

ซีไอไลต์แบบขั้นสออดแทรกด้วยเกลือควอเทอร์นารีแอมโมเนียมเป็นตัวเร่งปฏิกิริยา
สำหรับเอสเทอร์ฟิเคชันของกลีเซอรอล

นายชิตพัทธ์ นุ่มนึ่ง

วิทยานิพนธ์นี้เป็นส่วนหนึ่งของการศึกษาตามหลักสูตรปริญญาวิทยาศาสตรมหาบัณฑิต
สาขาวิชาปิโตรเคมีและวิทยาศาสตร์พอลิเมอร์

คณะวิทยาศาสตร์ จุฬาลงกรณ์มหาวิทยาลัย
บทคัดย่อและแฟ้มข้อมูลฉบับเต็มของวิทยานิพนธ์ตั้งแต่ปีการศึกษา 2554 ที่ให้บริการในคลังปัญญาจุฬาฯ (CUIR)
เป็นแฟ้มข้อมูลของนิสิตเจ้าของปีการศึกษา 2554 ทางบัณฑิตวิทยาลัย

The abstract and full text of theses from the academic year 2011 in Chulalongkorn University Intellectual Repository (CUIR)
are the thesis authors' files submitted through the Graduate School.

LAYERED ZEOLITES INTERCALATED WITH QUATERNARY AMMONIUM
SALTS AS CATALYSTS FOR ESTERIFICATION OF GLYCEROL

Mr. Chitatat Numnim

A Thesis Submitted in Partial Fulfillment of the Requirements
for the Degree of Master of Science Program in Petrochemistry and Polymer Science
Faculty of Science
Chulalongkorn University
Academic Year 2011
Copyright of Chulalongkorn University

Thesis Title LAYERED ZEOLITES INTERCALATED WITH QUATERNARY
 AMMONIUM SALTS AS CATALYSTS FOR ESTERIFICATION
 OF GLYCEROL
By Mr. Chitatat Numnim
Field of Study Petrochemistry and Polymer Science
Thesis Advisor Assistant Professor Chawalit Ngamcharussrivichai, Ph.D.

Accepted by the Faculty of Science, Chulalongkorn University in Partial Fulfillment
of the Requirements for the Master's Degree

.....Dean of the Faculty of Science
(Professor Supot Hannongbua, Dr. rer. nat.)

THESIS COMMITTEE

.....Chairman
(Associate Professor Supawan Tantayanon, Ph.D.)

.....Thesis Advisor
(Assistant Professor Chawalit Ngamcharussrivichai, Ph.D.)

.....Examiner
(Associate Professor Voravee Hoven, Ph.D.)

.....External Examiner
(Anawat Ketcong, Ph.D.)

ชิตทัตต์ นุ่มนึ่ง : ซีโอไลต์แบบชั้นสอดแทรกด้วยเกลือควอเทอร์นารีแอมโมเนียมเป็นตัวเร่งปฏิกิริยาสำหรับเอสเทอร์ฟิเคชันของกลีเซอรอล. (LAYERED ZEOLITES INTERCALATED WITH QUATERNARY AMMONIUM SALTS AS CATALYSTS FOR ESTERIFICATION OF GLYCEROL) อ.ที่ปรึกษาวิทยานิพนธ์หลัก: ผศ.ดร. ขวลิต งามจรัสศรีวิชัย, 108 หน้า.

งานวิจัยนี้ศึกษาการเตรียม MCM-22 สอดแทรกด้วยเกลือควอเทอร์นารีแอมโมเนียม ได้แก่ เททระโพรพิลแอมโมเนียมไฮดรอกไซด์ (TPAOH) เททระบิวทิลแอมโมเนียมไฮดรอกไซด์ (TBAOH) เททระบิวทิลแอมโมเนียมแอซิเตท (TBAAc) ซิทิลไตรเมทิลแอมโมเนียมโบรไมด์ (CTAB) การสังเคราะห์ MCM-22(P) ใช้วิธีไฮโดรเทอร์มัล MCM-22 และ ITQ-2 เตรียมได้จากการเผาและการดีลามิเนชันของ MCM-22(P) ตามลำดับ การสอดแทรก MCM-22 ด้วย CTAB และ TPAOH หรือ TBAOH ทำโดยรีฟลักซ์ MCM-22(P) กับสารละลาย TPAOH/CTAB หรือ TBAOH/CTAB ตามลำดับ ที่อุณหภูมิ 80 องศาเซลเซียสเป็นเวลา 16 ชั่วโมง MCM-22 และ ITQ-2 ถูกอิมเพกเนทด้วยกรดฟอสฟอริกทั้งสติก (HPW) วิเคราะห์สมบัติของตัวเร่งปฏิกิริยาที่เตรียมได้ด้วยเทคนิคต่างๆ ได้แก่ การเลี้ยวเบนของรังสีเอกซ์ การสูญเสียน้ำหนักด้วยความร้อน เทคนิคการดูดซับแก๊สไนโตรเจน กัดองจุลทรรศน์ อิเล็กตรอนแบบส่องกราด การตรวจวัดสมบัติความเป็นกรด และศึกษาผลของเกลือควอเทอร์นารีแอมโมเนียม ปริมาณกรดฟอสฟอริกทั้งสติก อัตราส่วนโดยโมล กลีเซอรอลต่อกรดลอริก อุณหภูมิปฏิกิริยา ปริมาณตัวเร่งปฏิกิริยา และระยะเวลาทำปฏิกิริยาต่อการเปลี่ยนของกรดลอริกและการกระจายของผลิตภัณฑ์ พบว่าตัวเร่งปฏิกิริยา 40HPW/ITQ-2 ให้ผลได้ของโมโนกลีเซอไรด์สูงที่สุดเท่ากับ 45.5 เปอร์เซ็นต์ ที่การเปลี่ยนของกรดลอริกเท่ากับ 57.4 เปอร์เซ็นต์ ภายใต้ภาวะการทำปฏิกิริยาที่เหมาะสม คือ อัตราส่วนโดยโมลของกลีเซอรอลต่อกรดลอริกเท่ากับ 1 ปริมาณตัวเร่งปฏิกิริยา 4 เปอร์เซ็นต์โดยน้ำหนักของกรดลอริก และระยะเวลาทำปฏิกิริยา 5 ชั่วโมงที่อุณหภูมิ 110 องศาเซลเซียส

สาขาวิชา ปิโตรเคมีและวิทยาศาสตร์พอลิเมอร์ ลายมือชื่อนิสิต.....

ปีการศึกษา2554.....ลายมือชื่อ อ.ที่ปรึกษาวิทยานิพนธ์หลัก.....

5272696223: MAJOR PETROCHEMISTRY AND POLYMER SCIENCE

KEYWORDS: MWW ZEOLITES / MCM-22 / ITQ-2 / QUATERNARY AMMONIUM SALTS / ESTERIFICATION / GLYCEROL

CHITATAT NUMNIM: LAYERED ZEOLITES INTERCALATED WITH QUATERNARY AMMONIUM SALTS AS CATALYSTS FOR ESTERIFICATION OF GLYCEROL. ADVISOR: ASST. PROF. CHAWALIT NGAMCHARUSSRIVICHAI, Ph.D., 108 pp.

This research aimed to study the preparation of MCM-22 intercalated with quaternary ammonium salts, including tetrapropylammonium hydroxide (TPAOH), tetrabutylammonium hydroxide (TBAOH), tetrabutylammonium acetate (TBAAC), and cetyltrimethylammonium bromide (CTAB). MCM-22(P) was synthesized by using hydrothermal method. MCM-22 and ITQ-2 were attained by calcination and delamination of MCM-22(P), respectively. The intercalation of MCM-22 with CTAB and TPAOH or TBAOH can be prepared by refluxing MCM-22(P) with the solution of TPAOH/CTAB or TBAOH/CTAB, respectively, at 80 °C for 16 h. MCM-22 and ITQ-2 were impregnated with phosphotungstic acid (HPW). The synthesized catalysts were characterized by means of X-ray diffraction (XRD), thermogravimetric/differential thermal analysis (TG/DTA), nitrogen adsorption-desorption technique, scanning electron microscopy (SEM), and acidity measurement. Effects of quaternary ammonium salt, phosphotungstic acid amount, molar ratio of glycerol to lauric acid, reaction temperature, catalyst amount, and reaction time on lauric acid conversion and products distribution were investigated. Due to an enhancement of the catalyst acidity, it was found that 40HPW/ITQ-2 giving the highest monoglycerides yield of 45.5% at the lauric acid conversion of 57.4% under the suitable conditions, the molar ratio of glycerol/lauric acid of 1, the catalyst mass of 4 wt.% based on weight of lauric acid, the reaction time of 5 h at 110 °C.

Field of Study: Petrochemistry and Polymer Science Student's Signature.....

Academic Year:2011..... Advisor's Signature.....

ACKNOWLEDGEMENTS

The author would like to express his sincere gratitude to his advisor, Asst. Prof. Dr.Chawalit Ngamcharussrivichai for his excellent supervision, inspiring guidance and encouragement throughout this research. The author also would like to acknowledge Assoc. Prof. Dr.Supawan Tantayanon, Assoc. Prof. Dr.Voravee Hoven and Dr.Anawat Ketcong for serving as chairman and members of thesis committee, respectively.

The author wishes to express his thankfulness to all people in the associated institutions for their kind assistance and collaboration.

Many thanks are going to the technicians at the Department of Chemical Technology, Chulalongkorn University.

The author also gratefully acknowledged the funding supports from the Center for Petroleum, Petrochemicals and Advanced Materials (NCE-PPAM) and the PTT Public Company Limited.

Finally, the author wishes to express his deep gratitude to his family for their love, support, understanding and encouragement throughout the graduate study.

CONTENTS

	Page
Abstract in Thai.....	iv
Abstract in English.....	v
Acknowledgements.....	vi
Contents.....	vii
List of Tables.....	xi
List of Figures.....	xiii
List of Abbreviations.....	xvi
 CHAPTER	
I INTRODUCTION.....	1
1.1 Statement of problems.....	1
1.2 Objectives.....	2
1.3 Scopes of work.....	3
II THEORY AND LITERATURE REVIEWS.....	4
2.1 Monoglycerides.....	4
2.1.1 Structure of monoglycerides.....	4
2.1.2 Synthesis of monoglycerides.....	4
2.1.3 Application of monoglycerides.....	7
2.2 Acid-catalyzed esterification.....	8
2.3 Glycerol.....	9
2.3.1 Structure of glycerol.....	9
2.3.2 Synthesis of glycerol.....	9
2.3.3 Application of glycerol.....	10
2.4 Fatty acids.....	12
2.4.1 Saturated fatty acids.....	12
2.4.2 Unsaturated fatty acids.....	13
2.5 Catalysts.....	15
2.5.1 Properties of industrial catalysts.....	15
2.5.2 Types of catalysts.....	16
2.5.3 Step in a heterogeneous catalytic reaction.....	17
2.6 Molecular sieves.....	19
2.7 Zeolites.....	19
2.7.1 Zeolite structures.....	20

CHAPTER	Page
2.7.2 Properties of zeolites.....	22
2.7.2.1 Acid sites of zeolites.....	22
2.7.2.2 Shape and size selectivity.....	23
2.7.3 Factors influence zeolite formation.....	24
2.7.3.1 Reaction mixture components.....	25
2.7.3.2 Temperature.....	25
2.7.3.3 Time	26
2.8 MWW zeolite	26
2.8.1 Synthesis of MCM-22.....	27
2.8.2 Synthesis of ITQ-2.....	27
2.9 Quaternary ammonium salts.....	29
2.10 Heteropoly acid.....	31
2.11 Literature review.....	32
III EXPERIMENTAL	36
3.1 Chemicals	36
3.1.1 Chemicals for synthesis of catalysts.....	36
3.1.2 Chemicals for adsorption study.....	36
3.1.3 Chemicals for esterification reaction.....	37
3.1.4 Chemicals for analysis of reaction products.....	37
3.2 Instruments and equipments.....	37
3.2.1 Instruments and equipments for synthesis of catalysts.....	37
3.2.2 Instruments and equipments for esterification.....	38
3.2.3 Instruments for analysis of reaction product.....	39
3.3 Catalyst preparation.....	40
3.3.1 Synthesis of MCM-22.....	40
3.3.2 Synthesis of ITQ-2.....	42
3.3.3 Ion exchange of MCM-22 and ITQ-2.....	43
3.3.4 Synthesis of MCM-22 intercalated with quaternary ammonium salts.....	43
3.3.5 Synthesis of MCM-22 intercalated with quaternary ammonium salts/CTAB.....	43
3.3.6 Synthesis of MCM-22 and ITQ-2 zeolite supported phosphotungstic acid.....	44
3.4 Study of adsorption study.....	44
3.5 Esterification of glycerol with lauric acid.....	45

CHAPTER	Page
3.5.1 Study on the effect of type of catalysts.....	45
3.5.2 Study on the effect of molar ratio of glycerol to lauric acid.....	45
3.5.3 Study on the effect of reaction temperature.....	45
3.5.4 Study on the effect of catalysts amount.....	45
3.5.5 Study on the effect of CTAB amount.....	46
3.5.6 Study on the effect of reaction time.....	46
3.6 Reaction product analysis.....	46
3.7 Characterization of catalysts.....	47
3.7.1 X-ray powder diffraction (XRD).....	47
3.7.2 Thermogravimetric analysis (TGA).....	48
3.7.3 Nitrogen adsorption-desorption technique.....	49
3.7.4 Scanning electron microscope (SEM).....	51
3.7.5 Acid-base titration.....	53
3.7.6 Back titration.....	53
3.7.7 Acid strength (Hammett indicators).....	54
IV RESULTS AND DISCUSSION	56
4.1 Characterization of catalysts.....	56
4.1.1 X-ray powder diffraction (XRD).....	56
4.1.2 Thermogravimetric/Differential thermal analysis (TG/DTA).....	63
4.1.3 Nitrogen adsorption-desorption technique.....	67
4.1.4 Scanning electron microscope (SEM).....	69
4.1.5 Acidity of catalysts.....	73
4.1.6 Adsorption study.....	75
4.2 Esterification of glycerol with lauric acid.....	77
4.2.1 Esterification of glycerol with lauric acid over MCM-22 and ITQ-2.....	77
4.2.2 Catalytic activity of MCM-22 intercalated with quaternary ammonium salts/CTAB in esterification of glycerol with lauric acid.....	78
4.2.3 Effect of quaternary ammonium salt (CTAB) as phase transfer catalyst on esterification of glycerol with lauric acid.....	78
4.2.4 Adjustment of reactants and catalyst addition method.....	80

CHAPTER	Page
4.2.5 Catalytic activity of MCM-22 and ITQ-2 supported phosphotungstic acid catalysts in esterification of glycerol	82
4.2.6 Catalytic activity of MCM-22 and ITQ-2 impregnated with different amounts of phosphotungstic acid.....	83
4.3 Parameters affecting esterification of glycerol with lauric acid	85
4.3.1 Effect of molar ratio of glycerol to lauric acid.....	85
4.3.2 Effect of reaction temperature.....	86
4.3.3 Effect of catalysts amount.....	87
4.3.4 Effect of reaction time.....	88
V CONCLUSIONS AND RECOMMENDATIONS.....	89
5.1 Conclusions.....	89
5.2 Recommendations	90
REFERENCES.....	91
APPENDIX.....	97
VITAE.....	108

LIST OF TABLES

Table	Page
1.1 Structure of quaternary ammonium salts.....	3
2.1 Application of monoglycerides	7
2.2 Example of saturated fatty acids.....	12
2.3 Example of unsaturated fatty acids	14
2.4 Comparison of homogeneous and heterogeneous catalyst.....	17
2.5 IUPAC classification of porous materials.....	19
2.6 The effect of selected variables on the final crystalline products of zeolite crystallization	25
2.7 Example of anion activating quaternary ammonium salts.....	30
2.8 Example of accessible quaternary ammonium salts	31
2.9 Some acid and oxidation reactions catalyzed by heteropoly acids	32
3.1 Gas chromatograph conditions for determining glyceride products	39
3.2 Features of adsorption isotherms.....	51
3.3 Properties of Hammett indicators used for measurement of acid strength	54
4.1 Proposed structures of the catalysts prepared	60
4.2 Textural properties of MCM-22 and ITQ-2 loaded with different amounts of phosphotungstic acid	69
4.3 Acidity measurement of the catalysts prepared	74
4.4 Effect of catalyst types on lauric acid conversion and products distribution	77
4.5 Effect of MCM-22 intercalated with quaternary ammonium salts/CTAB on lauric acid conversion and products distribution.....	78
4.6 Effect of CTAB on lauric acid conversion and products distribution.....	79
4.7 Esterification results from adjustment of reactants and catalyst addition method.....	80
4.8 Effect of phosphotungstic acid supported on MCM-22 and ITQ-2 on esterification of glycerol with lauric acid in the presence or absence of CTAB.....	82

Table	Page
4.9 Effect of phosphotungstic acid loading on lauric acid conversion and products distribution in esterification of glycerol over HPW/MCM-22 and HPW/ITQ-2.....	83
4.10 Effect of molar ratio of glycerol to lauric acid on lauric acid conversion and products distribution in esterification of glycerol over 40HPW/ITQ-2.....	85
4.11 Effect of reaction temperature on lauric acid conversion and products distribution in esterification of glycerol over 40HPW/ITQ-2.....	86
4.12 Effect of catalyst amount on lauric acid conversion and products distribution in esterification of glycerol over 40HPW/ITQ-2.....	87

LIST OF FIGURES

Figure		Page
2.1	Chemical structure of monoglycerides.....	4
2.2	Esterification of glycerol with fatty acids.....	5
2.3	Transesterification of glycerol with fatty acid methyl esters.....	5
2.4	Transesterification of glycerol with triglycerides.....	5
2.5	Esterification of monoglycerides and diglycerides with fatty acids.....	6
2.6	Esterification of carboxylic acid and alcohol.....	8
2.7	Mechanism of acid-catalyzed esterification.....	8
2.8	Chemical structure of glycerol.....	9
2.9	Saponification of triglycerides with alkali.....	10
2.10	Transesterification of triglycerides with alcohol.....	10
2.11	Commodity chemicals from glycerol.....	11
2.12	The structure and general formula of fatty acids.....	12
2.13	Comparison of the <i>trans</i> -isomer and the <i>cis</i> -isomer of oleic acid.....	13
2.14	The relationship between activation energy (E_a) and enthalpy (ΔH) of the reaction with and without a catalyst.....	15
2.15	Steps in heterogeneous catalysis.....	18
2.16	Simplified structure of tetrahedral network in zeolites.....	20
2.17	A primary building unit of zeolites.....	20
2.18	Secondary Building Units (SBU's) in zeolites.....	21
2.19	The structure of sodalite, zeolite A, and faujasite-type zeolites.....	21
2.20	Examples of the three types of pore openings in the porous material molecular sieves (a) an 8 ring pore opening (small pore), (b) a 10 ring pore opening (medium pore), and (c) a 12 ring pore opening (large pore).....	22
2.21	The generation of Brønsted and Lewis acid sites in zeolite.....	23
2.22	Three types of selectivity in zeolites: reactant, product, and transition-state shape selectivity.....	24
2.23	MWW frameworks.....	26
2.24	Scheme for the preparation of ITQ-2 obtained from MCM-22 precursor.....	28
2.25	Proposed structure for ITQ-2.....	28

Figure		Page
2.26	Structure of quaternary ammonium salts.....	29
2.27	Structure of phosphotungstic acid.....	32
3.1	The gas chromatograph column heating program.....	40
3.2	Preparation diagram for MCM-22.....	41
3.3	Preparation diagram for ITQ-2.....	42
3.4	Diagram for derivatization of reaction product.....	46
3.5	Diffraction of X-ray by regular planes of atoms.....	48
3.6	Perkin-Elmer Pyris Diamond thermogravimetric/differential thermal analyzer.....	49
3.7	The IUPAC classification of adsorption isotherm.....	50
3.8	Diagram for acid-base titration.....	53
3.9	Diagram for back titration.....	54
3.10	Hammett indicators used for measurement of acid strength.....	55
3.11	Example of the color change of Bromothymol blue.....	55
4.1	XRD patterns of (a) MCM-22(P), (b) MCM-22, (c) H-MCM-22, (d) ITQ-2, and (e) H-ITQ-2.....	56
4.2	Formation of MCM-22 by condensation of the MCM-22(P) upon calcinations: (a) the contraction of interlayer spacing of about 2 Å, (b) the accompanying change in the low angle XRD pattern.....	57
4.3	XRD patterns of MCM-22(P) and MCM-22 intercalated with quaternary ammonium salts: (a) MCM-22(P), (b) MCM-TPAOH, (c) MCM-TBAOH (d) MCM-TBAAc, and (e) MCM-CTAB.....	58
4.4	XRD patterns of MCM-22(P) and MCM-22 intercalated with quaternary ammonium salts and CTAB: (a) MCM-22(P), (b) MCM-TPAOH/CTAB, (c) MCM-TBAOH/CTAB, and (d) MCM-TBAAc/CTAB.....	60
4.5	XRD patterns of MCM-22 and HPW/MCM-22 with different loadings: (a) MCM-22, (b) 10HPW/MCM-22, (c) 20HPW/MCM-22, (d) 40HPW/MCM-22, and (e) 60HPW/MCM-22..	61
4.6	XRD patterns of ITQ-2 and HPW/ITQ-2 with different loadings: (a) ITQ-2, (b) 10HPW/ITQ-2, (c) 20HPW/ITQ-2, (d) 40HPW/ITQ-2, and (e) 60HPW/ITQ-2.....	61
4.7	XRD pattern of phosphotungstic acid	62
4.8	TG/DTG profile of MCM-22(P).....	63
4.9	TG/DTG profile of MCM-TPAOH.....	64
4.10	TG/DTG profile of MCM-TPAOH/CTAB.....	65

Figure	Page
4.11 TGA profiles of bulk phosphotungstic acid, ITQ-2, and 40HPW/ITQ-2.....	66
4.12 Nitrogen adsorption-desorption isotherms of (◆) MCM-22, (■) 10HPW/MCM-22, (▲) 20HPW/MCM-22, (+) 40HPW/MCM-22, and (x) 60HPW/MCM-22.....	68
4.13 Nitrogen adsorption-desorption isotherms of (◆) ITQ-2, (■) 10HPW/ITQ-2, (▲) 20HPW/ITQ-2, (+) 40HPW/ITQ-2, and (x) 60HPW/ITQ-2.....	68
4.14 SEM images of (a) MCM-22(P), (b) MCM-22, (c) H-MCM-22, (d) MCM TPAOH/CTAB, and (e) 40HPW/MCM-22.....	71
4.15 SEM images of (a) ITQ-2, (b) H-ITQ-2, and (c) 40HPW/ITQ-2.....	72
4.16 Adsorption isotherms of glycerol and lauric acid on various catalysts: (a) MCM-22(P), (b) MCM-22, (c) MCM-TPAOH/CTAB, and (d) 40HPW/ITQ-2 (Symbols: (■) lauric acid and (◆) glycerol).....	76
4.17 Effect of reaction time on glycerides yield and products distribution in esterification of glycerol over 40HPW/ITQ-2. Reaction conditions: Catalyst amount, 4 wt.%; glycerol/lauric acid molar ratio, 1; reaction temperature, 110 °C. (Symbols: (◆) lauric acid conversion, (■) monoglycerides yield, and (▲) diglycerides yield).....	88
A-1 Representative chromatogram of reaction mixture obtained from the esterification of glycerol with lauric acid over 40HPW/ITQ-2 catalyst....	98
A-2 Calibration curve of monolaurin standard solution	99
A-3 Calibration curve of dilaurin standard solution	100
A-4 Calibration curve of trilaurin standard solution	100
A-5 Calibration curve of lauric acid standard solution	101
A-6 Calibration curve of glycerol standard solution	102

LIST OF ABBREVIATIONS

Å	Angstrom
BET	Brunauer-Emmett-Teller
°C	Degree Celsius
GC	Gas chromatography
g	Gram (s)
h	Hour (s)
mL	Milliliter (s)
min	Minute (s)
M	Molarity
%	Percentage
SEM	Scanning electron microscopy
XRD	X-ray diffraction
TGA	Thermogravimetric analysis
TPAOH	Tetrapropylammonium hydroxide
TBAOH	Tetrabutylammonium hydroxide
TBAAc	Tetrabutylammonium acetate
CTAB	Cetyltrimethylammonium bromide
HMI	Hexamethylene imine
HPW	Phosphotungstic acid
μL	Microliter (s)

CHAPTER I

INTRODUCTION

1.1 Statement of Problems

In the last decade, the biodiesel production is increasing exponentially. In the production of biodiesel via transesterification of triglycerides with methanol, about 1 kg of crude glycerol is formed as a by-product for every 9 kg of biodiesel. Nowadays, glycerol surplus is becoming a matter of environmental and economic concern [1-4]. Therefore, new ideas to convert glycerol in more valuable compounds are needed. One important glycerol derivative is monoglycerides which are widely used as emulsifiers in food, pharmaceutical, and cosmetic products due to their physicochemical properties, basically the hydrophilic/hydrophobic balance [5-7].

There are two main synthetic routes for obtaining monoglycerides; direct esterification of glycerol with fatty acids and transesterification of glycerol with triglycerides or fatty acid methyl esters [8-10]. In both routes, the industrial processes use homogeneous catalysts. An acid catalyst such as sulfuric, phosphoric, or organic sulfonic acid is required in the esterification route, whereas the transesterification process involves a base-catalyzed reaction with a strong base such as KOH or $\text{Ca}(\text{OH})_2$ and high temperatures. These industrial processes lead to a mixture of monoglycerides (35 to 40 %), diglycerides (40 to 50%), and triglycerides (10 to 15%) and a molecular distillation is necessary to obtain greater monoglyceride enrichment. A drawback associated with using homogeneous catalysts is the need of a neutralization step with the formation of soaps and a high salt content, followed by another washing to remove the salt formed in the purification by which a large amount of wastewater is produced, representing a disadvantage of the homogeneous catalysis. Alternative methods for the preparation of monoglycerides include enzymatic alcoholysis of triglycerides and enzymatic esterification of glycerol and fatty acids. The drawbacks of the enzymatic methods are low space velocity and a relatively complex workup of the reaction mixture.

Recently, the application of heterogeneous acid catalysts to esterification/transesterification for monoglycerides syntheses has attracted considerable attention since the process can be simplified by using of a designed-column reactor packed with the solid catalysts. Consequently, the need of subsequent steps for the catalyst separation and the product purification can be reduced [11-13]. More importantly, the most of heterogeneous catalysts themselves are recyclable, less toxic and non-corrosive. Among many solid acid systems, zeolites have been widely used in numerous acid-catalyzed reactions due to their several advantages, such as high acidity, shape-selectivity, thermal stability, high surface area, less-corrosive, easy regeneration and separation from the liquid products [14-16]. This research has focused on an application of MWW layered zeolites as heterogeneous catalysts to the synthesis of monoglycerides via the esterification route. The major interest in MWW zeolites is brought from the fact that the layers can be swollen by intercalation with quaternary ammonium salts [17-19]. Both the property of quaternary ammonium salts act as phase transfer catalysts and the suitable interlayer space can facilitate the migration of reactants to acid sites, resulting in an enhancement of the esterification rates and the selectivity of monoglycerides [20-21].

The aim of this thesis is to prepare MWW layered zeolites intercalated with quaternary ammonium salts, including tetrapropylammonium hydroxide, tetrabutylammonium hydroxide, tetrabutylammonium acetate, and cetyltrimethylammonium bromide and use as catalysts for the esterification of glycerol with lauric acid. Effect of molar ratio of glycerol to lauric acid, reaction temperature, catalysts amount, reaction time on the conversion of lauric acid and the selectivity of monoglycerides were investigated.

1.2 Objectives

The objectives of this research are:

1. To synthesize layered zeolites intercalated with quaternary ammonium salts.
2. To study the esterification of glycerol with fatty acid over layered zeolites intercalated with quaternary ammonium salts.

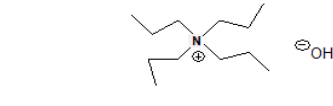
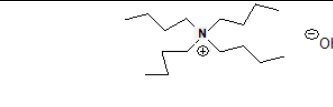
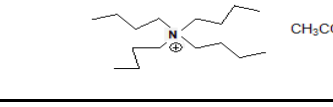
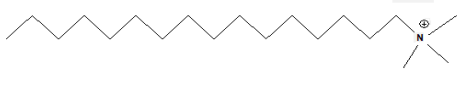
1.3 Scopes of work

1.3.1 To review previously published research articles related to this thesis.

1.3.2 To synthesize layered zeolites intercalated with quaternary ammonium salts.

The quaternary ammonium salts used in the study are listed in Table 1.1.

Table 1.1 Structure of quaternary ammonium salts

Quaternary ammonium salt	Structure
Tetrapropylammonium hydroxide (TPAOH)	
Tetrabutylammonium hydroxide (TBAOH)	
Tetrabutylammonium acetate (TBAAc)	
Cetyltrimethylammonium bromide (CTMAB)	

1.3.3 To characterize the prepared catalysts.

1.3.4 To study effects of esterification conditions on fatty acid conversion and monoglycerides selectivity.

- Amount of catalyst 0-6 wt.%
- Molar ratio of glycerol to fatty acid 1-3
- Reaction time 0.5-8 h
- Reaction temperature 100-130 °C

1.3.5 To summarize the results and write thesis.

CHAPTER II

THEORY AND LITERATURE REVIEWS

2.1 Monoglycerides

2.1.1 Structure of monoglycerides

Monoglycerides, also known as glycerol monoesters, are glycerides consisting of one fatty acid chain covalently bonded to a glycerol molecule through an ester linkage. The interest in monoglycerides resides in their structure comprising an aliphatic chain and two hydroxyl groups in the hydrophilic part. This structure causes surfactant action, which stabilizes emulsions. Monoglycerides can be broadly divided into two isomeric forms; α -monoglycerides and β -monoglycerides, depending on the position of the ester bond on the glycerol moiety [22].

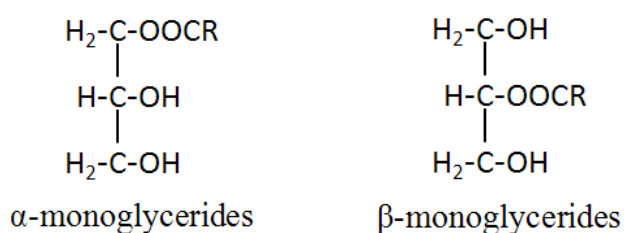


Figure 2.1 Chemical structure of monoglycerides.

2.1.2 Synthesis of monoglycerides

There are two main synthetic routes for obtaining monoglycerides [8-10]:

- (1) Esterification of glycerol with fatty acids over acid catalysts in nitrogen-rich atmosphere, as illustrated in Figure 2.2.

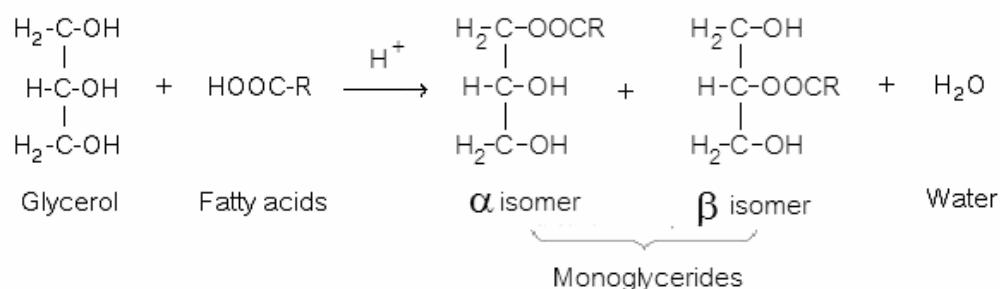


Figure 2.2 Esterification of glycerol with fatty acids.

- (2) Transesterification of glycerol with fatty acid methyl esters (Figure 2.3) or triglycerides (Figure 2.4) over basic catalysts in nitrogen-rich atmosphere.

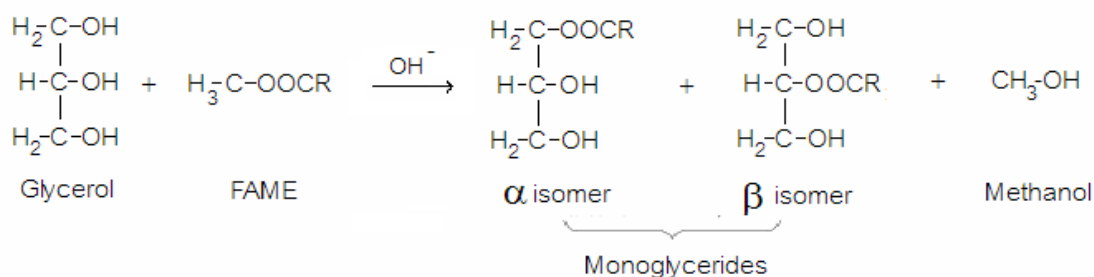


Figure 2.3 Transesterification of glycerol with fatty acid methyl esters.

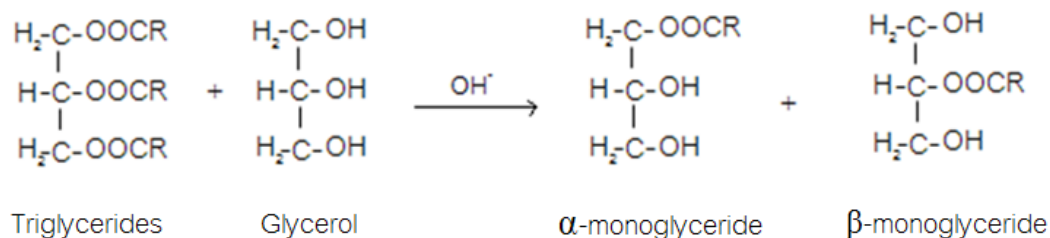


Figure 2.4 Transesterification of glycerol with triglycerides.

Monoglyceride synthesis by esterification or transesterification was transformed to diglycerides and triglycerides by consecutive reaction with fatty acids or fatty acid methyl esters, as shown in Figure 2.5.

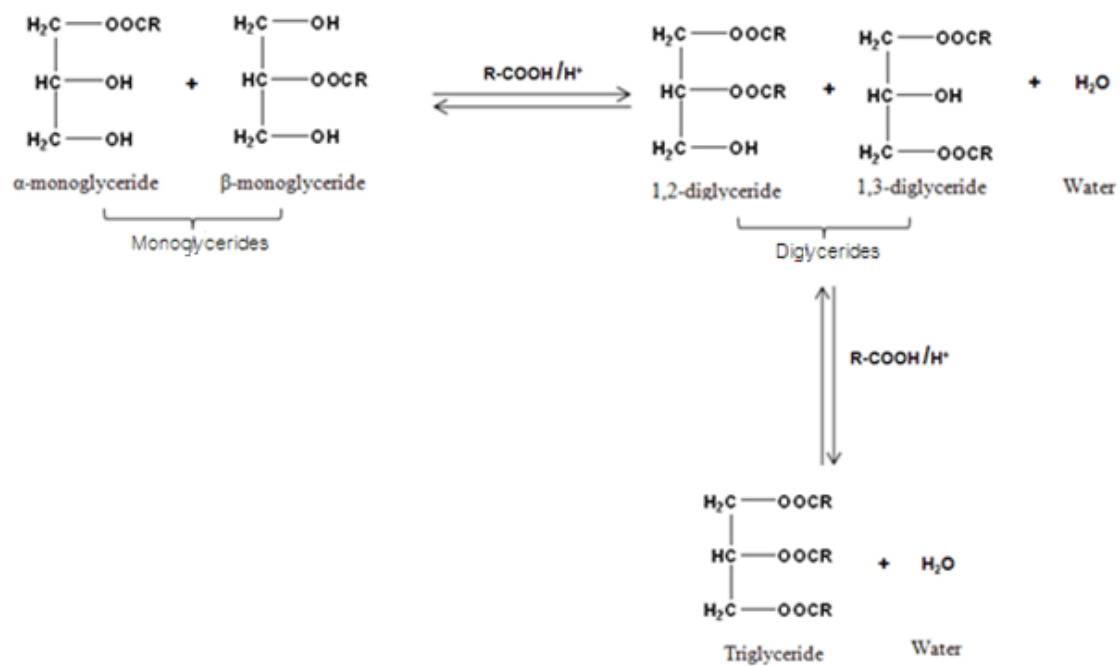


Figure 2.5 Esterification of monoglycerides and diglycerides with fatty acids.

2.1.3 Application of monoglycerides

Monoglycerides are valuable compounds with broad area of applications as summarized in Table 2.1.

Table 2.1 Application of monoglycerides

Food and drink	<ul style="list-style-type: none"> • Manufacture use as emulsifiers. • Used as filler and sweetener in low-fat food products such as cookies. • Used as humectants and sweetener in a wide range of products. • Manufacture of polyglyceryl ester as an additive in margarine and butter.
Personal care	<ul style="list-style-type: none"> • Used in a wide range of personal care products as an emollient, humectants, solvent and lubricant; including skin care, hair care, toothpastes, shaving creams and soaps.
Pharmaceuticals	<ul style="list-style-type: none"> • Used as a lubricant and humectant in pharmaceutical preparation such as suppositories, cough syrups and expectorants.
Polymers	<ul style="list-style-type: none"> • Producing polyether polyols for polyurethane foams and other flexible foams. • As a plasticizer in cellophane. • Production of alkyd resins for paints and coatings.

2.2 Acid-catalyzed esterification [23]

The most usual method for the preparation of esters is the reaction of carboxylic acid (fatty acid) and alcohol with elimination of water. Esterification is a reversible reaction, but is driven to completion by using of excess alcohol and removal of water.

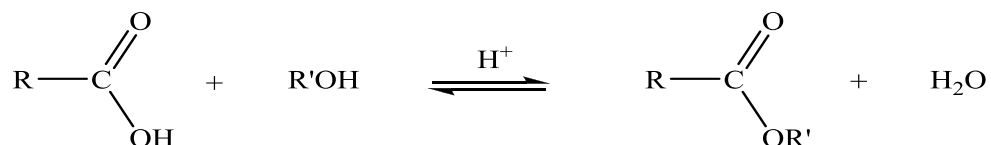


Figure 2.6 Esterification of carboxylic acid and alcohol.

The uncatalyzed reaction is usually too slow to be useful. The acid and alcohol can be reacted thermally, usually in the presence of an acid catalyst in an esterification reactor. Possible catalysts include sulfuric acid, tetra alkyl titanate, *p*-toluene sulfonic acid, anhydrous sodium hydrogen sulfate, and stannous octanoate. The mechanism of acid-catalyzed esterification is shown in Figure 2.7.

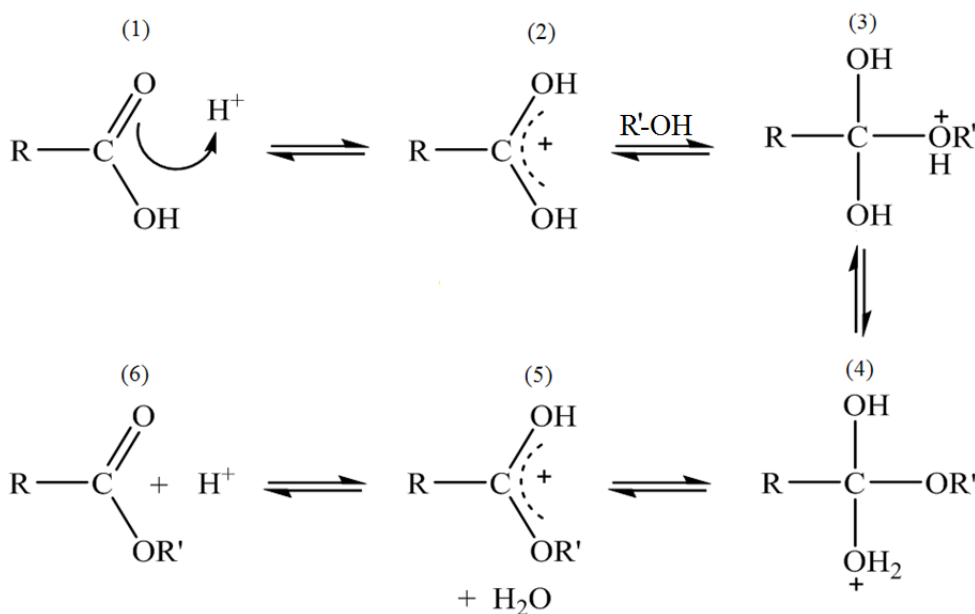


Figure 2.7 Mechanism of acid-catalyzed esterification [24].

Step 1: Protonation of the carbonyl group makes it more electrophilic.

Step 2: The oxygen atom of alcohol functions as the nucleophile attacking the electrophilic carbon atom in the $\text{C}=\text{O}$, with the electrons moving towards the oxonium ion, creating the tetrahedral intermediate.

Step 3: Deprotonate the alcoholic oxygen.

Step 4: Need to make an OH leave, it doesn't matter which one, so convert it into a good leaving group by protonation.

Step 5: Use the electrons of an adjacent oxygen to help "push out" the leaving group, a neutral water molecule.

Step 6: Deprotonation of the oxonium ion reveals the carbonyl group in the ester product.

2.3 Glycerol

2.3.1 Structure of glycerol

Glycerol, also well known as glycerin, and less commonly as 1,2,3-propanetriol, glyceritol, and glycol alcohol. Glycerol is a colorless, odorless, and sweet-tasting viscous liquid. It is hygroscopic because it absorbs water from the air then it was used as a moistener in cosmetic. It melts at 17.8 °C, boils with decomposition at 290 °C, and is miscible with water and ethanol [1-2]. The chemical structure for glycerol is shown in Figure 2.8.

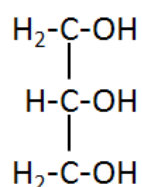


Figure 2.8 Chemical structure of glycerol.

2.3.2 Synthesis of glycerol

Glycerol can be found naturally in the form of fatty acid esters and also as important intermediates in the metabolism of living organisms. Traditionally, glycerol is obtained as a by-product in two different processes [1-2]:

(1) Saponification of triglycerides with alkali

The production of soap, sometimes called alkaline hydrolysis, converts triglycerides to glycerol and a mixture of salts of long-chain carboxylic acids, as can be seen in Figure 2.9.

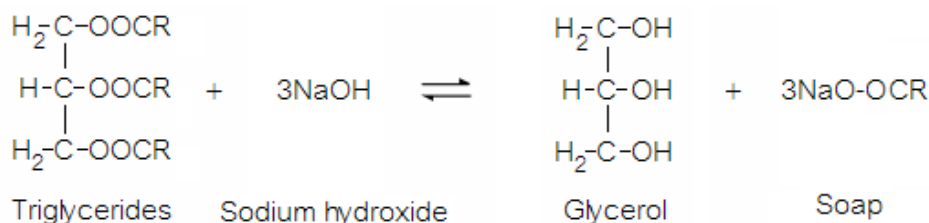


Figure 2.9 Saponification of triglycerides with alkali.

(2) Transesterification of triglycerides with alcohol

Transesterification of triglycerides with an alcohol forms monoesters and glycerol as the by-product (Figure 2.10). Principally, it is the action of one alcohol displacing another from ester. A catalyst is usually used to speed up the reaction and may be alkali, acid or enzymatic in nature. Sodium hydroxide is the most commonly used alkali catalyst, due to economic reasons and availability.

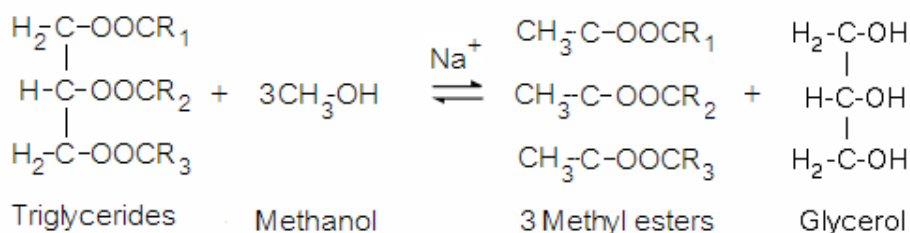


Figure 2.10 Transesterification of triglycerides with alcohol.

2.3.3 Application of glycerol

Glycerol is a potentially important biorefinery feedstock, available as a by-product in the production of biodiesel by transesterification of vegetable oils or animal fats. For every 9 kg of biodiesel produced, about 1 kg of a crude glycerol by-product is formed. Glycerol markets have reacted strongly to the increasing availability of glycerol. Although the global production of biodiesel is still very limited, the market price of glycerol has dropped rapidly. If the production of biodiesel increases, the supply of glycerol will be in

excess of demand. Therefore, new uses for glycerol need to be found. Although glycerol can be burned as a fuel, it can also be processed into more valuable commodity chemicals. Its highly functionalized nature means that glycerol can readily be oxidized, reduced, halogenated, etherified, and esterified to obtain alternative commodity chemicals. Glycerol derivatives from possible glycerol reactions are shown in Figure 2.11.

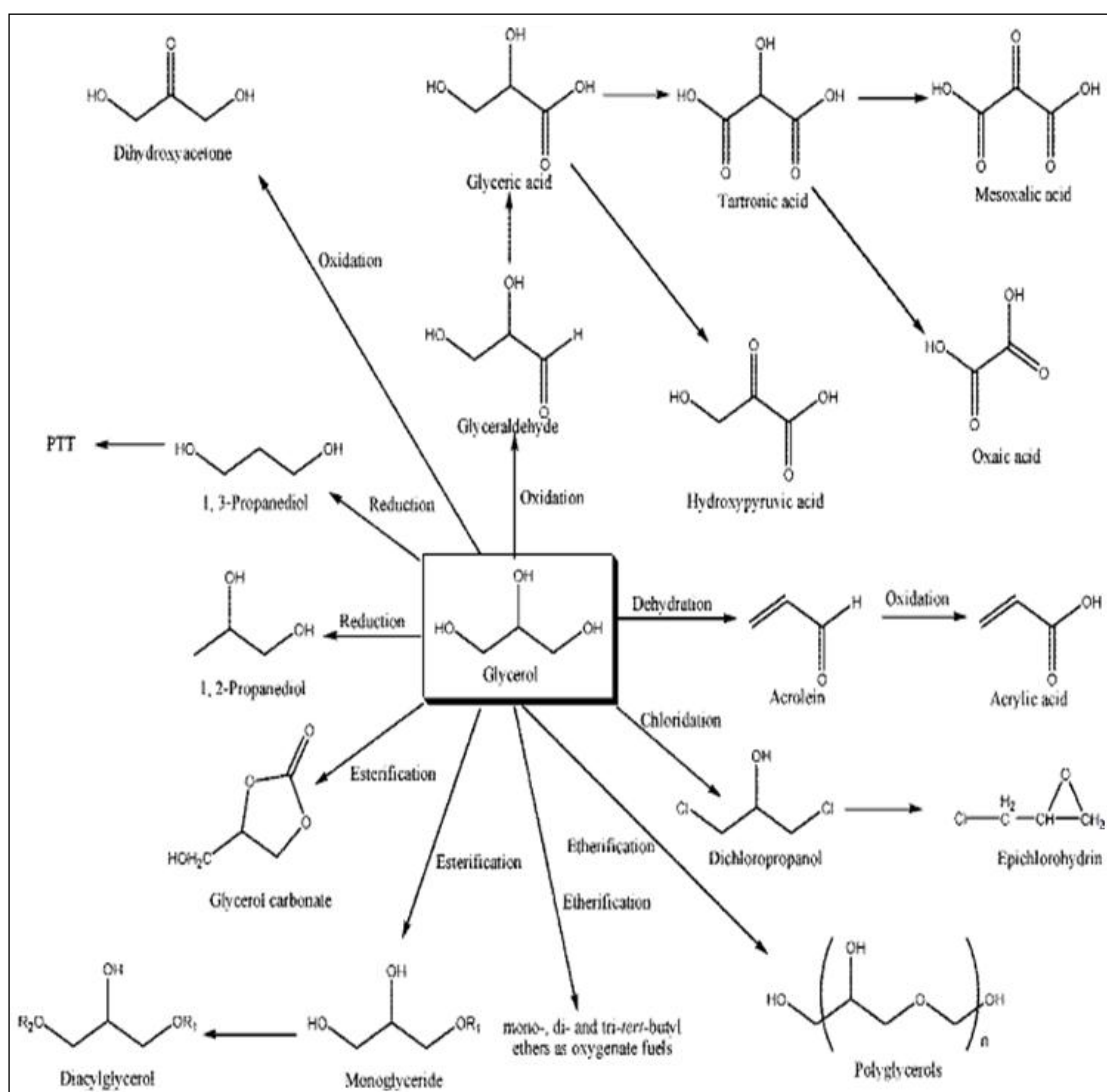


Figure 2.11 Commodity chemicals from glycerol [1].

2.4 Fatty acids [25]

Fatty acids are aliphatic monocarboxylic acids derived from or contained in esterified form in an animal or vegetable fat, oil or wax. Natural fatty acids commonly have a chain of 4 to 28 carbons (usually unbranched and even numbered), which may be saturated or unsaturated.

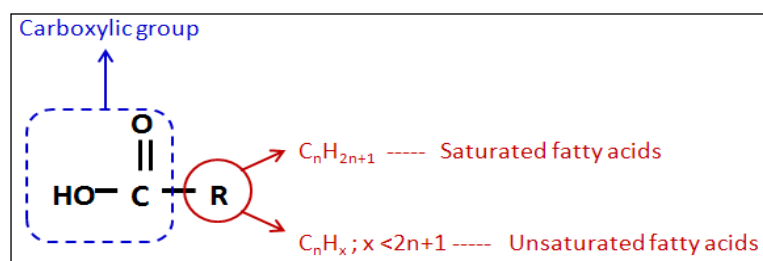


Figure 2.12 The structure and general formula of fatty acids.

2.4.1. Saturated fatty acids

Saturated fatty acids do not contain any double bonds or other functional groups along the chain. The term “saturated” refers to hydrogen, in that all carbons (apart from the carboxylic acid group) contain as many hydrogens as possible. Each carbon within the chain contains 2 hydrogen atoms. Saturated fatty acids form straight chains and, as a result, can be packed together very tightly, allowing living organisms to store chemical energy very densely. The saturated fatty acids are representatively shown in Table 2.2.

Table 2.2 Example of saturated fatty acids

Common name	IUPAC name	Chemical structure	C no. : db
Lauric	Dodecanoic acid	$CH_3(CH_2)_{10}COOH$	C12:0
Myristic	Tetradecanoic acid	$CH_3(CH_2)_{12}COOH$	C14:0
Palmitic	Hexadecanoic acid	$CH_3(CH_2)_{14}COOH$	C16:0
Stearic	Octadecanoic acid	$CH_3(CH_2)_{16}COOH$	C18:0

2.4.2 Unsaturated fatty acids

Unsaturated fatty acids are of similar form, except that one or more alkenyl functional groups exist along the chain, with each alkene substituting a single-bonded part of the chain with a double-bonded portion. The two next carbon atoms in the chain that are bound to either side of the double bond can occur in a *cis* or *trans* configurations. Figure 2.13 compares the structures of *trans*-isomer and *cis*-isomer of oleic acid.

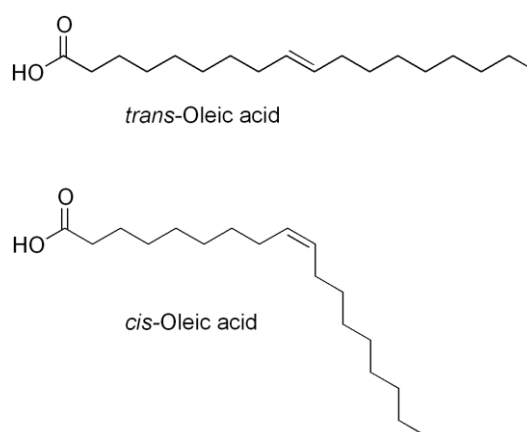


Figure 2.13 Comparison of the *trans*-isomer and the *cis*-isomer of oleic acid.

(a) *cis*-Isomer

A *cis* configuration means that adjacent carbon atoms are on the same side of the double bond. The rigidity of the double bond freezes its conformation and, in the case of the *cis* isomer, causes the chain to bend and restricts the conformational freedom of the fatty acid. The more double bonds the chain has in the *cis* configuration, the less flexibility it has. When a chain has many *cis* bonds, it becomes quite curved in its most accessible conformations. For example, oleic acid, with one double bond, has a link in it, whereas linoleic acid, with two double bonds, has a more pronounced bend. Alpha-linolenic acid, with three double bonds, favors a hooked shape. The effect of this is that, in restricted environments, such as when fatty acids are part of a phospholipid in a lipid bilayer, or triglycerides in lipid droplets, *cis* bonds limit the ability of fatty acids to be closely packed, and therefore could affect the melting temperature of the fat.

(b) *trans*-Isomer

A *trans* configuration, by contrast, means that the next two carbon atoms are bound to opposite sides of the double bond. As a result, they do not cause the chain to bend much, and their shape is similar to straight saturated fatty acids.

In most naturally occurring unsaturated fatty acids. Most fatty acids in the *trans* configuration (trans fats) are not found in nature and are the result of human processing. Examples of unsaturated fatty acids were presented in Table 2.3 [26].

Table 2.3 Example of unsaturated fatty acids

Common name	Chemical structure	C no. : db
Myristoleic acid	$\text{CH}_3(\text{CH}_2)_3\text{CH}=\text{CH}(\text{CH}_2)_7\text{COOH}$	C14:1
Palmitoleic acid	$\text{CH}_3(\text{CH}_2)_5\text{CH}=\text{CH}(\text{CH}_2)_7\text{COOH}$	C16:1
Oleic acid	$\text{CH}_3(\text{CH}_2)_7\text{CH}=\text{CH}(\text{CH}_2)_7\text{COOH}$	C18:1
Linoleic acid	$\text{CH}_3(\text{CH}_2)_4\text{CH}=\text{CHCH}_2\text{CH}=\text{CH}(\text{CH}_2)_7\text{COOH}$	C18:2

2.5 Catalysts

A catalyst is a substance that increases the rate of a chemical reaction by reducing the activation energy (E_a) as shown in Figure 2.14. The highest peak position performing the highest energy refers to the transition state. In typical reaction, the energy required to enter the transition state is high, whereas the energy to transition state decreases in the catalytic reaction. In addition, the catalyst may participate in multiple chemical transformations and is not consumed by the reaction.

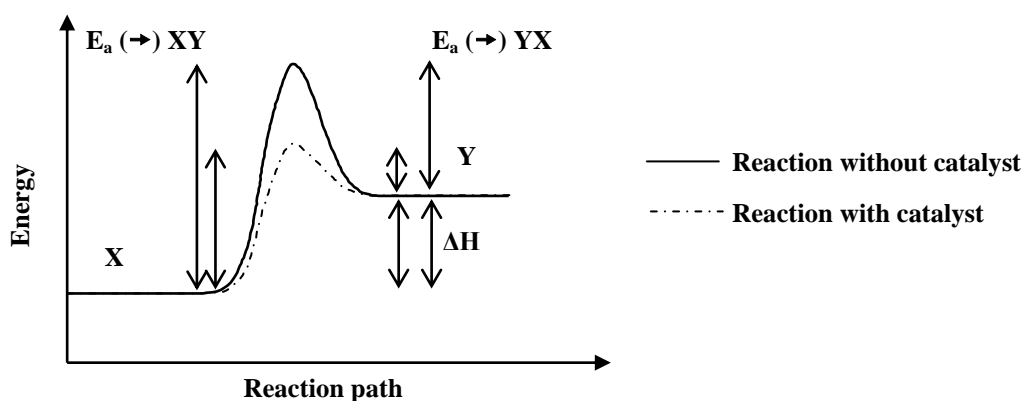


Figure 2.14 The relationship between activation energy (E_a) and enthalpy (ΔH) of the reaction with and without a catalyst [27].

2.5.1 Properties of industrial catalysts

In general, the suitable catalysts for industrial processes are considered mainly on the three properties [28]:

a) Activity is a measure of how fast one or more reactions proceed which can be defined in terms of kinetics. A high activity catalyst will be given high productivity when the less amount of the catalyst is utilized or the reaction is performed in mild operating condition, particularly temperature, which enhances selectivity and stability if the thermodynamic is more favorable. It is appropriate to measure reaction rates in the temperature that will be occurred in the reactor.

b) Selectivity of a reaction is the fraction of the starting material that is converted to the desired product. High selectivity catalyst produces high yield of a desired product, whereas undesirable competitive and consecutive reactions are suppressed. This means that the texture of the catalyst (in particular pore size and pore volume) should be improved

toward reducing limitation by internal diffusion, which in case of consecutive reactions rapidly reduces selectivity.

c) Stability of a catalyst determines its lifetime in industrial processes. Catalyst stability is influenced by various factors such as decomposition, coking and poisoning. Catalyst deactivation can be followed by measuring activity or selectivity as a function of time. Deactivated catalysts can often be regenerated before they ultimately have to be replaced. The catalyst lifetime is a crucial importance for the economics of process.

Nowadays, the efficient use of raw materials and energy is of major importance, and it is preferable to optimize existing processes than to develop new ones. For various reasons, the target quantities should be given the following order of priority:

Selectivity > Stability > Activity

2.5.2 Types of catalysts

Catalysts can be divided into two main types: homogeneous and heterogeneous. In a homogeneous reaction, the catalyst is in the same phase as the reactants. In a heterogeneous reaction, the catalyst is in a different phase from the reactants. Heterogeneous catalysts, phase boundaries are always present between the catalyst and the reactants, while catalyst, reactants, and products are present in the same phase in homogeneous catalysis. Homogeneous catalysts have a higher degree of dispersion than heterogeneous catalysts that only the surface atoms are active [28].

Due to their high degree of dispersion, homogeneous catalysts exhibit a higher activity per unit mass of metal than heterogeneous catalysts. The high mobility of the molecules in the reaction mixture results in more collision with substrate molecules. The reactant can approach the catalytically active center from any direction, and a reaction at an active center does not block the neighboring centers. This allows the use of lower catalyst concentrations and milder reaction conditions. Table 2.4 summarizes the advantages and disadvantages of the two classes of catalyst. The major disadvantage of homogeneous catalysts is the difficulty of separating the catalyst from product. Heterogeneous catalysts are either automatically removed in the process (e.g. gas-phase reactions in fixed-bed reactions) or they can be separated by simple methods such as centrifugation or filtration. In the case of homogeneous catalysts, more complicated processes such as distillation, liquid-liquid extraction and ion exchange must often be used.

Table 2.4 Comparison of homogeneous and heterogeneous catalyst

Consideration	Homogeneous catalyst	Heterogeneous catalyst
1. Active centers	All metal atoms	Only surface atoms
2. Concentration	Low	High
3. Selectivity	High	Low
4. Diffusion problems	Practically absent	Present (mass-transfer-controlled reaction)
5. Reaction conditions	Mild (50-200 °C)	Severe (often >250 °C)
6. Applicability	Limited	Wide
7. Activity loss	Irreversible reaction with product (cluster formation), poisoning	Sintering of the metal crystallites, poisoning
8. Structure/ Stoichiometry	Defined	Undefined
9. Modification possibility	High	Low
10. Thermal stability	Low	High
11. Catalyst separation	Sometimes laborious (chemical decomposition, distillation, extraction)	Fixed-bed: unnecessary Suspension: filtration
12. Catalyst recycling	Possible	Unnecessary (fixed-bed) or easy (suspension)
13. Cost of catalyst losses	High	Low

2.5.3 Step in a heterogeneous catalytic reaction [29].

In heterogeneous catalysis, the catalytic action involves the adsorption of reactant molecules on active sites on the surface of the solid catalysts therefore, the transport of those molecules from the fluid phase to the surface, where the catalytic reaction effectively occurs, must be considered in the general mechanism. Similarly, the molecules of the reaction products are eventually desorbed and transferred in the opposite direction from inside the solid pores to the fluid phase.

Hougen, Watson and others have broken down the steps that occur on a molecular scale in the following manner.

1. Mass transfer of reactants from the main body of the fluid to the gross exterior surface of the catalyst particle.
2. Molecular diffusion or flow of reactants from the exterior surface of the catalyst particle into the interior pore structure.
3. Chemisorptions of at least one of the reactants on the catalyst surface.
4. Reaction on the surface.
5. Desorption of adsorbed species from the surface of the catalyst.
6. Transfer of products from the interior catalyst pores to the gross external surface of the catalyst by ordinary molecular diffusion and/or Knudsen diffusion.
7. Mass transfer of products from the exterior surface of the particle into the bulk of the fluid.

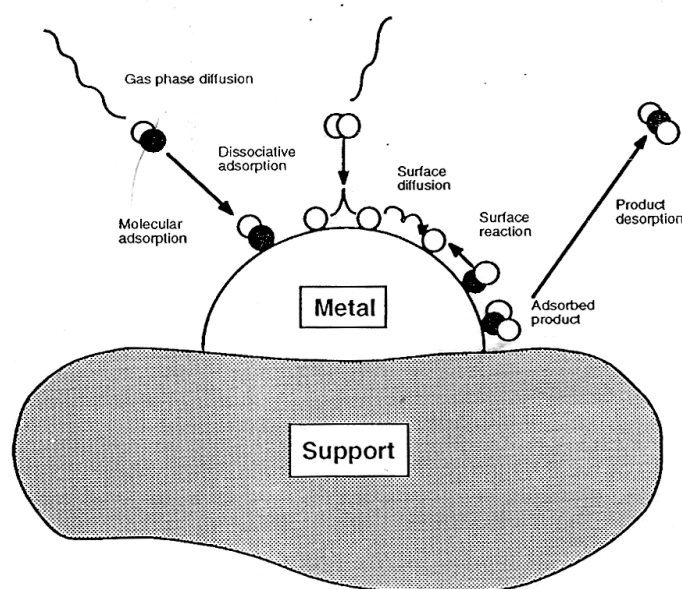


Figure 2.15 Steps in heterogeneous catalysis [30].

Several of these steps are shown in Figure 2.15. Of course, if the catalyst is nonporous, steps 2 and 6 are absent. Steps 1, 2, 6, and 7 are obviously physical processes, while steps 3 to 5 are basically chemical in character. The rates of the various steps depend on a number of factors in addition to the concentration profiles of the reactant and product species.

Steps 1 and 7 are highly dependent on the fluid flow characteristics of the system. The mass velocity of the fluid steam, the particle size, and the diffusional characteristics of the various molecular species are the pertinent parameters on which the rates of these steps depend. These steps limit the observed rate only when the catalytic reaction is very rapid and the mass transfer is slow. Anything that tends to increase mass transfer coefficients will enhance the rates of these processes. Since the rate of these steps are only slightly influenced by temperature, the influence of these processes on the overall conversion rate will vary as the temperature changes. Their influence is often negligible at low temperatures, but may be quite significant at higher temperatures.

2.6 Molecular sieves

Molecular sieves are porous materials that exhibit selective adsorption properties which can be classified on the IUPAC definitions into three main types depending on their pore sizes that are microporous materials, mesoporous materials, and macroporous materials. Properties and examples of these materials are shown in Table 2.5.

Table 2.5 IUPAC classification of porous materials

Type of porous molecular sieve	Pore size (Å)	Examples
Microporous materials	< 20	Zeolites, Activated carbon
Mesoporous materials	20 – 500	M41s, SBA-15, Pillared clays
Macroporous materials	> 500	Glasses

2.7 Zeolites

Zeolites, a type of molecular sieves, are crystalline aluminosilicates that contain uniform pores and cavities with molecular dimensions. The structures of zeolites consist of an extensive three-dimensional network of SiO_4 and AlO_4^- tetrahedral. The tetrahedral are cross-linked by sharing of the oxygen atoms as shown in Figure 2.16.

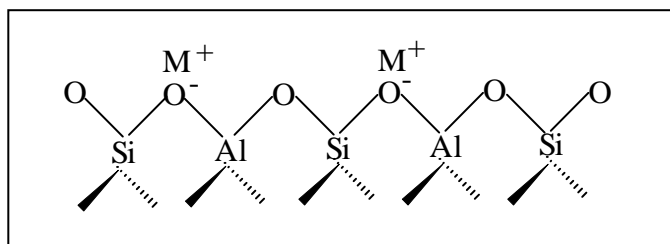
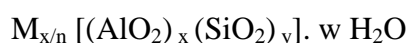


Figure 2.16 Simplified structure of tetrahedral network in zeolites [14].

The AlO_2^- tetrahedral in the structure determines the framework charge. This is balanced by cations that occupy nonframework positions. The structure formula of a zeolite is best expressed for the crystallographic unit cell as:



Where M is the cation of valence n, generally from the group I or II ions, although other metals, nonmetals, and organic cations are also possible, w is the number of water molecules. Water molecules presented are located in the channels and cavities, as the cations that neutralize the negative charge created by the presence of the AlO_2^- tetrahedral unit in the structure.

2.7.1. Zeolite structures

The structure of zeolite consists of a three-dimension framework of the tetrahedral primary building units when tetrahedral atoms are silicon and/or aluminum as shown in Figure 2.17.

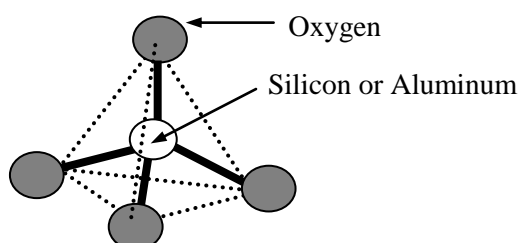


Figure 2.17 A primary building unit of zeolites [14].

A secondary building unit (SBU) consists of selected geometric groupings of those tetrahedral. There are sixteen such building units, which can be used to describe all of the known porous materials structures; for example, 4, 5, 6 and 8-member single rings, 4-4, 6-6, and 8-8-member double rings, and 4-1, 5-1 and 4-4-1 branched rings. The secondary building units are shown in Figure 2.18.

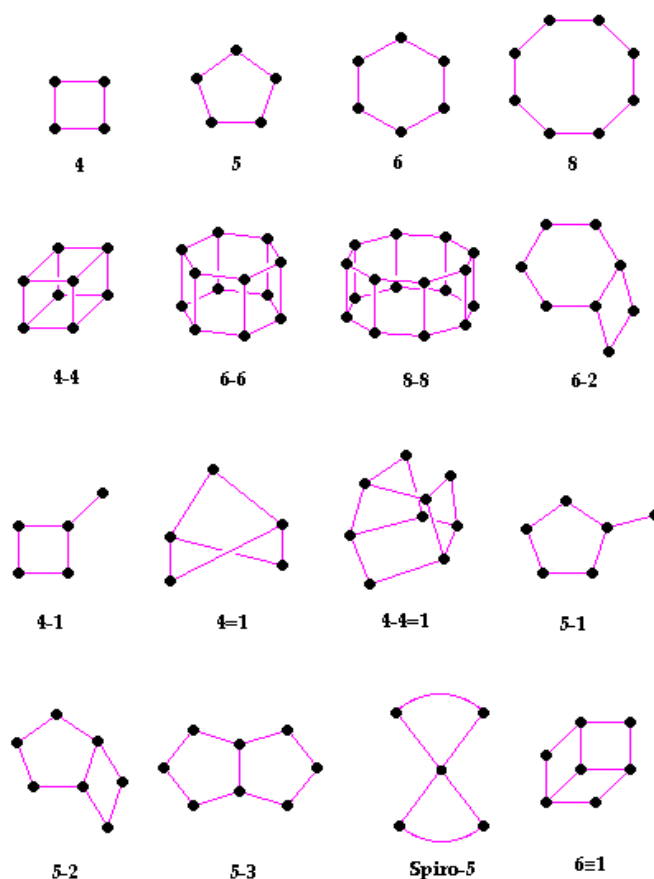


Figure 2.18 Secondary Building Units (SBU's) in zeolites [31].

Most zeolite frameworks can be generated from several different SBUs. For example, the sodalite framework can be built from either the single 6-member ring or the single 4-member ring. Some of them are shown in Figure 2.19.

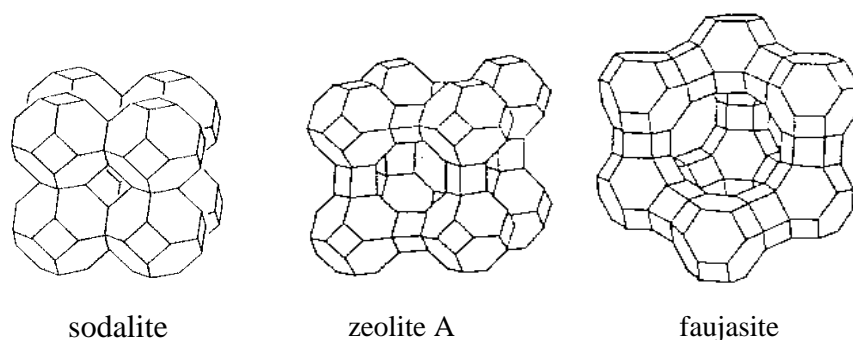


Figure 2.19 The structure of sodalite, zeolite A, and faujasite-type zeolites.

The different ring sizes found in zeolites, based on the different number of tetrahedral atoms defining the opening, are shown in Figure 2.20. The ring sizes are often mentioned as the number of oxygen atoms which are equal to the number of tetrahedral atoms.

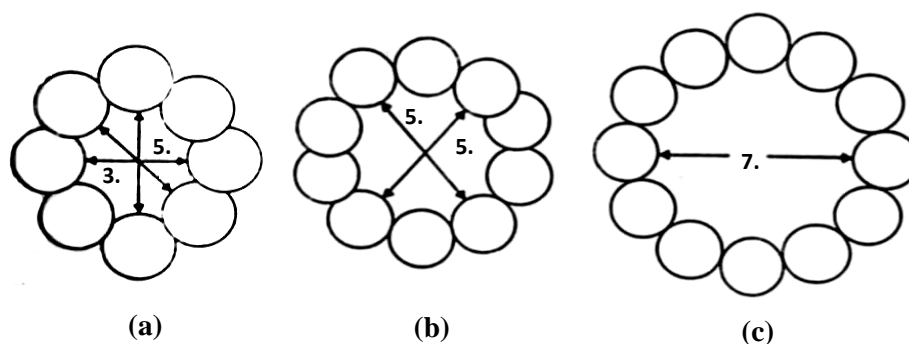


Figure 2.20 Examples of the three types of pore openings in the porous material molecular sieves (a) an 8 ring pore opening (small pore), (b) a 10 ring pore opening (medium pore), and (c) a 12 ring pore opening (large pore) [14].

2.7.2 Properties of zeolites

2.7.2.1 Acid sites of zeolites

Most industrial applications of zeolites are based upon technology adapted from the acid silica/alumina catalysts originally developed for the acid-catalyzed reaction. This means that the activity required is based upon the production of “Brønsted acid sites” arising from the creating ‘hydroxyls’ within the zeolites pore structure. These hydroxyls are formed by ammonium exchange followed by a calcination step. Zeolites, as normally synthesized, usually have Na^+ balancing the framework charges, but these can be readily exchanged for protons by direct reaction with an acid, giving hydroxyl groups, the Brønsted acid sites. Alternatively, if the zeolite is not stable in acid solution, it is common to use the ammonium (NH_4^+) salt, and then heat it so that ammonia is driven off, leaving a proton. Further heating removes water from Brønsted site, exposing a tricoordinated Al ion, which has electron-pair acceptor properties; this is identified as a “Lewis acid site”. A scheme for the formation of these sites is shown in Figure 2.21. The surfaces of zeolites can display either Brønsted or Lewis acid sites, or both, depending on how the zeolite is prepared. Brønsted sites are converted into Lewis sites as the temperature is increased above $500\text{ }^\circ\text{C}$, and water is driven off.

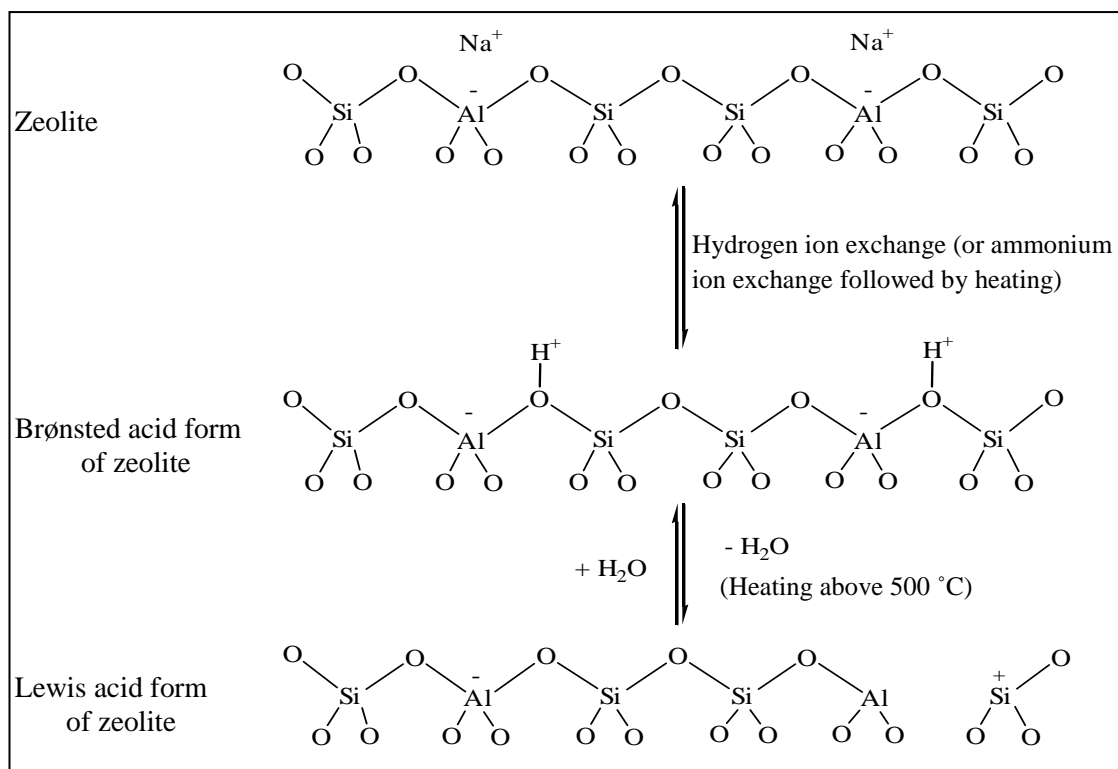


Figure 2.21 The generation of Brønsted and Lewis acid sites in zeolite [15].

2.7.2.2 Shape and size selectivity

Shape and size selectivity plays a very important role in catalysis. Highly crystalline and regular channel structures are among the principal features that zeolite used as catalysts offer over other materials. Shape selectivity is divided into 3 types: reactant shape selectivity, product shape selectivity and transition-state shape selectivity. These types of selectivities are shown in Figure 2.22. Reactant selectivity means that only starting materials of a certain size and shape can penetrate into the interior of the zeolite pores and undergo reaction at the catalytically active sites. Starting material molecules that are larger than the pore apertures cannot react. Product selectivity arises when, corresponding to the cavity size of a zeolite, only products of a certain size and shape that can exit from the pore system are formed. Restricted transition-state shape selectivity is a kinetic effect arising from the local environment around the active site: the rate constant for a certain reaction mechanism is reduced if the necessary transition state is too bulky to form readily.

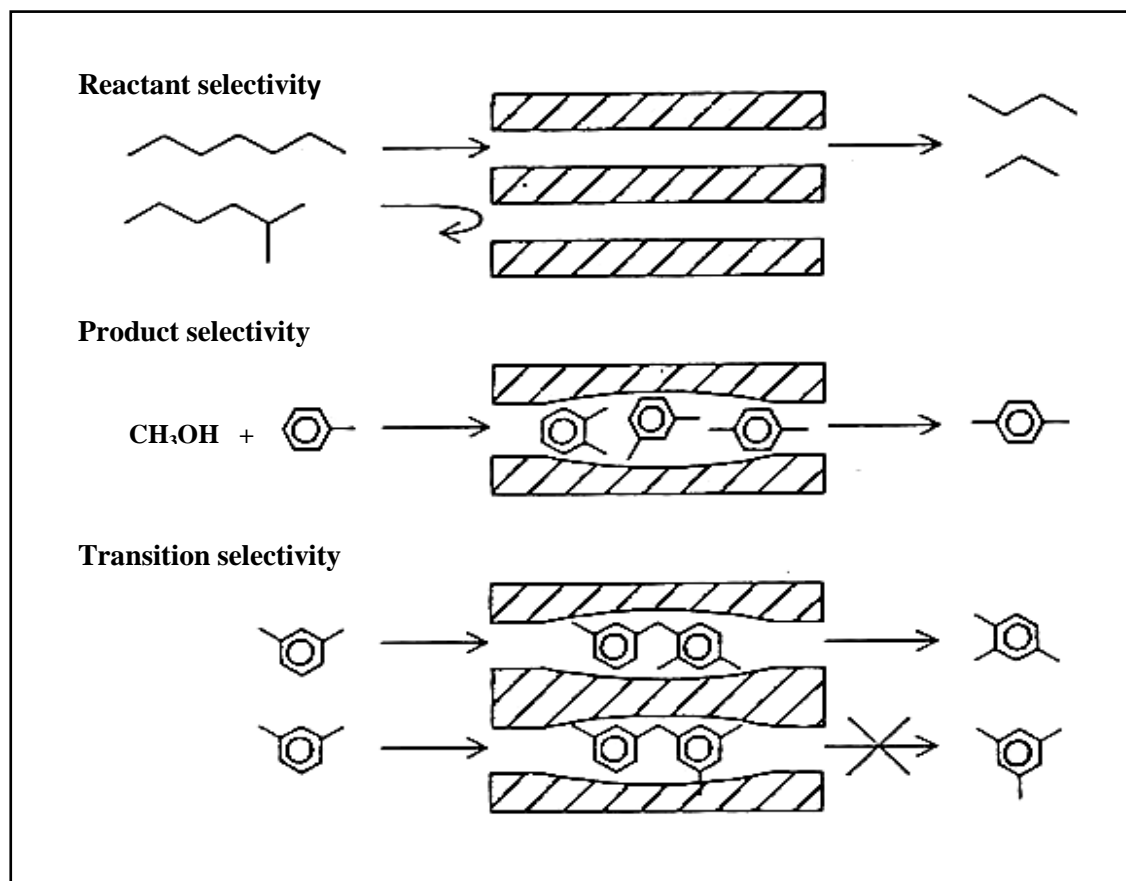


Figure 2.22 Three types of selectivity in zeolites: reactant, product, and transition-state shape selectivity [16].

Heterogeneous catalysis is important in fine-chemical and pharmaceutical manufacture and in petroleum refining. Many of the catalysts used by these industries are based on aluminosilicates, which combine high stability with excellent activity in acid mediated reactions. Within this class of material, zeolites microporous crystalline aluminosilicates with three-dimensional framework structures have attracted particular attention: they are significantly more active than the layered structures (clays) and mesoporous structures.

2.7.3 Factors influence zeolite formation

Three variables have a major influence on crystallization of zeolite structures [32-34]: the gross composition of the reaction mixture, temperature, and time. There are also history-dependent factors such as digestion or aging period, and order of mixing. A list of individual factors contributing to the synthesis of zeolite structure is provided below:

2.7.3.1 Reaction mixture components

Each component in the reactant mixture contributes to specific characteristic of the gel and to the final material obtained [34-35]. Table 2.6 provides a broad listing of individual components of the mixture and the primary influence within that reaction mixture.

Table 2.6 The effect of selected variables on the final crystalline products of zeolite crystallization

Reaction mixture composition (mole ratio)	Primary influence
SiO ₂ /Al ₂ O ₃	Framework composition
H ₂ O	Rate, crystallization mechanism
OH ⁻	Silicate molecular weight, OH ⁻ concentration
Inorganic cations	Structure, cation distribution
Organic additives	Structure, framework aluminum content

The SiO₂/Al₂O₃ ratio, the hydroxide content of the gel, and the presence of inorganic cations will also contribute to determine which structure will finally crystallize. The crystallization of a particular zeolite structure from the gel system containing these components strongly depends on the SiO₂/Al₂O₃ ratio of the starting gel mixture. The inorganic or organic cations not only influence the crystal structure, but they may also influence other features of the final crystalline products, such as morphology and crystal size. The hydroxide content enhances the formation of soluble silicate but too much hydroxide concentration catalyzes the formation of dense material such as quartz. The latter inhibits the zeolite formation.

2.7.3.2 Temperature

Temperature influences several factors in zeolite synthesis; it can alter the obtained zeolite phase as well as change the induction period before the start of crystallization [34-36]. This induction period decreased with increasing temperature. For

any mixture as the increasing temperature, the rate of crystallization increased. However, as the temperature change, conditions may favor formation of other phases.

2.7.3.3 Time

Time as a parameter can be optimized in the synthesis of many zeolites [34-37]. Many of interesting zeolites are metastable phase, and can recrystallize to other more stable structures which can be observed under certain conditions with prolonged reaction time. Crystallization parameters must be adjusted to minimize the time needed to obtain the desired crystalline phase.

2.8 MWW zeolite

MCM-22 is designed as MWW structure and has the same topology with PSH-3, SSZ-25, and ERB-1. MWW frameworks are shown in Figure 2.23. This type of zeolite has large pockets (inner diameter = 0.71 nm) on the external surface and two independent pore systems with 10-membered rings (10 MR): one is defined by the two-dimensional sinusoidal channels, and the other by the 12 MR supercages, with dimension of $0.71 \times 0.71 \times 18.1 \text{ nm}^3$. There is the former micropore, which is designed as an interlayer micropore, in the layer possessing the MWW framework, whereas the latter one is an intralayer micropore which exists between the layers.

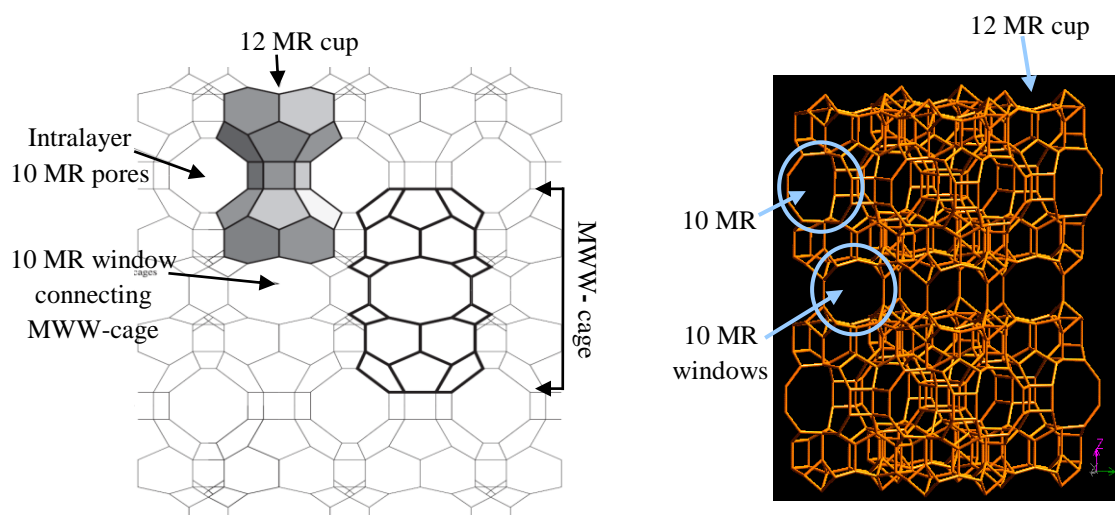


Figure 2.23 MWW frameworks [38].

2.8.1 Synthesis of MCM-22

The hydrothermal synthesis of MCM-22 has been studied in details using hexamethyleneimine as an organic template. MCM-22 having $\text{SiO}_2/\text{Al}_2\text{O}_3$ ratios around 30 could be obtained as a pure phase for a relatively broad range of OH/SiO_2 ratios, whereas crystallization from a parent mixture with low aluminum contents yielded a mixture of the MWW phase with the MFI or the FER phase. Mochida and co-workers [39] reported that the seeding in the hydrothermal synthesis of MCM-22 zeolite could avoid the formation of the undesired phase. These early reports as well as the original patent [40], indicate that stirring or rotating in hydrothermal crystallization is necessary to obtain a high quality MWW phase. Crystallization by using hexamethyleneimine under the static conditions yielded a pure phase of MCM-22 for narrow ranges of synthetic parameters, such as gel composition, crystallization period and temperature. The rotating crystallization yielded isolated hexagonal thin plates, which was around 1 μm in width, of MCM-22 crystals, whereas the static crystallization gave crystals composed by the aggregation of the hexagonal thin plates. Much attention has been paid on the unique crystalline structure due to possibilities in application to many catalytic reactions.

However, MCM-22 zeolites present some limitations when large reactant molecules are involved, especially in liquid-phase systems as is frequently the case in the synthesis of fine chemicals. Attempts to improve the diffusion of reactants to the catalytic sites have so far focused on increasing the zeolite pore sizes as well as decreasing zeolite crystal size. Recent work has described a new zeolitic material (ITQ-2) in which a layered zeolite precursor is delaminated in much the same way as the layered structure of a clay may be unbound, resulting in an aluminosilicate whose zeolite-type catalytic sites are contained within thin, readily accessible sheets. Then the delamination process can improve the accessibility of the catalytic sites to large molecules [41].

2.8.2 Synthesis of ITQ-2

ITQ-2 has been prepared by swelling and exfoliating the MCM-22 precursor (Figure 2.24). The process is so-called delamination. Typically, the swelling was carried out by mixing MCM-22 precursor with cetyltrimethylammonium bromide and tetrapropylammonium hydroxide aqueous solution. The mixture was refluxed at 80 °C for 16 h. The layers in the swollen MCM-22 precursor were stripped apart by placing the slurry in an ultrasound bath for 1 h.

ITQ-2 consists of monolayers of MWW structure (approximately 2.5 nm thick) with an extremely high external surface. These monolayers consist of a hexagonal array of cups that penetrate into the monolayers from both sides. These cups would have an aperture of approximately 0.7 nm, formed by a 12 MR. The cups meet at centre of the layer, forming a double 6 MR window that connects the cups, bottom to bottom. As a result, a smooth 10 MR channel system runs in between the cups, inside the sheet (Figure 2.25). ITQ-2 zeolite showed high catalytic activities in the reactions of large molecules inaccessible to the 10MR micropore system, if compared with MCM-22 zeolite. This is due to high external surface area of the delaminated structure, which gives a large amount of structurally accessible acid sites.

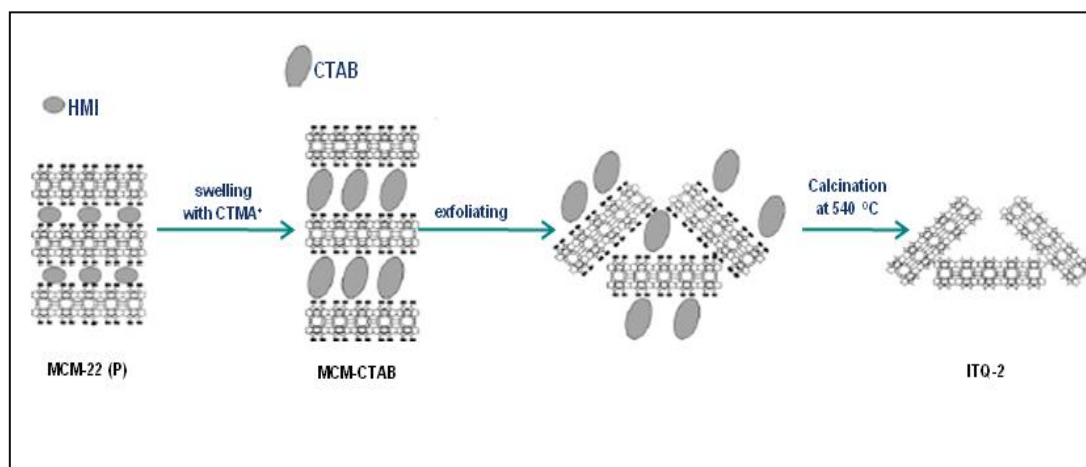


Figure 2.24 Scheme for the preparation of ITQ-2 obtained from MCM-22 precursor [18].

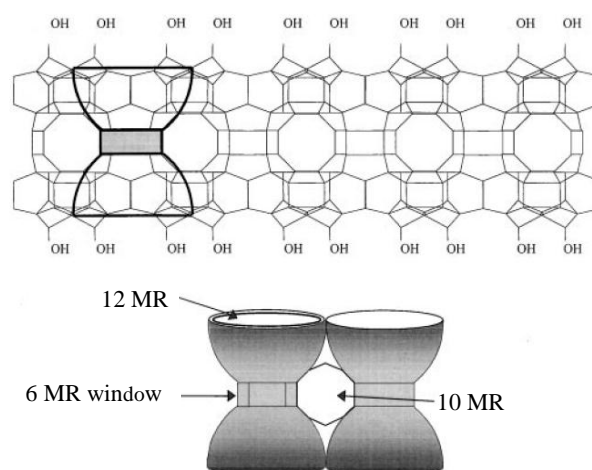


Figure 2.25 Proposed structure for ITQ-2 [53].

2.9 Quaternary ammonium salts

Quaternary ammonium salts are salts of quaternary ammonium cation with an anion. The structure of quaternary ammonium salts consists of polyatomic ions (NR_4^+) are positively charged and negatively charge of anion (X^-), R being an alkyl group or an aryl group. The common structure of quaternary ammonium salts is shown in Figure 2.26.

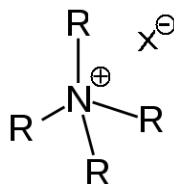


Figure 2.26 Structure of quaternary ammonium salts.

Quaternary ammonium salts are valuable compounds with wide applications such as:

- Antimicrobials

Quaternary ammonium salts are amphoteric surfactants that are widely used for the control of bacterial growth in clinical and industrial environments. Broad-spectrum antimicrobial activity and surfactant properties have made quaternary ammonium salts such as benzalkonium chloride the favored hygienic adjuncts in disinfectant cleansing formulations, and they have been increasingly deployed in domestic cleaning products over the last decade. The antimicrobial action of quaternary ammonium salts involves perturbation of cytoplasmic and outer membrane lipid bilayers through association of the positively charged quaternary nitrogen with the polar head groups of acidic phospholipids. The hydrophobic tail subsequently interacts with the hydrophobic membrane core. At concentrations normally used for application to inanimate surfaces, quaternary ammonium salts form mixed-micelle aggregates with hydrophobic membrane components that solubilize membrane and lyse the cells. Lethality occurs through generalized and progressive leakage of cytoplasmic materials.

- Osmolytes

Quaternary ammonium salts can act as osmolytes, which stabilize osmotic pressure in cells, specifically glycine betaine. They are soluble in the solution within a cell, or in the surrounding fluid. They play a role in maintaining cell volume and fluid balance. For example, when a cell swells due to external osmotic pressure, membrane channels open and allow efflux of osmolytes which carry water with them, restoring normal cell volume.

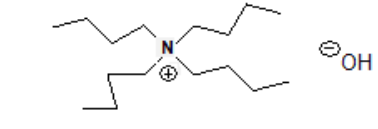
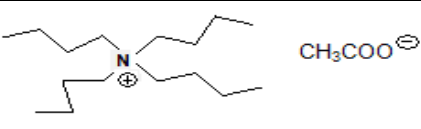
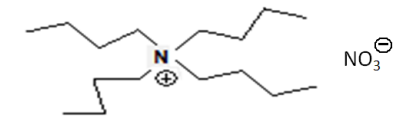
- Phase transfer catalysts

Quaternary ammonium salts can act as phase-transfer catalysts (PTCs) to accelerate the slow reaction that stems from poor interaction between the reactants. The reaction between two reactants present in two separate phases is often inhibited because of inability of the reagents to interact with each other. The rate of such reactions can be enhanced by using a catalyst known as a phase transfer catalyst. The phase-transfer catalysis is a well-known concept, in which, an organic-soluble reactant and an aqueous-soluble reactant are brought together by the use of a small quantity of catalyst which transports one reactant across the interface into the other phase to enhance the reaction rate, overcome mass transfer limitation. Quaternary ammonium salt has unique capability to dissolve in both organic and aqueous solution and hence widely used as a phase-transfer catalyst. Phase transfer catalytic processes are industrially important and environmentally friendly since they produce less industrial waste and consume less energy than traditional processes. Quaternary ammonium salts as phase transfer catalysts can be divided into two types [42-43]:

- 1) Anion activating quaternary ammonium salts

Quaternary ammonium salts having four large alkyl groups are considered to activate anions by increasing the distance separating cation from anion in the ion pair.


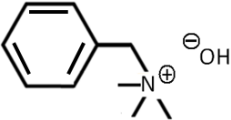
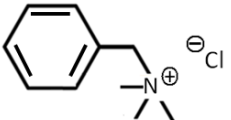
Table 2.7 Example of anion activating quaternary ammonium salts

Name	Structure
Tetrabutylammonium hydroxide (TBAOH)	
Tetrabutylammonium acetate (TBAAc)	
Tetrabutylammonium nitrate (TBANO₃)	

2. Accessible quaternary ammonium salts

Quaternary ammonium salts having one large group and three small groups are considered to be highly accessible because the openness of the structure allows relatively close association of the anion with the cation.

Table 2.8 Example of accessible quaternary ammonium salts

Name	Structure
Cetyltrimethylammonium bromide (CTAB)	
Benzyltrimethylammonium hydroxide (BTMAOH)	
Benzyltrimethylammonium chloride (BTMACl)	

2.10 Heteropoly acid [44-49]

Heteropoly acid (HPA) is a class of acid made up of a particular combination of hydrogen and oxygen with certain metals and non-metals. To qualify as a heteropoly acid, the compound must contain:

- a metal such as tungsten or molybdenum, termed the addenda atom
- oxygen
- an element generally from the *p*-block of the periodic table, such as silicon or phosphorus, termed the hetero atom
- acidic hydrogen atoms

The metal addenda atoms linked by oxygen atoms form a cluster with the hetero-atom inside bonded via oxygen atoms. Due to the possibilities of there being different combinations of addenda atoms and different types of hetero atoms, there are a lot of heteropoly acids.

Heteropoly acids have several advantages, such as low volatility, low corrosiveness, high thermal stabilities and strong Brønsted acidity, which make them extensively used as acid and oxidation catalysts for several chemical reactions. As shown in Table 2.9.

Table 2.9 Some acid and oxidation reactions catalyzed by heteropoly acids [44]

Heteropoly acids	Reactions
$\text{Cs}_{25}\text{H}_{0.5}\text{PW}_{12}\text{O}_{40}$	alkylation of isobutene by butene
$\text{Pd}_{15}\text{PW}_{12}\text{O}_{40}$	isomerisation of alkanes
$\text{H}_3\text{PW}_{12}\text{O}_{40}$	alkylation of aromatics
$\text{H}_3\text{PMo}_{12}\text{O}_{40}$	Isobutane to methacrylic acid
$\text{H}_3\text{PMo}_{10}\text{V}_2\text{O}_{40}$	Isobutyric acid to methacrylic acid

Among many heteropoly acids, phosphotungstic acid ($\text{H}_3\text{PW}_{12}\text{O}_{40}$ or HPW) have received the most attention due to simple preparation, most stable, and highest Brønsted acidity.

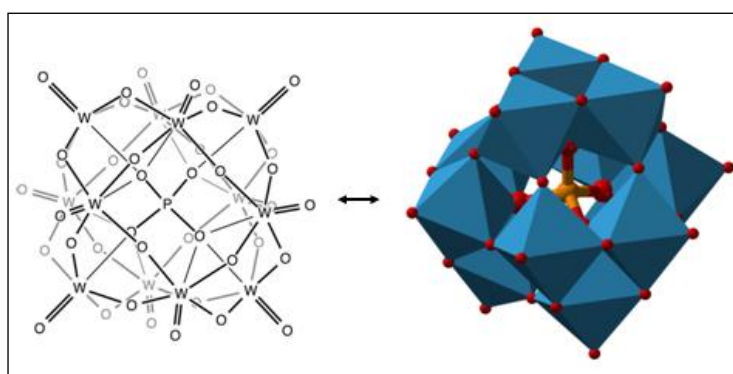


Figure 2.27 Structure of phosphotungstic acid [49].

2.11 Literature review

Frontera *et al.* [17] investigated the formation of ITQ-2 from different MCM-22(P) materials. The delamination process of ITQ-2 by MCM-22(P) is articulated in different treatment steps:

- swelling of a MCM-22(P) sample at 80 °C (swollen product)
- ultrasound treatment (sonicated product)
- calcination (ITQ-2)

The final solid ITQ-2 is formed by disordered individual sheets of crystalline layers. A relevant loss of ordered material is obtained after the swelling treatment. The preparation of ITQ-2 is favoured by decreasing aluminium content of the MCM-22(P). Moreover, the time of ultrasound treatment is a very important parameter to obtain a final product with good adsorption properties.

Xue *et al.* [50] studied the selective synthesis of *p*-xylene by vapor phase alkylation of toluene with dimethyl carbonate over MgO modified MCM-22. MgO modified MCM-22 was prepared by impregnation of MCM-22 with an aqueous solution of magnesium nitrate. The X-ray diffraction results show that the structure of MCM-22 is retained after MgO modification. BET surface area and micropore area decrease markedly with further increase in MgO content due to the high MgO content may cause partial blockage of the pore of MCM-22. Acidity characterization results showed that the number of Brønsted acid sites on MCM-22 decreased significantly after MgO modification, which resulted in a decrease in activity. Selectivity for *p*-xylene was improved greatly over MgO modified MCM-22, which can be attributed to effective suppression of xylene isomerization by the reduction in external surface Brønsted acid sites.

Aguilar *et al.* [18] investigated the alkylation of biphenyl with propylene in gas phase over two zeolites: MCM-22 and ITQ-2. The influence of zeolite structure on the activity and selectivity was discussed. The results indicate that the dimensions of 10 MR channels inhibited the diffusion of the bulky reactants inside the zeolitic pores and, explains also the high *o*-IPBP selectivity. The activity in alkylation followed the order: ITQ-2 > MCM-22. It was because the surface area of ITQ-2 is higher than that of MCM-22.

Calgaroto *et al.* [51] studied the immobilization of porcine pancreatic lipase in MCM-22 zeolite with different Si/Al ratios (15, 25 and 50). Results showed that the material composition influenced significantly the immobilization process. Higher yields of immobilization and enzymatic activities were achieved when MCM-22 with Si/Al ratio of 25 was used as support.

Corma *et al.* [19] studied the synthesis of layered zeolitic organic-inorganic materials by intercalation and stabilization of arylic silsesquioxane molecules between inorganic zeolitic MWW layers. The organic linkers are conformed by two condensed silyl-arylic groups from disilane molecules, such as 1,4-bis(triethoxysilyl)benzene, which

react with the external silanol groups of the zeolitic layers. The layered zeolitic organic-inorganic materials contain micropores within the inorganic layers and a well-defined mesoporous system in between the organic linkers. An amination post-treatment introduces basic groups in the organic linkers close to the acid sites present in the structural inorganic counterpart. Through this methodology it has been possible to prepare bifunctional acid-base catalysts where the acid sites are of zeolitic nature located in the inorganic building blocks and the basic sites are part of the organic structure. The resultant materials can act as bifunctional acid-base catalysts for performing a two-step cascade reaction that involves the catalytic conversion of benzaldehyde dimethylacetal into benzylidene malononitrile.

Ghesti *et al.* [52] investigated the synthesis of cerium (III) trisdodecylsulfate trihydrate as a Lewis acid-surfactant-combined catalyst for the production of alkyl esters by solvent-free transesterification and esterification reactions. The results showed that cerium trisdodecylsulfate is active for both the transesterification of vegetable oils and the esterification of FFAs with alcohols. By changing several reaction parameters, such as molar ratio, temperature, time, catalyst amount, and type of alcohol, conversion efficiencies greater than 95% were observed for the transesterification of soybean oil with ethanol and methanol. In addition, the esterification of oleic acid with ethanol demonstrated that the catalyst is able to produce the ethyl esters in the presence of water.

Zhang *et al.* [20] investigated the synthesis of biodiesel through transesterification of soybean oil with methanol over KOH and used quaternary ammonium salts (such as cetyltrimethylammonium bromide, tetrabutylammonium hydroxide, tetrabutylammonium acetate, tetrabutylammonium nitrate, benzyltrimethylammonium hydroxide and tetrabutylammonium hydrogen sulphate) as phase transfer catalysts. Experimental results showed that methyl ester content higher than 96.5 wt.% was achieved after only 15 min of transesterification, suitable phase transfer catalysts (tetrabutylammonium hydroxide and tetrabutylammonium acetate) can facilitate the interphase transfer of species between the polar methanol/glycerol phase and non-polar oil phase, overcome mass transfer limitation and speed up reaction rates between two immiscible phases.

Wibowo *et al.* [21] studied the preparation of montmorillonite intercalated with quaternary ammonium salts (cetyltrimethylammonium bromide and tetrabutylammonium bromide) as catalysts for the esterification of glycerol with lauric acid. The X-ray diffraction results showed that after intercalation with cetyltrimethylammonium bromide and tetrabutylammonium bromide, the interlayer spaces increased from 1.1 nm to 1.9 and

1.7 nm, respectively. The quaternary ammonium salts held between the layers increased hydrophobicity of the catalysts. It would promote the diffusion of organic reactants to the acid sites to a certain extent, leading to some improvement of the catalytic activity. At the same time, the hydrophilic ammonium group would accelerate the aqueous–organic phase reaction.

CHAPTER III

EXPERIMENTAL

3.1 Chemicals

3.1.1 Chemicals for synthesis of catalysts

1. Sodium hydroxide (NaOH) (AR grade, Merck)
2. Hexamethyleneimine (HMI) (AR grade, Fluka)
3. Fumed silica (SiO₂) (Aerosil 200, Degussa)
4. Sodium aluminate (NaAlO₂) (AR grade, Sigma Aldrich)
5. Ammonium nitrate (NH₄NO₃) (AR grade, Sigma Aldrich)
6. Cetyltrimethylammonium bromide (CTAB) (AR grade, Sigma Aldrich)
7. Tetrapropylammonium hydroxide (TPAOH) (AR grade, Sigma Aldrich)
8. Tetrabutylammonium hydroxide (TBAOH) (AR grade, Sigma Aldrich)
9. Tetrabutylammonium acetate (TBAAc) (AR grade, Sigma Aldrich)
10. Phosphotungstic acid (HPW) (AR grade, Fluka)
11. Methanol (CH₃OH) (AR grade, Qrec)

3.1.2 Chemicals for adsorption study

1. Lauric acid (C₁₂H₂₄O₂) (AR grade, Qrec)
2. Glycerol (C₃H₈O₃) (AR grade, Ajax Finechem)
3. 1,4-Dioxane (C₄H₈O₂) (99%, Qrec)

3.1.3 Chemicals for esterification reaction

1. Lauric acid ($C_{12}H_{24}O_2$) (AR grade, Qrec)
2. Glycerol ($C_3H_8O_3$) (AR grade, Ajax Finechem)
3. Nitrogen gas (99.99%, TIG)

3.1.4 Chemicals for analysis of reaction products

1. Monolaurin ($C_{15}H_{30}O_4$) (99%, Sigma Aldrich)
2. Dilaurin ($C_{27}H_{52}O_5$) (99%, Sigma Aldrich)
3. Trilaurin ($C_{39}H_{74}O_6$) (99%, Sigma Aldrich)
4. Methyl heptadecanoate ($C_{18}H_{36}O_2$) (99.5%, Fluka)
5. Pyridine (C_5H_5N) (AR grade, Qrec)
6. n-Heptane (C_7H_{16}) (99%, Merck)
7. *N*-Methyl-*N*-(trimethylsilyl)trifluoroacetamide (MSTFA) (99%, Sigma Aldrich)

3.2 Instruments and equipments

3.2.1 Instruments and equipments for synthesis of catalysts

1. Spatula
2. Desiccator
3. Analytical balance
4. Beaker, 50, 100, and 250 mL
5. Polyethylene beaker, 100, 250, and 500 mL
6. Volumetric flask, 100, 250, and 500 mL

7. Three-neck round bottom flask 1000 mL
8. Stopper
9. Hot plate stirrer
10. Magnetic bar
11. Peristaltic pump
12. Filter paper No. 42
13. Oven
14. Thermometer
15. pH meter
16. Paraffin bath
17. Suction flask and vacuum pump
18. Hydrothermal and Parr reactor
19. Teflon bottle
20. Centrifuge
21. Crucible
22. Muffle furnace

3.2.2 Instruments and equipments for esterification

1. Three-neck round bottom flask 50 mL
2. Dropping funnel
3. Condenser
4. Thermometer
5. Paraffin bath

6. Hot plate stirrer
7. Magnetic bar
8. Teflon tube

3.2.3 Instruments for analysis of reaction product

Reaction products from the esterification were quantitatively analyzed with an Agilent Technologies 7890A gas chromatograph (GC) equipped with a 15-m DB-5HT capillary column and a flame ionization detector (FID). The gas chromatograph conditions and column heating programs are summarized in Table 3.1 and Figure 3.1, respectively. The chromatograms of standard solution are shown in APPENDIX.

Table 3.1 Gas chromatograph conditions for determining glyceride products

Conditions	Value
Carrier gas (He) flow rate	3.0 mL/min
Make up gas (N ₂) pressure	40 mL/min
Hydrogen pressure (for FID)	30 mL/min
Air pressure (for FID)	400 mL/min
Detector temperature	340 °C
Split ratio	Off
Injection port temperature	340 °C
Inject volume	0.1 µL
Initial column temperature	50 °C
Final column temperature	340 °C

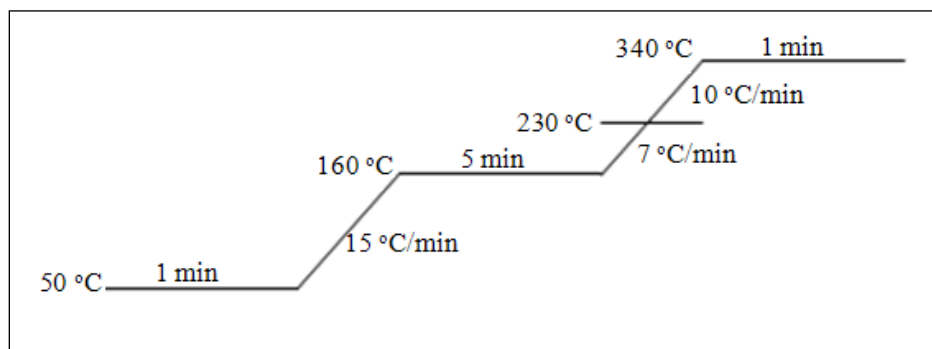


Figure 3.1 The gas chromatograph column heating program.

After course of the reaction, the catalyst was separated from the reaction mixture by filtration. The reaction mixture was immediately diluted with pyridine to stop the reaction. The glyceride products were quantified according to an internal standard method. Methyl heptadecanoate (C_{17}) was used as an internal standard. *N*-methyl-*N*-(trimethylsilyl)trifluoroacetamide (MSTFA) was used to convert the fatty acid remaining and the products containing hydroxyl groups to more volatile derivatives. The calculation of percent lauric acid conversion, percent yield and selectivity of glyceride products can be seen in APPENDIX.

3.3 Catalyst preparation

3.3.1 Synthesis of MCM-22

The MCM-22 precursor was prepared using HMI as the structure directing agent. Fumed silica and $NaAlO_2$ were used as silica and aluminium source, respectively. More specifically, a sample with $SiO_2/Al_2O_3 = 30$ was prepared in the following way: 21.00 g of fumed silica and 1.62 g of NaOH were dissolved in 167.70 g of deionized water under vigorous stirring for 90 min. Subsequently, 31.24 g of HMI was added dropwise and stirred for 90 min. Then, a solution of 2.65 g of $NaAlO_2$ in 83.85 g of water was added slowly into the mixture. After stirring for 90 min, the resulting gel (molar composition of 1 SiO_2 : 0.020 NaOH: 0.033 Al_2O_3 : 0.9 HMI: 40 H_2O) was transferred into a hydrothermal synthesis reactor under rotating conditions (rotating speed = 30 rpm, temperature = 150 °C and time = 7 days). The solid product was filtered and washed with deionized water until the filtrate pH was below 9.

Subsequently, the washed solid was dried at room temperature for 24 h at which precursor of MCM-22 was obtained. Then, the precursor was calcined in a muffle furnace at 540 °C for 8 h to remove the organic template and to yield MCM-22 zeolite. The procedure for MCM-22 preparation is showed in Figure 3.2.

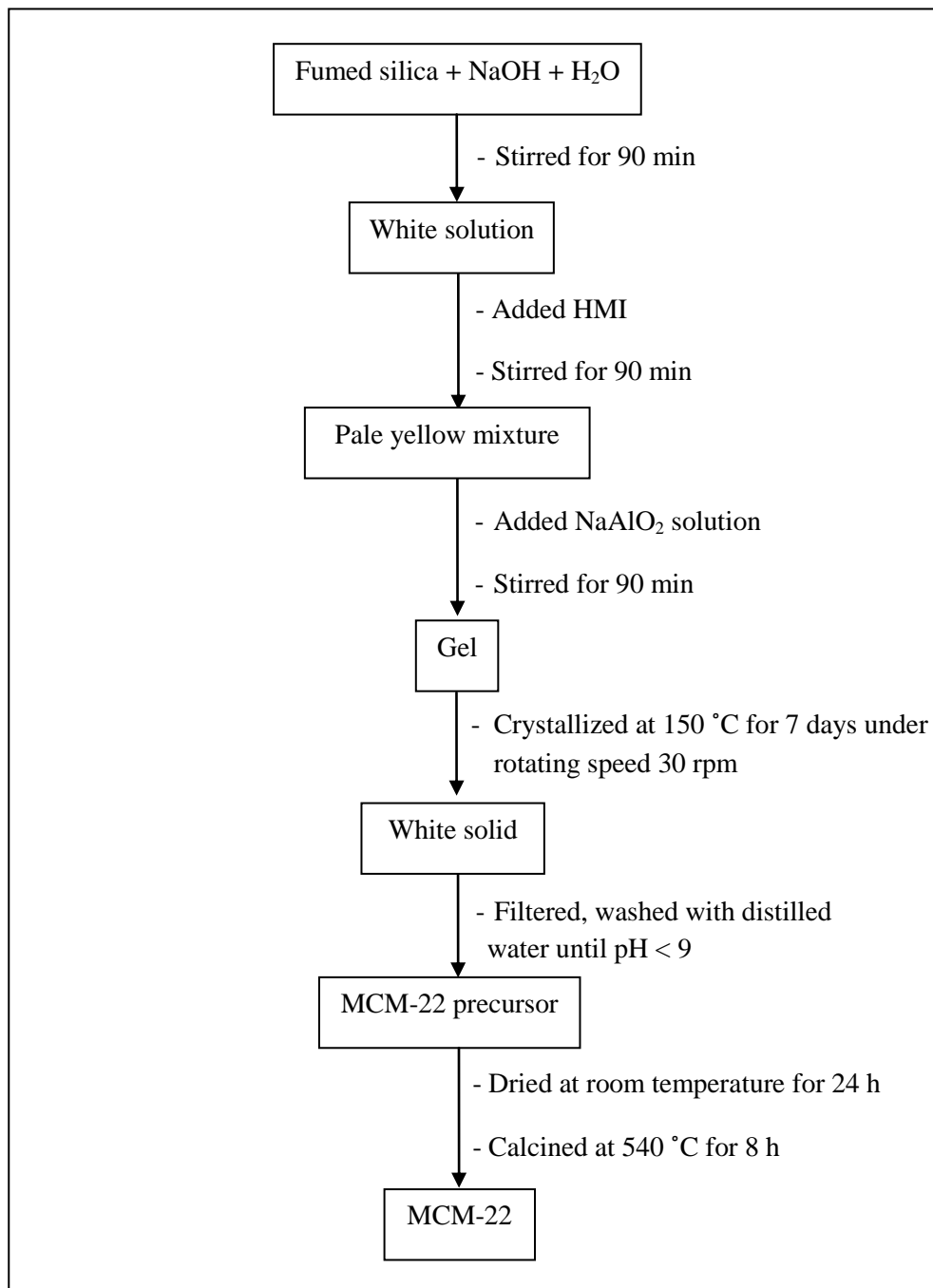


Figure 3.2 Preparation diagram for MCM-22.

3.3.2 Synthesis of ITQ-2

ITQ-2 was synthesized by swelling MCM-22 precursor with CTAB. Typically, 2.7 g of MCM-22 precursor was suspended in 48.0 g of deionized water containing 15.23 g of CTAB and 33.0 g of 20 wt.% tetrapropylammonium hydroxide aqueous solution. The mixture was refluxed at 80 °C for 16 h. The layers in the swollen MCM-22 precursor were stripped apart by placing the slurry in an ultrasound bath for 1 h. During the ultrasound treatment, care was taken to ensure that the temperature did not exceed 50 °C in order to prevent the occurring of MCM-41 phase. Subsequent addition of a few drops of concentrated hydrochloric acid, until the pH below 2, allowed harvesting of the solid by centrifuging. After being dried at 80 °C for 12 h, the organic material was removed by calcination at 580 °C for 12 h, yielding ITQ-2. The procedure for ITQ-2 preparation was illustrated in Figure 3.3.

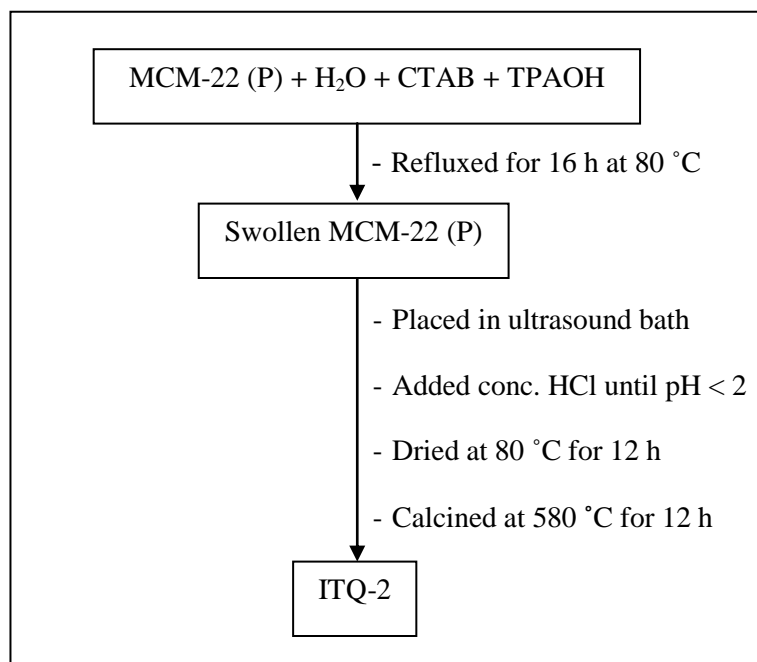


Figure 3.3 Preparation diagram for ITQ-2.

3.3.3 Ion exchange of MCM-22 and ITQ-2

MCM-22 and ITQ-2 were converted into H-form by following procedure: 1.0 g of MCM-22 or ITQ-2 was suspended in 100 mL of 1 M NH_4NO_3 . The mixture was stirred at 80 °C for 3 h and then filtered. This cycle was repeated two times in order to achieve maximum exchange into H-form. Then, it was calcined at 540 °C for 8 h using a muffle furnace. The resultant solids were designated as H-MCM-22 or H-ITQ-2, respectively.

3.3.4 Synthesis of MCM-22 intercalated with quaternary ammonium salts

Typically, 2.7 g of MCM-22 precursor was suspended in 58.1 g of deionized water containing 6.5 g of quaternary ammonium salts. The weight ratio of the mixture was 1 MCM-22 precursor: 2.4 quaternary ammonium salts: 21.5 H_2O . The mixture was then refluxed at 80 °C for 16 h. The solid product was collected by centrifuge, washed with deionized water, and dried at room temperature for 24 h. The catalysts prepared were denoted as MCM- x where x is type of quaternary ammonium salts such as CTAB, TPAOH, TBAOH, TBAAc.

3.3.5 Synthesis of MCM-22 intercalated with quaternary ammonium salts/CTAB

Typically, 2.7 g of MCM-22 precursor was suspended in 58.1 g of deionized water containing 15.2 g of CTAB and 6.5 g of quaternary ammonium salts. The weight ratio of the mixture was 1 MCM-22 precursor: 5.64 CTAB: 2.4 quaternary ammonium salts: 21.5 H_2O . The mixture was then refluxed at 80 °C for 16 h. The solid product was collected by centrifuge, washed with deionized water, and dried at room temperature for 24 h. The catalysts prepared were denoted as MCM- x /CTAB where x is type of quaternary ammonium salts such as TPAOH, TBAOH, TBAAc.

3.3.6 Synthesis of MCM-22 and ITQ-2 zeolite supported phosphotungstic acid

A series of catalysts having 10 wt.%, 20 wt.%, 40 wt.%, and 60 wt.% loading of phosphotungstic acid on MCM-22 and ITQ-2 were synthesized. Phosphotungstic acid was supported on MCM-22 and ITQ-2 by an incipient-wetness impregnation method. Typically, 1 g of MCM-22 or ITQ-2 was suspended in 20 mL of methanol solution to which a certain amount of phosphotungstic acid was added. After stirring the suspension at room temperature for 24 h, the solvent was evaporated. The catalyst was dried at 100 °C for 12 h and then kept in a desiccator. The prepared catalysts were denoted as (x)HPW/MCM-22 or (x)HPW/ITQ-2 where x is the weight percent of phosphotungstic acid loaded.

3.4 Study of adsorption study

Study on adsorption of glycerol and lauric acid on the catalyst prepared was performed in the following way: 0.05 g of catalysts was suspended in 25 mL of a solution of glycerol or lauric acid in 1,4-dioxane. The solution with different concentrations (0.05 M, 0.10 M, 0.25 M, and 0.40 M) was prepared. After stirring at room temperature for 24 h, the catalyst was removed by filtration and the amount of glycerol or lauric acid remaining was determined by a GC analysis. The adsorption capacity and equilibrium concentration were calculated based on following equation:

$$\text{Adsorption capacity (mol/g)} = \frac{\left(\frac{\text{mass of reactants initial (g)} - \text{mass of reactants remaining (g)}}{\text{molecular weight of reactants (g/mol)}} \right)}{\text{mass of catalyst (g)}} \quad (1)$$

$$\text{Equilibrium concentration (mol/L)} = \frac{\left(\frac{\text{mass of reactants remaining (g)}}{\text{molecular weight of reactants (g/mol)}} \right)}{\text{volume of solution (L)}} \quad (2)$$

3.5 Esterification of glycerol with lauric acid

Esterification of glycerol with lauric acid was carried out in a 50-mL three-neck round bottom flask equipped with N₂ line (flow rate of 50 mL/min). A water-cooled condenser was connected to the gas outlet in order to remove the water generated as by-product. The reaction temperature was controlled by a paraffin bath. In a typical reaction, glycerol and lauric acid at a certain glycerol/lauric acid molar ratio were added into the flask. The total weight of the reactants was maintained at 20.0 g. After stirring for 15 min, a catalyst was added into the reaction mixture under stirring. Several reaction parameters were adjusted to optimize the reaction conditions. After course of the reaction, the catalyst was separated from the reaction mixture by filtration. The reaction mixture was immediately diluted with pyridine for a GC analysis.

3.5.1 Study on the effect of type of catalysts

Esterification of glycerol with lauric acid was carried out under suitable conditions using MCM-22 and their derivatives as the catalysts.

3.5.2 Study on the effect of molar ratio of glycerol to lauric acid

The molar ratio of glycerol to lauric acid was varied in the range of 1-3.

3.5.3 Study on the effect of reaction temperature

The effect of reaction temperature was varied in the range of 100-130 °C.

3.5.4 Study on the effect of catalysts amount

The amount of catalyst was changed to 0 wt.%, 2 wt.%, 4 wt.%, and 6 wt.% based on weight of lauric acid.

3.5.5 Study on the effect of CTAB amount

The various amounts of CTAB, 0 wt.%, 2 wt.%, 6 wt.%, and 15 wt.% based on weight of lauric acid, were applied to the reaction.

3.5.6 Study on the effect of reaction time

The reaction time was varied in the range of 0.5-8 h.

3.6 Reaction product analysis

Liquid mixture attained after the esterification was derivatized by following procedure: 0.10 g of the reaction mixture was added into a vial. Then, 100 μL of MSTFA was used to convert the lauric acid and glycerol remaining and the products in the form of monoglycerides and diglycerides to more volatile derivatives. After a subsequent shake for 1 min and leaving at room temperature for 25 min, 100 μL of 30 mg/mL of methyl heptadecanoate as internal standard was added. The volume of solution was adjusted with n-heptane. The derivertization procedure was illustrated in Figure 3.4.

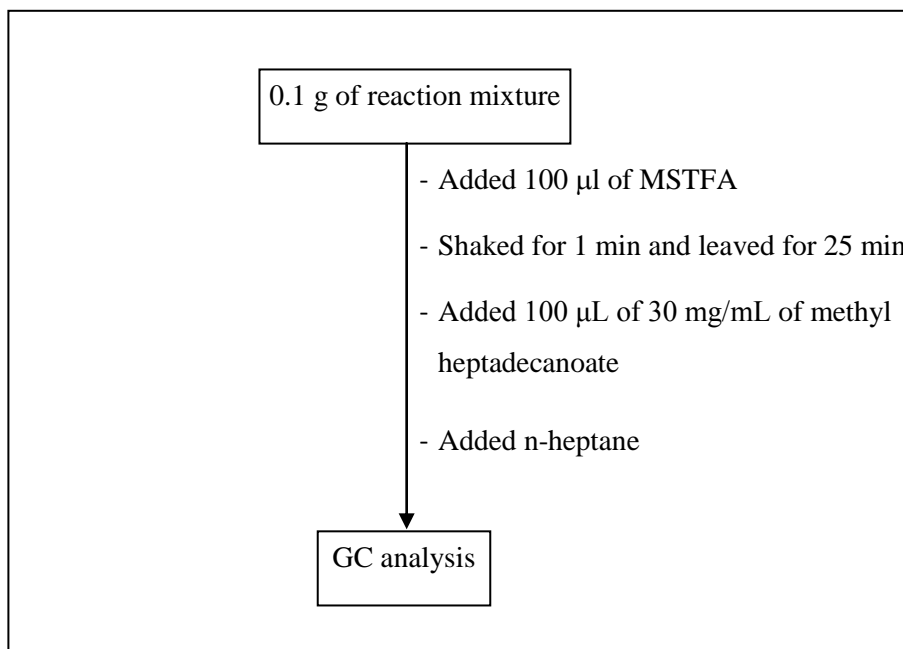


Figure 3.4 Diagram for derivertization of reaction product.

The glycerides content was determined by an Agilent Technologies 7890A gas chromatograph equipped with a 15-m DB-5HT capillary column and a flame ionization detector (FID). The gas chromatograph conditions and column heating programs are shown in Table 3.1 and Figure 3.1, respectively. The amount of lauric acid remaining and the glycerides composition was calculated based on the internal standardization method by using methyl heptadecanoate as an internal standard.

3.7 Characterization of catalysts

3.7.1 X-ray powder diffraction (XRD)

X-ray powder diffraction (XRD) is an instrumental technique used for identification of minerals, as well as other crystalline materials. XRD is a technique in which a collimated beams of nearly monochromatic X-rays is directed onto the flat surface of a relatively thin layer of finely ground material. XRD can provide additional information beyond basic identification. If the sample is a mixture, XRD data can be analyzed to determine the proportion of the different minerals present. Other information obtained can include the degree of crystallinity of the minerals present, possible deviations of the minerals from their ideal compositions, the structural state of the minerals and the degree of hydration for minerals that contain water in their structure. For samples available as larger crystals or in a crystal morphology that favors a preferred orientation, it has to be assured that all individual crystallites are randomly oriented when analyzed, that can be achieved by, e.g., carefully sample grinding. Figure 3.5 shows a monochromatic beam of X-ray incident on the surface of crystal at an angle θ . The scattered intensity can be measured as a function of scattering angle 2θ . The resulting XRD pattern efficiently determines the different phases present in the sample.

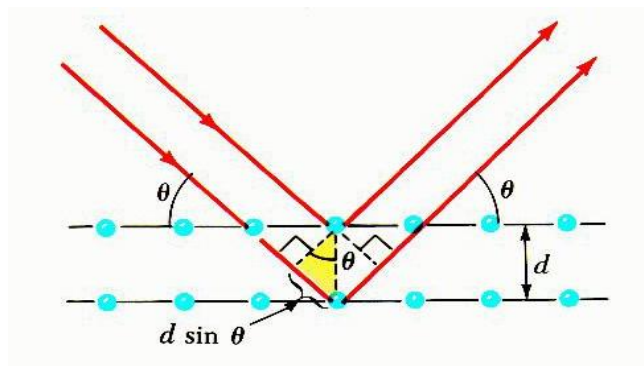


Figure 3.5 Diffraction of X-ray by regular planes of atoms.

Using this method, Bragg's law is able to determine the interplanar spacing of the samples, from diffraction peak according to Bragg angle.

$$n\lambda = 2 d \sin\theta$$

Where the integer n is the order of the diffracted beam, λ is the wavelength; d is the distance between adjacent planes of atoms (the d -spacings) and θ is the angle of between the incident beam and these planes.

The XRD patterns of synthesized catalysts were identified using a Rigaku D/MAX-2200 Ultima⁺ X-ray diffractometer equipped with Cu target X-ray tube (40 kV, 30mA) at 2-theta angle between 1.0 to 40.0 degree with a scan speed of 5.0 degree/min and sampling width of 0.02 degree. The scattering slit, divergent slit and receiving slit were fixed at 0.5 degree, 0.5 degree, and 0.3 mm, respectively. The measured diffractograms were analyzed using MDI software.

3.7.2 Thermogravimetric analysis (TGA)

Thermogravimetric analysis or TGA is a type of testing that is performed on samples to determine changes in weight in relation to change in temperature. Such analysis relies on a high degree of precision in three measurements: weight, temperature, and temperature change. As many weight loss curves look similar, the weight loss curve may require transformation before results may be interpreted. A

derivative weight loss curve can be used to tell the point at which weight loss is most apparent. Again, interpretation is limited without further modifications and deconvolution of the overlapping peaks may be required.

TGA is commonly employed in research and testing to determine characteristics of materials such as polymers, to determine degradation temperatures, absorbed moisture content of materials, the level of inorganic and organic components in materials, decomposition points of explosives, and solvent residues. It is also often used to estimate the corrosion kinetics in high temperature oxidation.

Thermal stability and weight loss of the catalysts were analyzed using a Perkin-Elmer Pyris Diamond thermogravimetric/differential thermal analyzer. Approximately 10 mg of catalyst was used and the temperature was ramped from room temperature to 1,000 °C under nitrogen at a heating rate of 8 °C/min. Degradation temperatures of the samples was calculated from TGA plot.



Figure 3.6 Perkin-Elmer Pyris Diamond thermogravimetric/Differential thermal analyzer.

3.7.3 Nitrogen adsorption-desorption technique

The N₂ adsorption-desorption technique is used to classify the porous materials and its physical properties such as surface area, pore volume, pore diameter and pore-size distribution of solid catalysts. Adsorption of gas by a porous material is described by an adsorption isotherm, the amount of adsorbed gas by the material at a fixed

temperature as a function of pressure. Porous materials are frequently characterized in terms of pore sizes derived from gas sorption data [54-55]. The IUPAC classification of adsorption isotherms is illustrated in Figure 3.7.

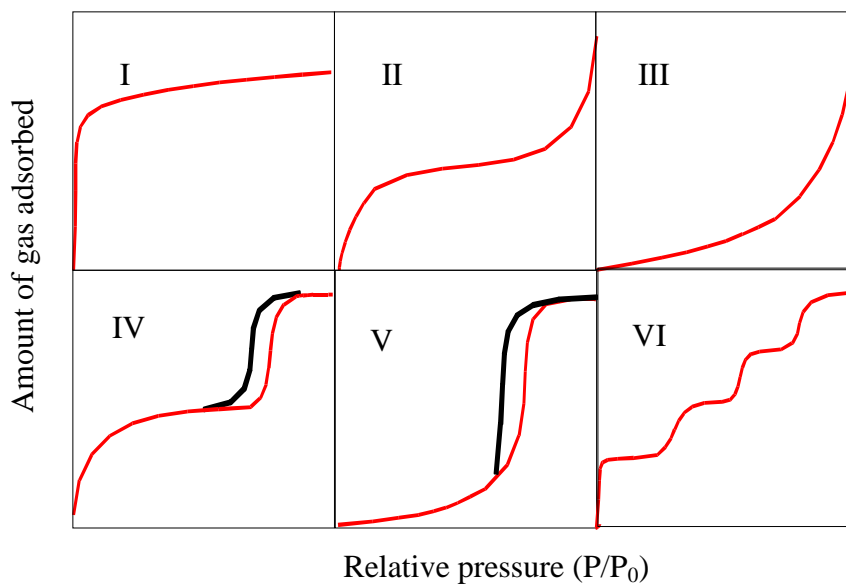


Figure 3.7 The IUPAC classification of adsorption isotherm [54].

As shown in Table 3.2, adsorption isotherms base on the strength of the interaction between the sample surface and adsorptive. Pore size distribution is measured by the use of nitrogen adsorption/desorption isotherm at liquid nitrogen temperature and relative pressures (P/P_0) ranging from 0.05-0.1. The large uptake of nitrogen at low P/P_0 indicates filling of the micropores ($<20 \text{ \AA}$) in the adsorbent. The linear portion of the curve represents multilayer adsorption of nitrogen on the surface of the sample, and the concave upward portion of the curve represents filling of mesoporous and macropores. The multipoint Brunauer, Emmett and Teller (BET) method is commonly used to measure total surface area.

$$\frac{1}{W[(P_0/P)-1]} = \frac{1}{W_m C} + \frac{C-1}{W_m C} (P/P_0) \quad (3)$$

Where W is the weight of nitrogen adsorbed at a given P/P_0 , W_m is the weight of gas to give monolayer coverage, and C is a constant that is related to the heat of adsorption. A slope and intercept are used to determine the quantity of nitrogen

adsorbed in the monolayer and calculate the surface area. For a single point method, the intercept is taken as zero or a small positive value, and the slope from the BET plot is used to calculate the surface area. The surface area depends upon the method used, as well as the partial pressures at which the data are collected.

Table 3.2 Features of adsorption isotherms

Type	Interaction between sample surface and gas adsorbate	Porosity	Example of sample-adsorbate
I	relatively strong	Micropores	activated carbon-N ₂
II	relatively strong	Nonporous	oxide-N ₂
III	weak	Nonporous	carbon-water vapor
IV	relatively strong	Mesopore	silica-N ₂
V	weak	Micropores	
		Mesopore	activated carbon-water vapor
VI	relatively strong sample surface has an even distribution of energy	Nonporous	graphite-Kr

N₂ adsorption-desorption isotherms and BET specific surface area of the catalysts were carried out using a BEL Japan, BELSORP-mini instrument. The materials weights were nearly 40 mg and weighted exactly after pretreatment at 150 °C for 3 h before each measurement.

3.7.4 Scanning electron microscope (SEM)

Scanning electron microscope (SEM) has unique capabilities for analyzing surfaces and morphology of materials. It is analogous to the reflected light microscope, although different radiation sources serve to produce the required illumination. Whereas the reflected light microscope forms an image from light reflected from a sample surface, the SEM uses electrons for image formation. The different wavelength of these radiation sources result in different resolution levels:

electron have much shorter wavelength than light photons, and shorter wavelength are capable of generating the higher resolution information. Enhanced resolution in turn permits higher magnification without loss of detail. The maximum magnification of the light microscope is about 2,000 times; beyond this level is “empty magnification”, or the point where increased magnification does not provide additional information. This upper magnification limit is a function of the wavelength of visible light, 2,000 Å, which equal the theoretical maximum resolution of conventional light microscope. In comparison, the wavelength of electron is less than 0.5 Å, and theoretically the maximum magnification of electron beam instrument is beyond 800,000 times. Because of instrumental parameters, practical magnification and resolution limits are about 75,000 times and 40 Å in a conventional SEM. The SEM consists basically of four systems:

1. The *illuminating/imaging system* produces the electron beam and directs it onto the sample.
2. The *information system* includes the data released by the sample during electron bombardment and detectors which discriminate among analyze these information signals.
3. The *display system* consists of one or two cathode-ray tubes for observing and photographing the surface of interest.
4. The *vacuum system* removes gases from the microscope column which increase the mean free path of electron, hence the better image quality.

The morphology and particle sizes of the catalysts were observed using a JEOL JSM-6480 LV scanning electron microscope. All samples were coated with spluttering gold under vacuum.

3.7.5 Acid-base titration

The amount of acid sites on a catalyst was quantified using 2.0 M sodium chloride solution as an ion-exchange agent. Approximately 0.05xx g of a catalyst was exchanged with 15 mL of 2.0 M sodium chloride solution for 30 min under constant agitation at room temperature. The mixture was titrated with 0.01 M sodium hydroxide solution by using phenolphthalein as an indicator.

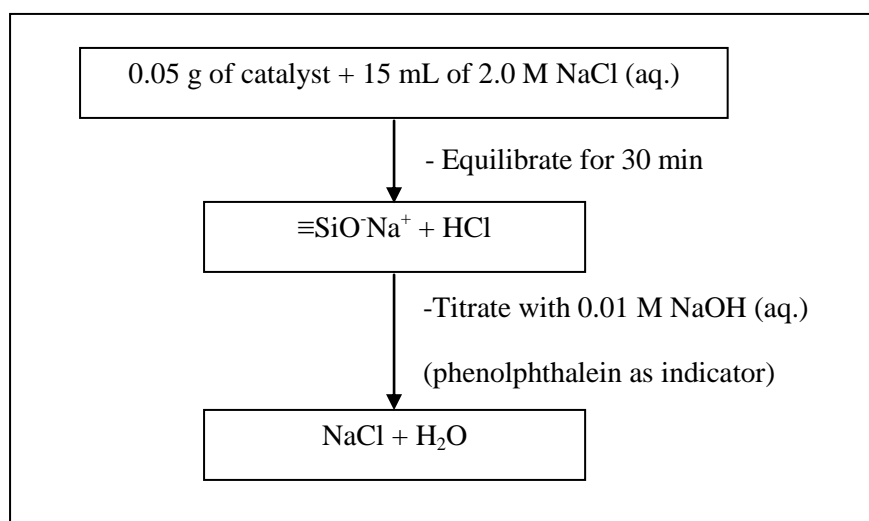


Figure 3.8 Diagram for acid-base titration.

3.7.6 Back titration

The amount of acid sites on a catalyst was quantitatively measured by back titration method. Approximately 0.05xx g of a catalyst was stirred with 100 mL of 0.04 M sodium hydroxide solution for 30 min at room temperature, and then catalyst was separated by a filtration. After that, titration with 0.2 M hydrochloric acid solution was performed by using phenolphthalein as an indicator.

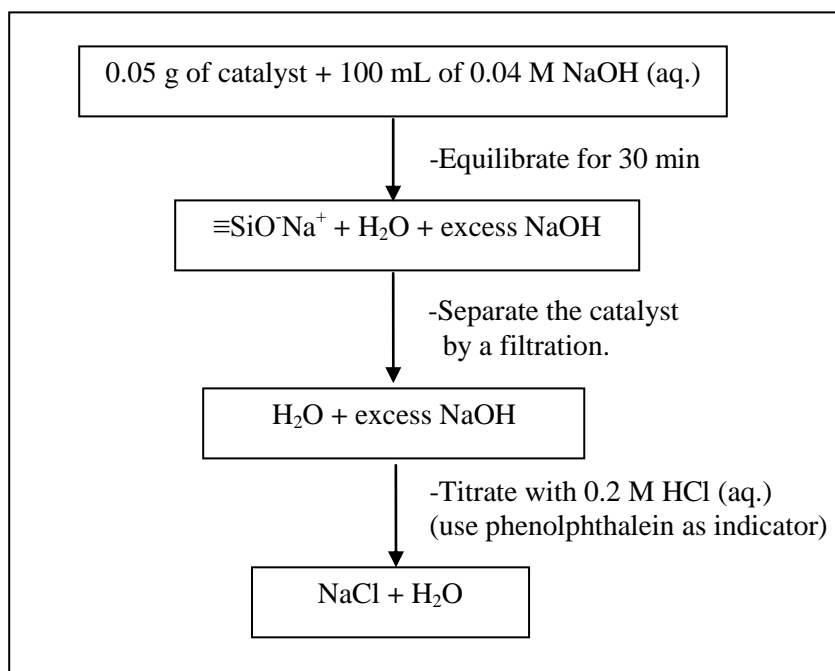


Figure 3.9 Diagram for back titration.

3.7.7 Acid strength (Hammett indicators)

Acid strength of the acid catalysts was measured by Hammett indicators. Approximately 0.1 g of a catalyst was dried at 120 °C for 16 h. The catalyst was added to a test tube, followed by adding 3 mL of 0.1 wt.% solution of indicator in benzene and observing a change of indicator color. The properties of Hammett indicators used in the present study are listed in Table 3.3.

Table 3.3 Properties of Hammett indicators used for measurement of acid strength

Hammett indicators	M.W.	Basic color	Acid color	pK _a
Methyl red	269.30	yellow	Red	4.2
Neutral red	288.78	yellow	Red	6.8
Bromothymol blue	624.39	blue	Red	7.2
Phenolphthalein	318.32	pink	Colorless	9.8



Figure 3.10 Hammett indicators used for measurement of acid strength.

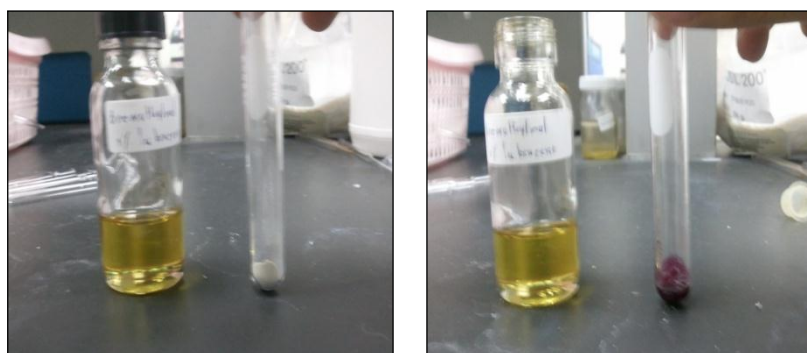


Figure 3.11 Example of the color change of Bromothymol blue.

CHAPTER IV

RESULTS AND DISCUSSION

4.1 Characterization of catalysts

4.1.1 X-ray powder diffraction (XRD)

The XRD patterns of MCM-22(P), MCM-22, H-MCM-22, ITQ-2, and H-ITQ-2 zeolites are shown in Figure 4.1.

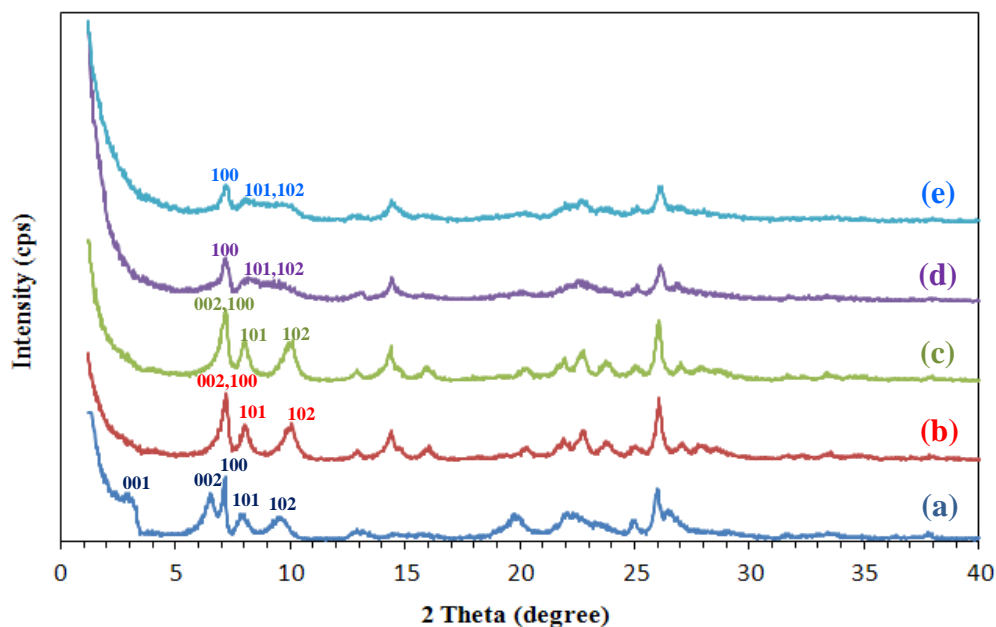


Figure 4.1 XRD patterns of (a) MCM-22(P), (b) MCM-22, (c) H-MCM-22, (d) ITQ-2, and (e) H-ITQ-2.

The XRD pattern of the MCM-22(P) in Figure 4.1(a) exhibited five peaks locating at $2\theta = 3.0^\circ$, 6.5° , 7.1° , 7.9° , and 9.6° , which were indexed as (001), (002), (100), (101), and (102) diffraction planes, respectively. The pattern corresponded to the layer structure of MCM-22(P). The broad characteristics of (001) peak at $2\theta = 3.0^\circ$ can be assigned to the presence of organic template (HMI) in the structure of MCM-22(P). The diffraction peak belonging to (002) plane ($2\theta = 6.5^\circ$) indicated the interlayer space in the structure of MCM-22(P). The structure integrity of each MWW

layer was reflected by the peak at $2\theta = 7.1^\circ$, relating to (100) plane. Additionally, the presence of the peaks of (101) and (102) plane indicated the ordering of the MWW layers stacking in the vertical direction.

In the case of MCM-22, the broad band at $2\theta = 3.0^\circ$ disappeared due to the removal of the organic template by the calcination (Figure 4.1(b)). The peaks relating to (101) and (102) planes were still discrete, confirming that the ordering of the MWW layer stack was preserved after the calcination. The (100) plane of the intralayer ($2\theta = 7.1^\circ$) are still observed, indicating that the structure integrity of each MWW layer was retained. The calcination resulted in the contraction of interlayer spacing as reflected by a shift of the interlayer (002) plane to higher 2θ at which the peak was merged with the peak of intralayer (100) plane. The structural change upon the calcination of MCM-22(P) can be explained by the schematic drawing in Figure 4.2.

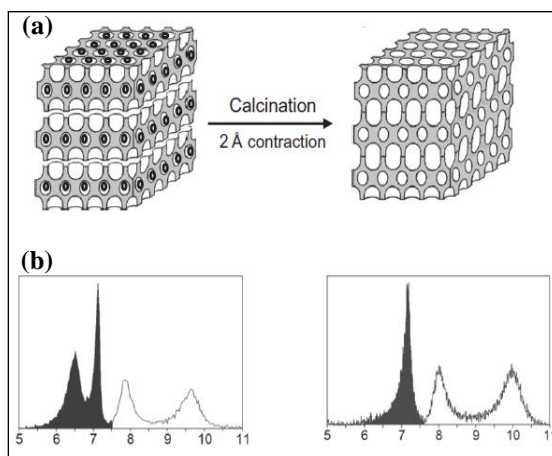


Figure 4.2 Formation of MCM-22 by condensation of MCM-22(P) upon calcination: (a) the contraction of interlayer spacing of about 2 Å, (b) the accompanying change in the low angle XRD pattern [50].

Figure 4.1(c) shows the XRD pattern of H-MCM-22. In comparison with that of MCM-22 (Figure 4.1(b)), the XRD pattern of H-MCM-22 was not changed, implying that the structure of MCM-22 was retained without any deformation of the MWW structure after the NH_4NO_3 treatment.

The XRD pattern of ITQ-2 is shown in Figure 4.1(d). ITQ-2 did not show the interlayer peak at $2\theta = 6.5^\circ$ due to the separation of MWW layers from each other by

the delamination process. The structure integrity of each MWW layer was preserved during the delamination as deduced from the (100) peak of the intralayer. It can be seen that, the interlayer (101) and (102) planes become broad, which showed a loss of registry along the vertical direction. These results indicated that the layers in MCM-22(P) can be separated by the delamination process, yielding ITQ-2.

Figure 4.1(e) reveals the XRD pattern of H-ITQ-2. Comparing to that of ITQ-2 (Figure 4.1(d)), the XRD pattern of H-ITQ-2 was not significantly altered, indicating that the structure of ITQ-2 was retained after the ion exchange with the NH_4NO_3 solution.

The XRD patterns of MCM-22 intercalated with various quaternary ammonium salts are presented in Figure 4.3(b-e). It can be seen that the XRD pattern of the resulting MCM-22 was not changed after the intercalation process when compared to that of MCM-22(P) (Figure 4.3(a)). Moreover, the peak of (002) plane still appeared, indicating the retention of interlayer spacing in the structure of MCM-22. These results suggested that quaternary ammonium salts cannot be successfully intercalated into the interlayer spacing of MCM-22.

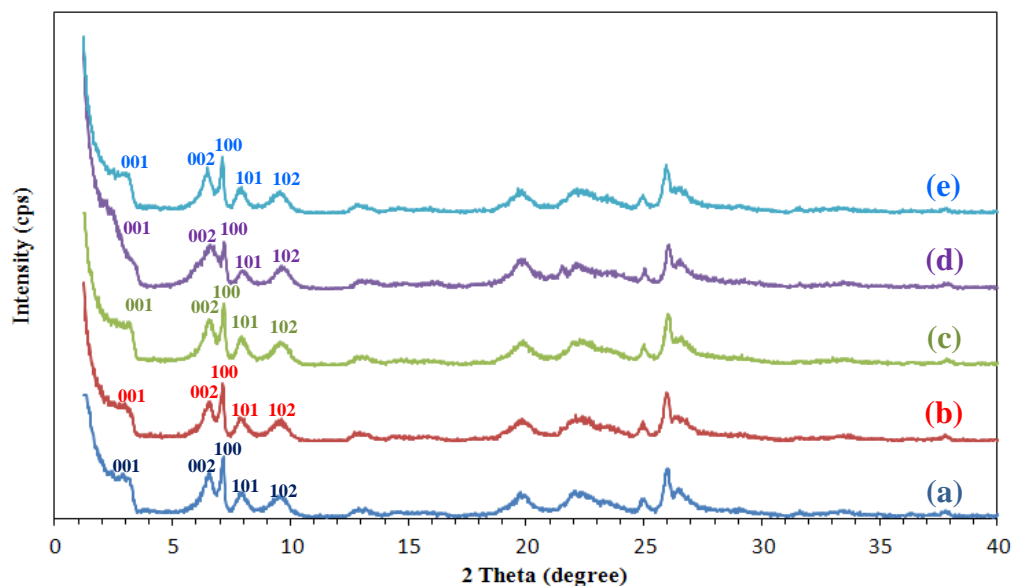


Figure 4.3 XRD patterns of MCM-22(P) and MCM-22 intercalated with quaternary ammonium salts: (a) MCM-22(P), (b) MCM-TPAOH, (c) MCM-TBAOH (d) MCM-TBAAc, and (e) MCM-CTAB.

Figure 4.4 shows the XRD patterns of MCM-22 intercalated with quaternary ammonium salts in the presence of CTAB. MCM-TPAOH/CTAB (Figure 4.4(b)) and MCM-TBAOH/CTAB (Figure 4.4(c)) had very similar patterns. The (002) peak at $2\theta = 6.5^\circ$, corresponding to the interlayer spacing, was shifted to 1.7° , indicating an increase in the space between the MWW layers. In addition, the interlayer peaks at 2θ in the range of $8-10^\circ$ were combined together, reflecting a loss of registry along the vertical direction. These results suggested that the intercalation by using TPAOH (or TBAOH) together with CTAB can intercalate both CTAB and TPAOH (or TBAOH) molecules into the interlayer space of MCM-22.

However, the XRD pattern of MCM-22 intercalated with TBAAc/CTAB (Figure 4.4(d)) was very similar to that of the parent MCM-22(P) (Figure 4.4(a)). The retention of the peak at $2\theta = 6.5^\circ$ indicated that the space between the layers of MCM-22 was still the same. These results implied that TBAAc cannot be inserted into the interlayer space of MCM-22 by using the present method. This behavior may be related to the size and basicity of the anion. Acetate anion (CH_3COO^-) should be excluded from the interlayer region as its large size, while hydroxide anion (OH^-) possesses a higher basicity and a smaller size enough to diffuse in between the layers. Therefore, TPAOH and TBAOH, with the assistance of CTAB, can diffuse into the interlayer spacing. Table 4.1 summarizes the proposed structures of the catalysts prepared based on the XRD results.

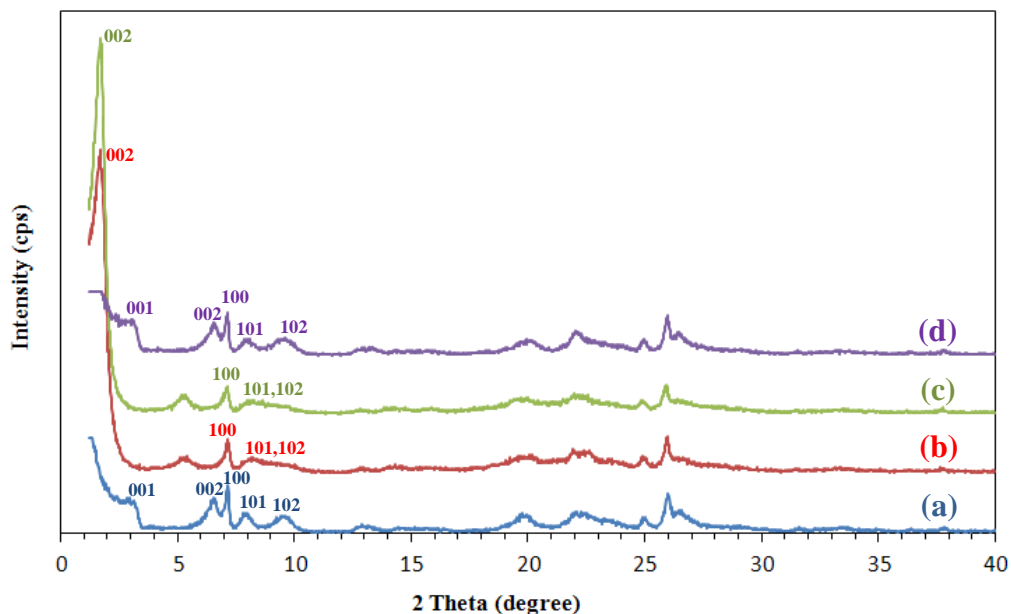
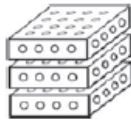
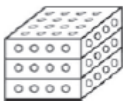
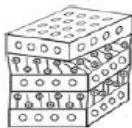
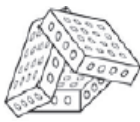


Figure 4.4 XRD patterns of MCM-22(P) and MCM-22 intercalated with quaternary ammonium salts and CTAB: (a) MCM-22(P), (b) MCM-TPAOH/CTAB, (c) MCM-TBAOH/CTAB, and (d) MCM-TBAAc/CTAB.

Table 4.1 Proposed structures of the catalysts prepared

MCM-22(P), MCM-TPAOH MCM-TBAOH, MCM-TBAAc MCM-CTAB, MCM-TBAAc/CTAB	MCM-22 H-MCM-22	MCM-TPAOH/CTAB MCM-TBAOH/CTAB	ITQ-2 H-ITQ-2
			

The XRD patterns of MCM-22 and HPW/MCM-22 with different loadings are shown in Figure 4.5. It is clear that the increase in the amount of phosphotungstic acid impregnated on MCM-22 significantly decreased the peak intensity of MCM-22. It should be attributed to an occurrence of disorder in the structure of MCM-22. No diffraction peak of bulk phosphotungstic acid (Figure 4.7) was observed for the supported catalysts. These results indicated that the phosphotungstic acid was well dispersed on MCM-22. HPW/ITQ-2 exhibited similar behavior (Figure 4.6).

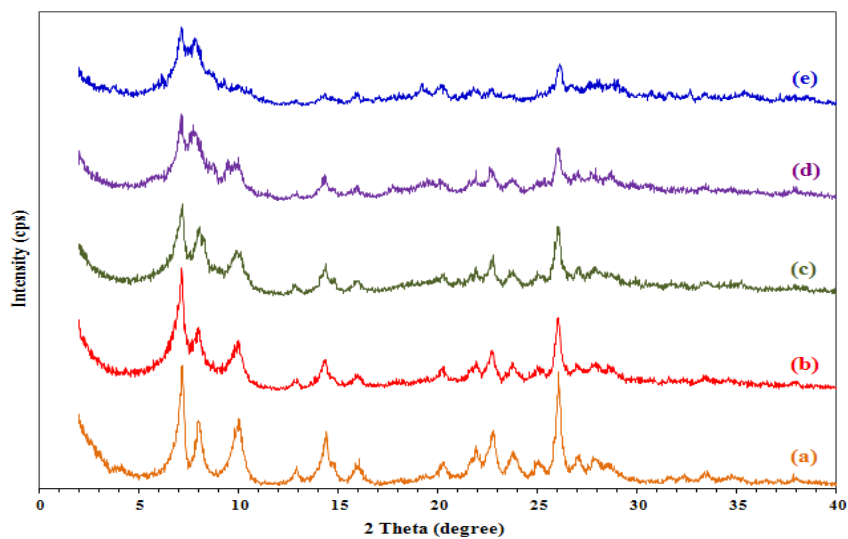


Figure 4.5 XRD patterns of MCM-22 and HPW/MCM-22 with different loadings: (a) MCM-22, (b) 10HPW/MCM-22, (c) 20HPW/MCM-22, (d) 40HPW/MCM-22, and (e) 60HPW/MCM-22.

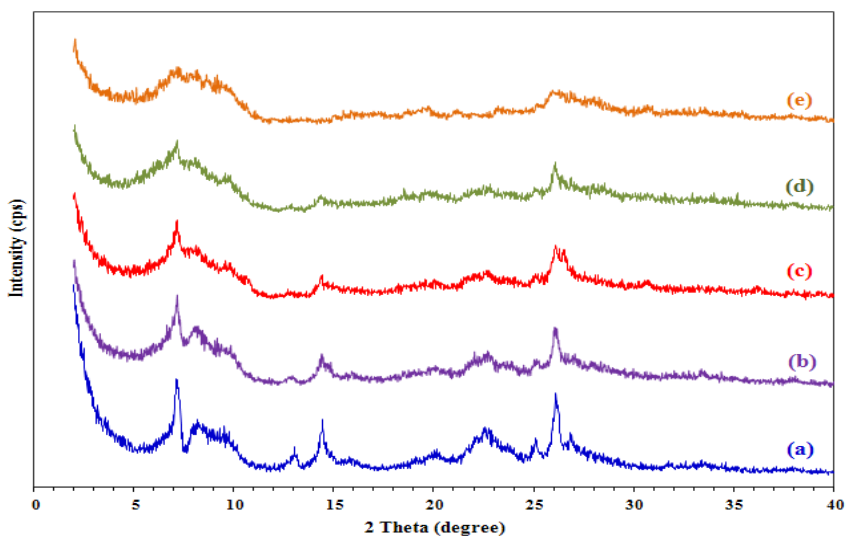


Figure 4.6 XRD patterns of ITQ-2 and HPW/ITQ-2 with different loadings: (a) ITQ-2, (b) 10HPW/ITQ-2, (c) 20HPW/ITQ-2, (d) 40HPW/ITQ-2, and (e) 60HPW/ITQ-2.

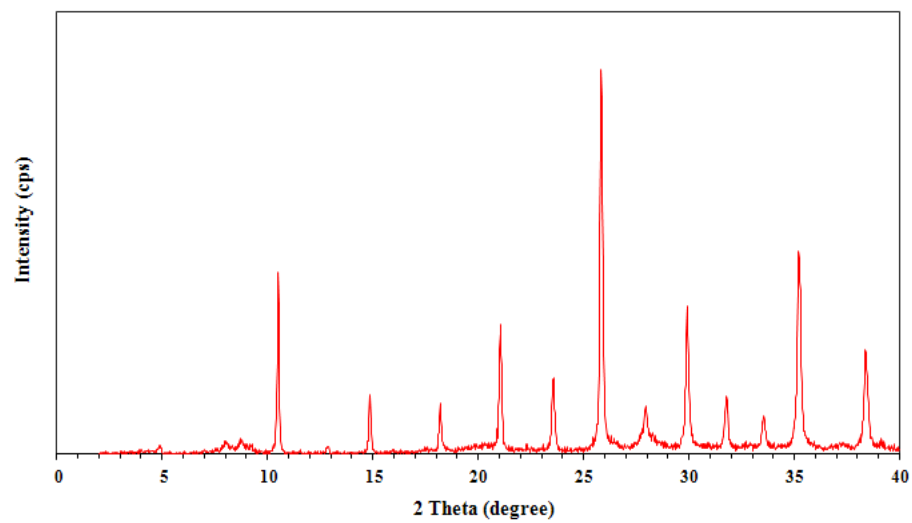


Figure 4.7 XRD pattern of phosphotungstic acid.

4.1.2 Thermogravimetric/Differential thermal analysis (TG/DTA)

The thermal stability and the weight loss of the prepared catalysts were analyzed with a thermogravimetric/differential thermal analyzer. The decomposition pattern of MCM-22(P) exhibited a three-step weight loss (Figure 4.8). The first weight loss of 2.8% from room temperature to 160 °C corresponded to the loss of physisorbed water. The weight loss of about 3.0% in the second step (up to 270 °C) was due to the decomposition of organic template (HMI) from the interlayer, while the subsequent weight loss of 11.1% between 350 °C and 510 °C was due to the decomposition of organic template from the intralayer.

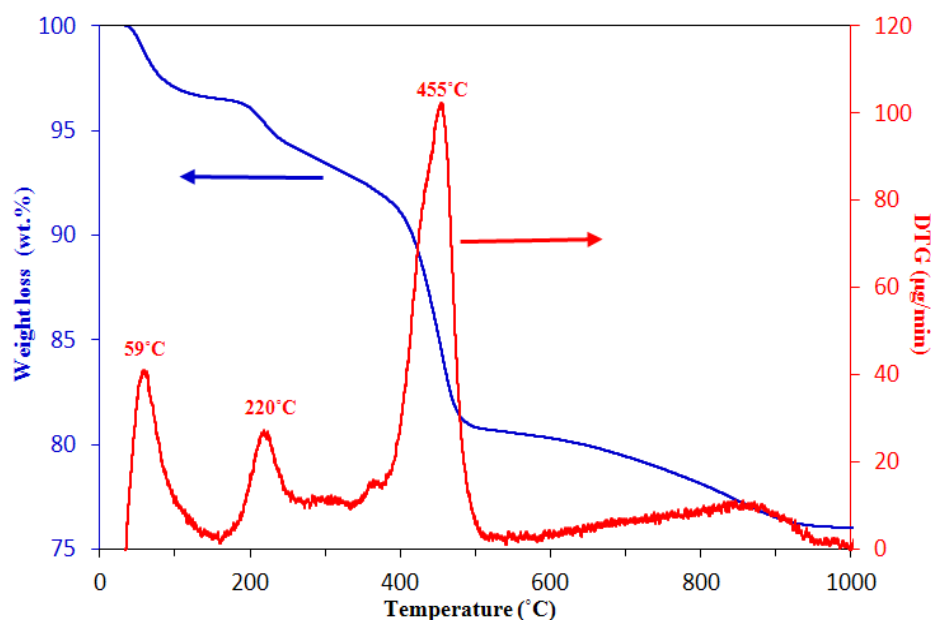


Figure 4.8 TG/DTG profile of MCM-22(P).

The TG/DTG profile in Figure 4.9 illustrated that the degradation of MCM-TPAOH occurred in three steps. The first weight loss of 3.0% from room temperature to 160 °C corresponded to the loss of physisorbed water. The weight loss of about 2.0% in the second step (up to 250 °C) was due to the decomposition of organic template from the interlayer, while the subsequent weight loss of 10.6% between 350 °C and 510 °C was due to the decomposition of organic template from the intralayer. In comparison with MCM-22(P) (Figure 4.8), the TG/DTG results obtained from MCM-TPAOH were similar to those of MCM-22(P) (Figure 4.8). These results indicated that the quaternary ammonium salts cannot be introduced into the interlayer spacing of MCM-22(P).

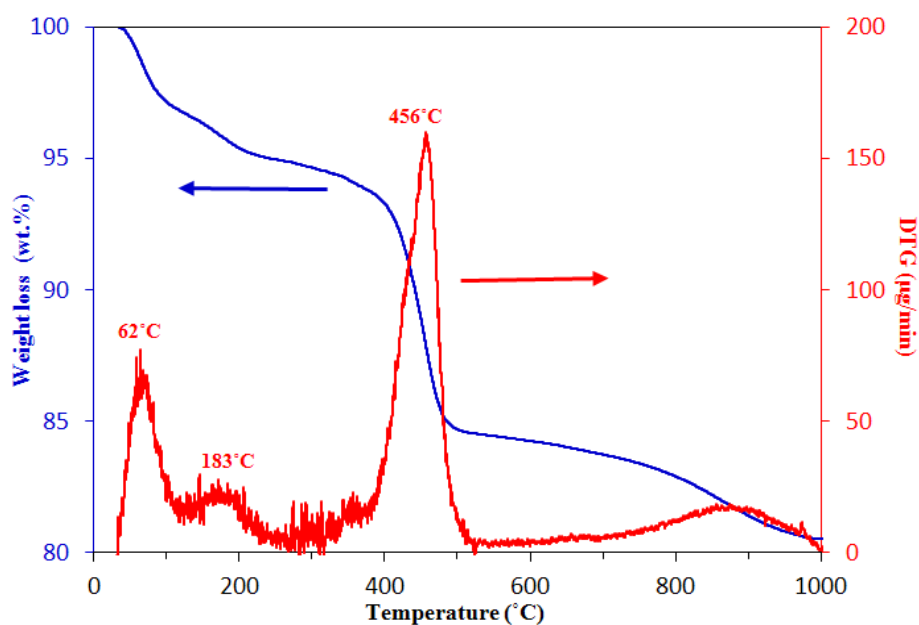


Figure 4.9 TG/DTG profile of MCM-TPAOH.

Figure 4.10 showed the TG/DTG profile of MCM-TPAOH/CTAB, which has three-step weight loss. The first weight loss of 2.9% (up to 140 °C) corresponded to the desorption of physisorbed water. The weight loss of 13.5% in the second step was due to the decomposition of CTAB and TPAOH from the interlayer, and the third weight loss of 22.1% up to 520 °C corresponded to the loss of CTAB and TPAOH from the intralayer. In comparison with that of MCM-22(P) (Figure 4.8), the TG/DTG obtained from MCM-TPAOH/CTAB shown a similar decomposition pattern. At the same decomposition steps, MCM-TPAOH/CTAB exhibited higher loss of weight when compared to MCM-22(P). It should be because CTAB has higher molecular weight than HMI. These results indicated that CTAB and TPAOH can be introduced into the interlayer space of MCM-22(P).

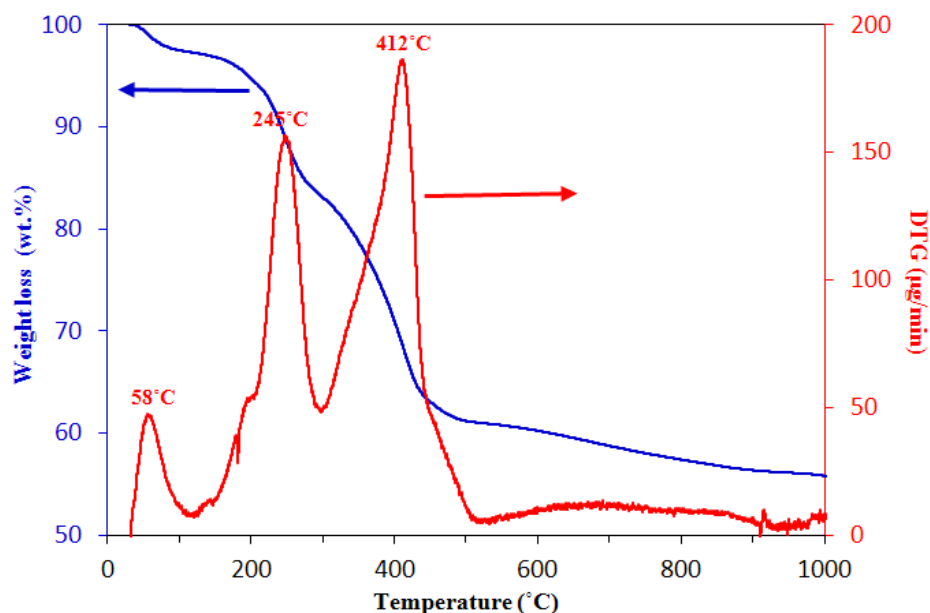


Figure 4.10 TG/DTG profile of MCM-TPAOH/CTAB.

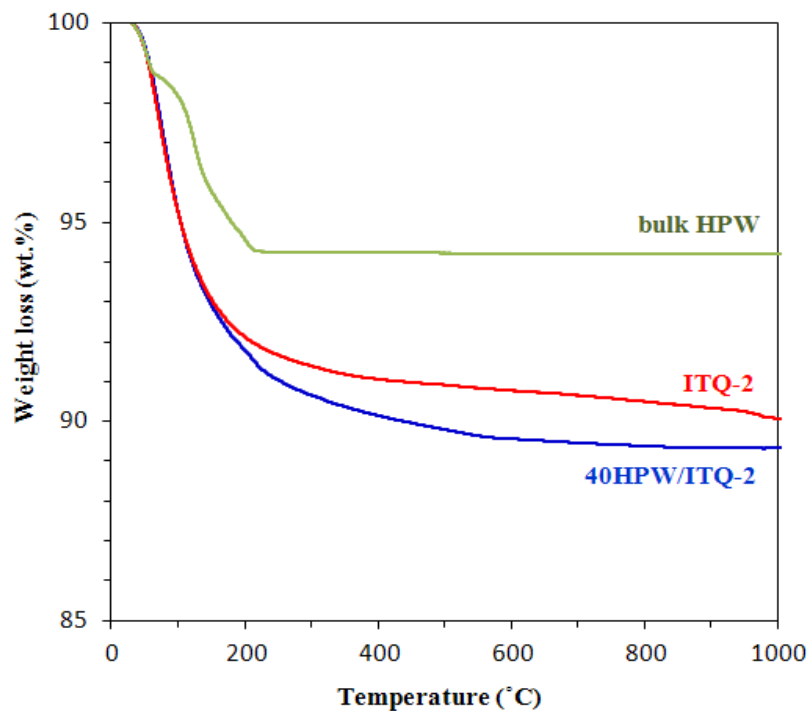


Figure 4.11 TGA profiles of bulk phosphotungstic acid, ITQ-2, and 40HPW/ITQ-2.

The thermal analysis has been carried out on bulk phosphotungstic acid, ITQ-2 and 40HPW/ITQ-2. The analysis results are shown in Figure 4.11. The TGA of bulk phosphotungstic acid showed a weight loss of about 4% up to a temperature of 160 °C, indicating a loss of adsorbed water. The gradual weight loss of about 2% up to 500 °C corresponded to the dehydroxylation of acidic groups to form WO_3 and PO_x species. The TGA profile of ITQ-2 showed a weight loss of about 9% from room temperature to 500 °C, which should be attributed to the loss of physisorbed water and the dehydroxylation of structural -OH groups. The TGA of 40HPW/ITQ-2 showed a weight loss of about 7% up to 160 °C due to the loss of adsorbed water molecules. A gradual weight loss of about 3% up to 500 °C was also observed. This result implied that the thermal stability of HPW was increased after its impregnation on ITQ-2 support. This may be caused by a formation of intermolecular bondings between ITQ-2 surface and phosphotungstic acid.

4.1.3 Nitrogen adsorption-desorption technique

The nitrogen adsorption-desorption isotherms of MCM-22 and ITQ-2 supporting different amounts of phosphotungstic acid are shown in Figure 4.12 and Figure 4.13, respectively. All catalysts exhibited type I isotherm of IUPAC classification, which is a characteristic pattern of microporous materials. The hysteresis loop at high relative pressure indicated the presence of mesopores that may be generated from interparticle voids. The textural properties derived from the isotherms of these catalysts are summarized in Table 4.2. MCM-22 support had the total specific surface area of $440 \text{ m}^2/\text{g}$, the external surface area of $97 \text{ m}^2/\text{g}$ and the internal surface area of $343 \text{ m}^2/\text{g}$. In the case of ITQ-2, the delamination process increased the total specific surface area and the external surface area to 588 and $97 \text{ m}^2/\text{g}$, respectively, due to the separation of MWW layers.

Additionally, the total specific surface area of HPW/MCM-22 and HPW/ITQ-2 was decreased with increasing the loading of phosphotungstic acid in the catalysts. It should be due to a blockage of the zeolite pores by the phosphotungstic acid clusters.

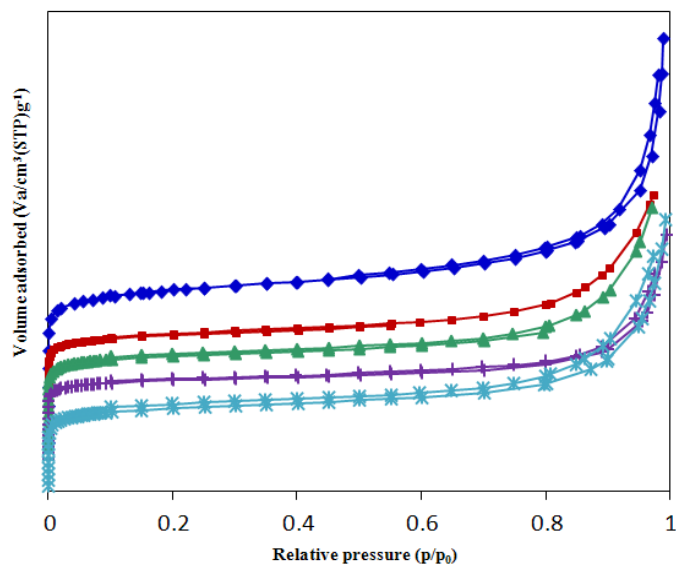


Figure 4.12 Nitrogen adsorption-desorption isotherms of (♦) MCM-22, (■) 10HPW/MCM-22, (▲) 20HPW/MCM-22, (+) 40HPW/MCM-22, and (×) 60HPW/MCM-22.

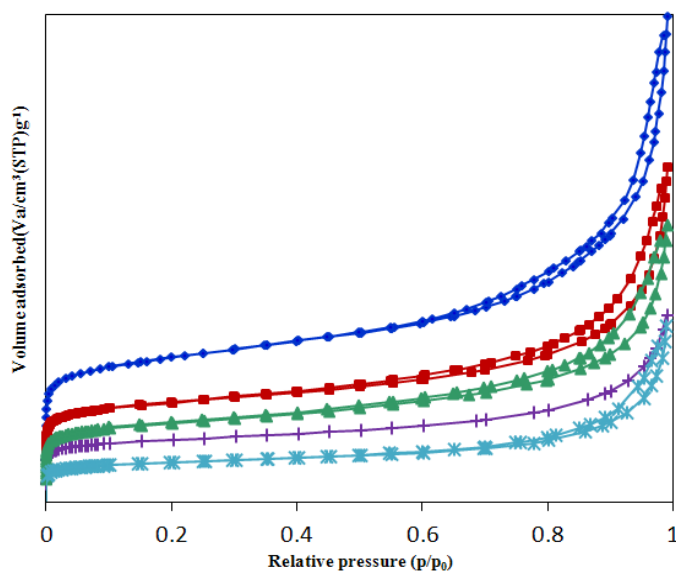


Figure 4.13 Nitrogen adsorption-desorption isotherms of (♦) ITQ-2, (■) 10HPW/ITQ-2, (▲) 20HPW/ITQ-2, (+) 40HPW/ITQ-2, and (×) 60HPW/ITQ-2.

Table 4.2 Textural properties of MCM-22 and ITQ-2 loaded with different amounts of phosphotungstic acid

Catalysts	Total specific surface area ^a (m ² /g)	External surface area ^b (m ² /g)	Internal surface area (m ² /g)	Micropore volume ^b (cm ³ /g)
MCM-22	440	97	343	0.15
10HPW/MCM-22	287	68	219	0.08
20HPW/MCM-22	264	67	196	0.08
40HPW/MCM-22	237	56	182	0.07
60HPW/MCM-22	227	69	158	0.06
ITQ-2	588	327	261	0.10
10HPW/ITQ-2	383	206	177	0.07
20HPW/ITQ-2	307	194	114	0.04
40HPW/ITQ-2	259	133	126	0.05
60HPW/ITQ-2	215	103	112	0.04

^a Calculated using the BET plot method.

^b Calculated using the t-plot method.

4.1.4 Scanning electron microscope (SEM)

The SEM images of MCM-22(P), MCM-22, H-MCM-22, MCM-TPAOH/CTAB, and 40HPW/MCM-22 are displayed in Figure 4.14. MCM-22(P) (Figure 4.14(a)) and MCM-22 (Figure 4.14(b)) exhibited an aggregate of platelets with irregular shape. The average size of diameter of about 0.8 μm . The SEM image of H-MCM-22 suggested that the treatment of MCM-22 with NH_4NO_3 , followed by the calcination, splited out the MCM-22 platelets but maintained their size (Figure 4.14(c)). The particles of MCM-22 packed densely after the intercalation with TPAOH and CTAB (Figure 4.14(d)). The SEM image of HPW impregnated on MCM-22 (Figure 4.14(e)) indicated the smaller size of platelet aggregates when compared to that of MCM-22 as a result of the destruction of the MWW structure by the acid conditions used in the impregnation.

Figure 4.15 illustrates the SEM images of ITQ-2, H-ITQ-2, and 40HPW/ITQ-2. The particles of these samples also possessed the platelet-like morphology similarly to MCM-22 but with smaller size. The average diameter of ITQ-2 is around 0.5 μm . Figure 4.15(b) shows the SEM image of H-ITQ-2. In comparison with that of ITQ-2 (Figure 4.15(a)), the morphology of H-ITQ-2 was not changed, implying that the structure of parent ITQ-2 was retained after the NH_4NO_3 treatment. The impregnation of HPW onto ITQ-2 (Figure 4.15(c)) broke down the platelets to smaller size (0.3 μm). These results were in accordance with the XRD results that indicated the destruction of the zeolite structure.

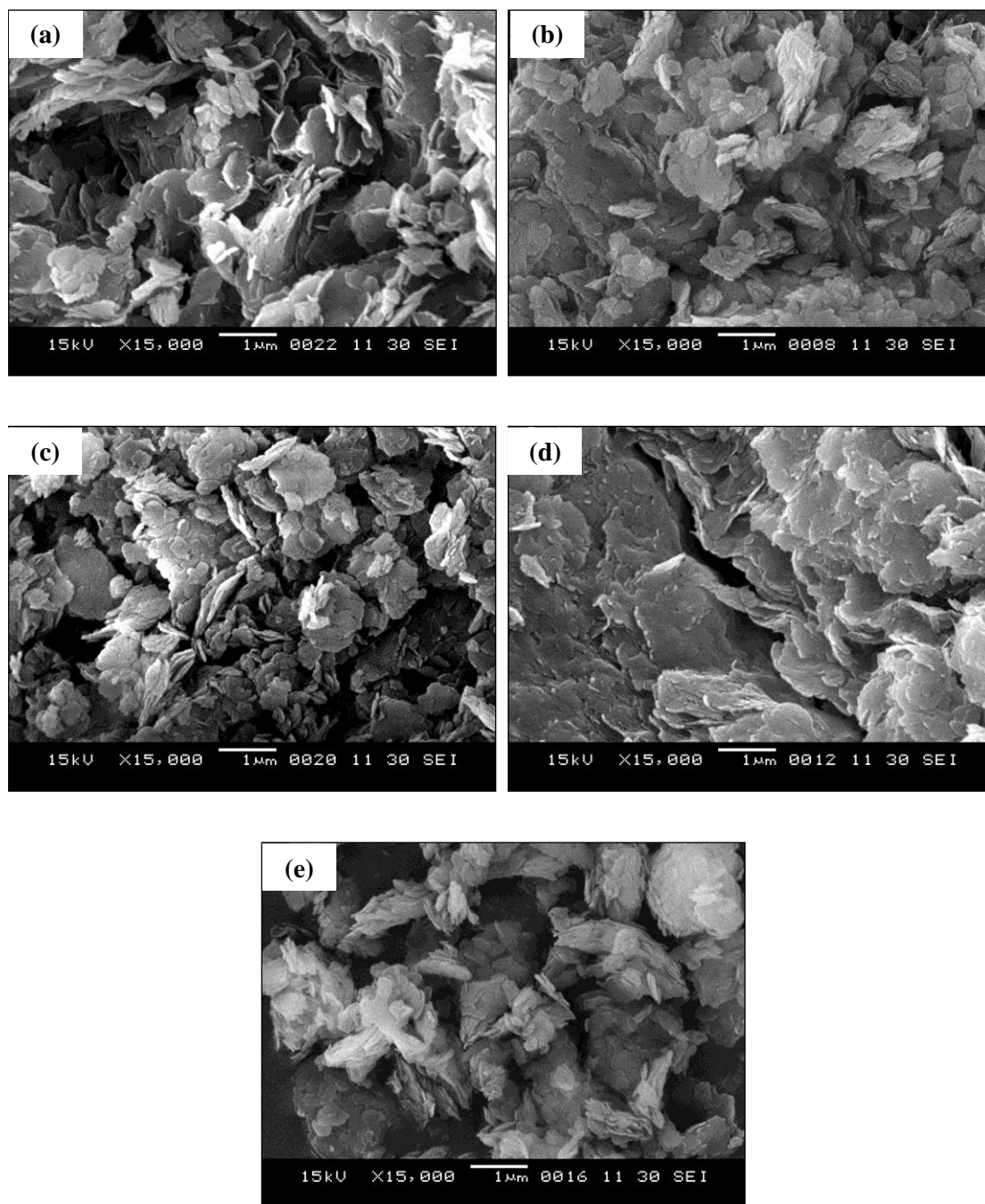


Figure 4.14 SEM images of (a) MCM-22(P), (b) MCM-22, (c) H-MCM-22, (d) MCM-TPAOH/CTAB, and (e) 40HPW/MCM-22.

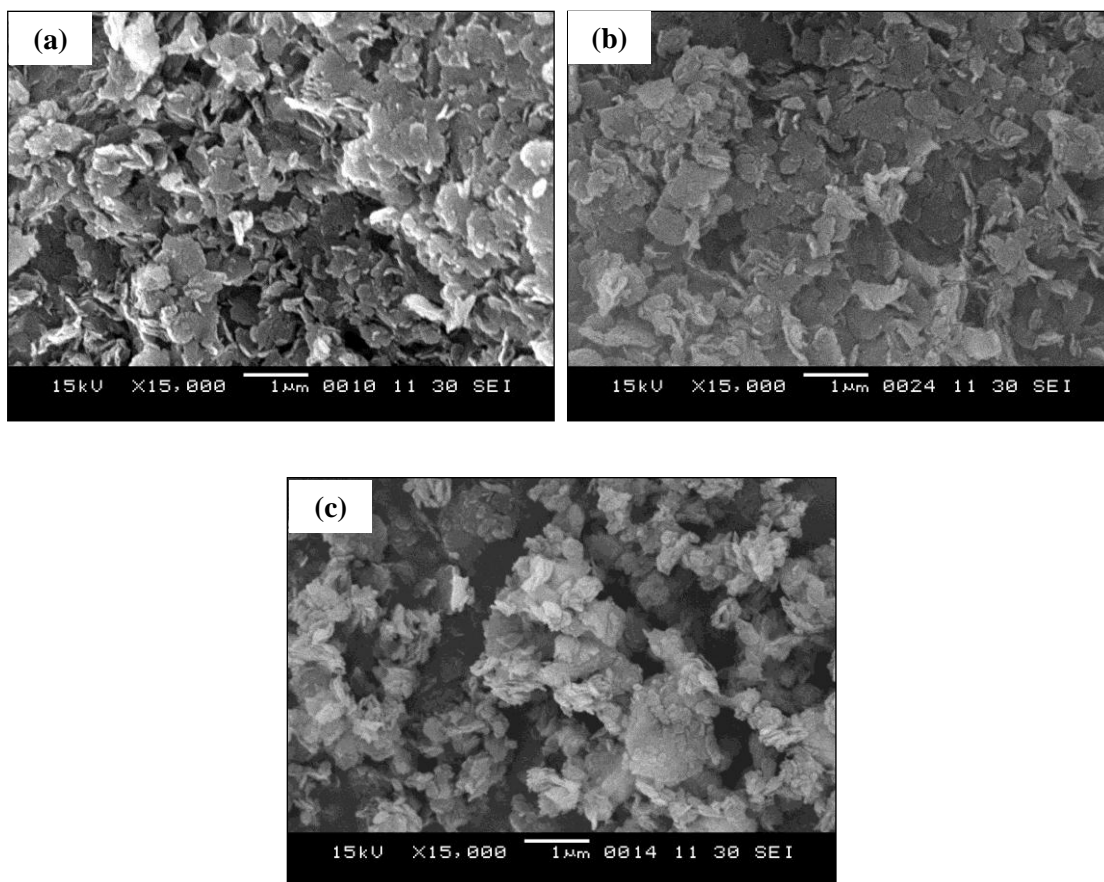


Figure 4.15 SEM images of (a) ITQ-2, (b) H-ITQ-2, and (c) 40HPW/ITQ-2.

4.1.5 Acidity of catalysts

The amount of acid sites containing in a catalyst usually expressed as millimole of acid sites per unit weight of catalyst. The prepared catalysts were quantitatively measured for the amount of acid sites by back titration and acid-base titration method using sodium chloride as an ion-exchange agent. Furthermore, the acid strength of the catalysts were determined by using Hammett indicators. The results are summarized in Table 4.3. MCM-22(P) had the acid amount of 0.79 mmol/g (obtained from acid-base titration method). In comparison with MCM-22, MCM-22(P) exhibited lower acidity, probably due to the blockage of pores and acid sites by HMI molecules. ITQ-2 with higher total surface area possessed higher acid amount than MCM-22. The treatment with NH_4NO_3 , followed by the calcination enhanced the acidity of MCM-22 and ITQ-2 but their acid strength was similar. In the case of MCM-TPAOH/CTAB and MCM-TBAOH/CTAB, they were classified to base catalysts since pK_a was higher than 9.8. It should be due to the presence of TPAOH (or TBAOH) molecules in the interlayer space of MCM-22. The phosphotungstic acid supported on MCM-22 and ITQ-2 enhanced the acidity of MCM-22 and ITQ-2. The acid amount of HPW/MCM-22 and HPW/ITQ-2 was increased with increasing the loading of phosphotungstic acid in the catalysts.

Table 4.3 Acidity measurement of the catalysts prepared

Catalysts	Acid amount ^a (mmol/g)	Acid amount ^b (mmol/g)	Acid strength ^c
MCM-22(P)	0.79	0.91	pK _a < 4.2
MCM-22	0.89	1.02	pK _a < 4.2
H-MCM-22	0.92	1.05	pK _a < 4.2
MCM-TPAOH	0.77	0.89	pK _a < 4.2
MCM-TBAOH	0.69	0.92	pK _a < 4.2
MCM-TBAAc	0.76	0.96	pK _a < 4.2
MCM-CTAB	0.74	0.88	pK _a < 4.2
MCM-TPAOH/CTAB	-	-	pK _a > 9.8
MCM-TBAOH/CTAB	-	-	pK _a > 9.8
MCM-TBAAc/CTAB	0.77	0.84	pK _a < 4.2
ITQ-2	1.39	1.58	pK _a < 4.2
H-ITQ-2	1.44	1.62	pK _a < 4.2
10HPW/MCM-22	1.44	1.69	pK _a < 4.2
20HPW/MCM-22	3.04	3.21	pK _a < 4.2
40HPW/MCM-22	3.70	3.93	pK _a < 4.2
60HPW/MCM-22	3.72	4.02	pK _a < 4.2
10HPW/ITQ-2	2.67	2.91	pK _a < 4.2
20HPW/ITQ-2	3.21	3.39	pK _a < 4.2
40HPW/ITQ-2	4.06	4.34	pK _a < 4.2
60HPW/ITQ-2	4.11	4.38	pK _a < 4.2

^aAcid amount defined as millimole of acid per gram of catalyst, obtained by acid–base titration method.

^bAcid amount defined as millimole of acid per gram of catalyst, obtained by back titration method.

^cAcid strength obtained by using Hammett indicators.

4.1.6 Adsorption study

Adsorption of reactant molecules on catalyst surface is an important step in heterogeneous catalysis. Figure 4.16 shows the adsorption isotherms of glycerol and lauric acid on MCM-22(P), MCM-22, MCM-TPAOH/CTAB, and 40HPW/ITQ-2. The adsorption of glycerol on all catalysts exhibited type I isotherm of IUPAC classification, implying that glycerol was well adsorbed on the catalyst surface. It should be due to the hydrophilic character of the catalysts and glycerol molecules. However, the adsorption of lauric acid showed the isotherm of type III. Due to its hydrophobic nature, lauric acid was poorly adsorbed on the catalyst surface.

Figure 4.16(a) shows the adsorption isotherms of glycerol and lauric acid on MCM-22(P). In comparison with that of MCM-22 (Figure 4.16(b)), the adsorption capacity of MCM-22(P) was lower, probably due to the blockage of acid sites by HMI as suggested by the XRD results (Figure 4.1(a)) and the acidity measurement (Table 4.3). The adsorption isotherms of glycerol and lauric acid on MCM-TPAOH/CTAB is shown in Figure 4.16(c). The presence of TPAOH and CTAB in the interlayer space decreased the total amount of both reactants. The adsorption capacity of MCM-TPAOH/CTAB was even lower than that of MCM-22(P) (Figure 4.16(a)). This result should be related to the larger molecular size of CTAB that is more hindrance to the acid sites. However, it can be seen that MCM-TPAOH/CTAB selectively hampered the adsorption of glycerol, whereas the adsorption capacity of lauric acid was increased. This result suggested that the organic molecules introduced into the MCM-22 layer can enhance the hydrophobicity of the catalyst. The isotherms of glycerol and lauric acid adsorbed on 40HPW/ITQ-2 exhibited the highest capacity (Figure 4.16(d)). The separation of MWW layers by the delamination process to form the sheet-like structure (ITQ-2) should promote the diffusion of reactant molecules to the catalyst surface. Moreover, the impregnation of HPW increased the amount of acid sites (see Table 4.3), resulting in a surplus of the quantity of adsorption sites.

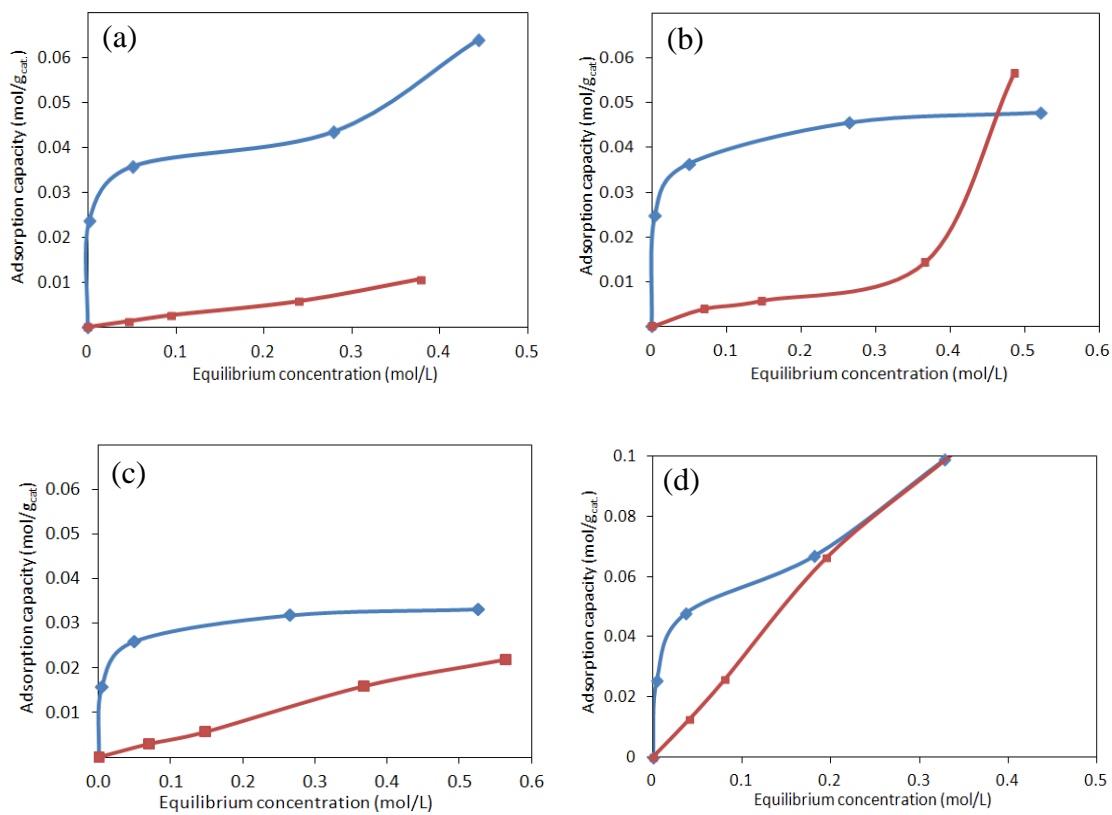


Figure 4.16 Adsorption isotherms of glycerol and lauric acid on various catalysts: (a) MCM-22(P), (b) MCM-22, (c) MCM-TPAOH/CTAB, and (d) 40HPW/ITQ-2 (Symbols: (■) lauric acid and (◆) glycerol).

4.2 Esterification of glycerol with lauric acid

4.2.1 Esterification of glycerol with lauric acid over MCM-22 and ITQ-2

The catalytic activity of MCM-22 and ITQ-2 in the esterification of glycerol with lauric acid was compared with that of MCM-22(P) and the proton-form zeolites as shown in Table 4.4.

Table 4.4 Effect of catalyst types on lauric acid conversion and products distribution

Catalysts	Lauric acid conversion (mol%)	Monoglycerides yield (mol%)	Glycerides selectivity (%)	
			mono	di
Blank	22.2	18.9	85.3	14.7
MCM-22(P)	29.9	23.5	78.7	21.3
MCM-22	32.5	27.8	85.5	14.5
H-MCM-22	35.0	28.4	81.1	18.9
ITQ-2	38.5	32.0	83.0	17.0
H-ITQ-2	39.8	29.4	73.9	26.1

Reaction conditions: Catalyst amount, 4 wt.%; glycerol/lauric acid molar ratio, 1; reaction temperature, 110 °C; reaction time, 5 h.

The esterification without catalyst gave the lauric acid conversion of 22.2% and the monoglycerides yield of 18.9%. Using MCM-22(P) increased the lauric acid conversion and the monoglycerides yield to 29.9% and 23.5%, respectively. Moreover, ITQ-2 showed higher lauric acid conversion and monoglycerides yield than MCM-22 since the delaminated zeolite possessed higher total surface area and larger amount of acid sites. In addition, it can be seen that the ion exchange with NH_4NO_3 solution to increase the acid amount did not significantly alter the conversion of lauric acid over MCM-22 and ITQ-2. However, it is likely that the formation of diglycerides was increased when the reaction was catalyzed by H-MCM-22 and H-ITQ-2.

4.2.2 Catalytic activity of MCM-22 intercalated with quaternary ammonium salts/CTAB in esterification of glycerol with lauric acid

The esterification activity of MCM-22 intercalated with quaternary ammonium salts/CTAB is presented in Table 4.5. By comparing to the parent MCM-22, MCM-TPAOH/CTAB and MCM-TBAOH/CTAB exhibited lower lauric acid conversion and monoglycerides yield. The decrease in the catalytic activity of MCM-TPAOH/CTAB and MCM-TBAOH/CTAB may be due to the blockage of pores and acid sites by the CTAB and TPAOH molecules introduced during the intercalation.

Table 4.5 Effect of MCM-22 intercalated with quaternary ammonium salts/CTAB on lauric acid conversion and products distribution

Catalysts	Lauric acid conversion (mol%)	Monoglycerides yield (mol%)	Glycerides selectivity (%)	
			mono	di
Blank	22.2	18.9	85.3	14.7
MCM-22	32.5	27.8	85.5	14.5
MCM-TPAOH/CTAB	24.4	21.5	88.4	11.6
MCM-TBAOH/CTAB	22.9	19.9	87.1	12.9

Reaction conditions: Catalyst amount, 4 wt.%; glycerol/lauric acid molar ratio, 1; reaction temperature, 110 °C; reaction time, 5 h.

4.2.3 Effect of quaternary ammonium salt (CTAB) as phase transfer catalyst on esterification of glycerol with lauric acid

Due to the miscibility of glycerol and lauric acid, the esterification is significantly limited by the mass transfer between two phases. In this study, CTAB was used as phase transfer catalyst. The esterification of glycerol with lauric acid catalyzed by using different catalysts in the present of CTAB is shown in Table 4.6.

Table 4.6 Effect of CTAB on lauric acid conversion and products distribution

Catalysts	CTAB amount (wt.%)	Lauric acid conversion (mol%)	Monoglycerides yield (mol%)	Glycerides	
				selectivity (%)	
				mono	di
Blank	-	22.2	18.9	85.3	14.7
	2	22.8	19.3	84.6	15.4
	6	22.5	19.2	85.2	14.8
MCM-22(P)	-	29.9	23.5	78.7	21.3
	2	29.7	24.1	81.4	18.7
	6	30.2	23.9	79.2	20.8
MCM-22	-	32.5	27.8	85.5	14.5
	2	32.1	27.0	84.0	16.0
	6	32.9	27.4	83.4	16.6
H-MCM-22	-	35.0	28.4	81.1	18.9
	2	36.8	27.7	75.2	24.8
	6	33.9	27.7	81.7	18.3
ITQ-2	-	38.5	32.0	83.0	17.0
	2	36.8	31.5	85.7	17.3
	6	38.2	31.7	83.0	17.0
H-ITQ-2	-	39.8	29.4	73.9	26.1
	2	36.7	30.3	82.5	17.5
	6	36.7	30.0	81.8	18.2
MCM-TPAOH/CTAB	-	24.4	21.5	88.4	11.6
	2	23.9	20.8	87.2	12.8
	6	25.0	21.9	87.9	12.1
MCM-TBAOH/CTAB	-	22.9	19.9	87.1	12.9
	2	24.8	21.8	88.0	12.0
	6	24.5	21.3	86.9	13.1

Reaction conditions: Catalyst amount, 4 wt.%; glycerol/lauric acid molar ratio, 1; reaction temperature, 110 °C; reaction time, 5 h.

These results indicated that CTAB had no significant effect on the lauric acid conversion and the monoglycerides yield although the CTAB amount was increased from 2 to 6 wt.% based on weight of lauric acid.

4.2.4 Adjustment of reactants and catalyst addition method

Since the surface of zeolite catalysts and glycerol molecules are hydrophilic, the direct addition of catalysts into the mixture of glycerol and lauric acid may favor the adsorption of glycerol onto the catalyst surface by which the diffusion of lauric acid molecules to the acid sites is hampered. Here, the method for the reactants and catalyst addition was adjusted by using ITQ-2 as the catalyst and CTAB as the phase transfer catalyst. The reaction results are summarized in Table 4.7.

Table 4.7 Esterification results from adjustment of reactants and catalyst addition method

Catalysts	CTAB amount (wt.%)	Lauric acid conversion (mol%)	Monoglycerides yield (mol%)	Glycerides selectivity (%)	
				mono	di
ITQ-2 ^a	-	38.5	32.0	83.0	17.0
ITQ-2 ^b	-	38.4	32.1	83.6	16.4
ITQ-2 ^c	-	36.9	30.4	82.5	17.5
ITQ-2 ^d	15	39.6	31.4	79.4	20.6
ITQ-2 ^e	15	37.4	30.7	82.1	17.9
ITQ-2 ^f	15	32.4	28.4	87.5	12.5
ITQ-2 ^g	-	39.5	31.5	79.9	20.1

Reaction conditions: Catalyst amount, 4 wt.%; glycerol/lauric acid molar ratio, 1; reaction temperature, 110 °C; reaction time, 5 h.

^a Mixed lauric acid with glycerol for 15 min, and then added ITQ-2.

^b Mixed lauric acid with ITQ-2 for 15 min, and then added dropwise glycerol for 3 min.

^c Mixed lauric acid with ITQ-2 for 15 min, and then added dropwise glycerol for 30 min.

^d Mixed lauric acid with glycerol for 15 min, and then added ITQ-2, CTAB.

^e Mixed lauric acid with ITQ-2 for 15 min, and then added dropwise the mixture of glycerol and CTAB for 3 min.

^f Mixed lauric acid with ITQ-2 for 15 min, and then added dropwise the mixture of glycerol and CTAB for 30 min.

^g Mixed lauric acid with glycerol for 15 min, and then added ITQ-2 + molecular sieve (4Å) 20 wt.% based on weight of ITQ-2.

The mixture of glycerol, lauric acid and ITQ-2 gave the lauric acid conversion and the monoglycerides yield of 38.5% and 32%, respectively. Changing the method to dropping of glycerol into the mixture of lauric acid and ITQ-2 within 3 or 30 min did not alter the reaction results. Moreover, the addition of CTAB in order to increase miscibility of lauric acid, glycerol and ITQ-2, lauric acid was mixed with ITQ-2 for 15 min and then the mixture of glycerol with CTAB was dropped for 3 and 30 min, cannot improve the lauric acid conversion and the monoglycerides yield.

One of the reaction products occurred in the esterification of glycerol with lauric acid is water, a well-known poison or inhibitor of the acid catalysts. In order to suppress or minimize the detrimental effect of water, a solid molecular sieve (pore size diameter of 4 Å), which is quite inactive in the esterification, was mixed with ITQ-2 and added to the reaction mixture. It can be seen that the elimination of water during the reaction by using a molecular sieve cannot increase the lauric acid conversion and the monoglycerides yield. These results also suggested that the reaction of glycerol and lauric acid was not limited by the poisoning of the acid sites but the catalyst acidity.

4.2.5 Catalytic activity of MCM-22 and ITQ-2 supported phosphotungstic acid catalysts in esterification of glycerol

In order to increase the catalytic activity of MCM-22 and ITQ-2 in the esterification, MCM-22 and ITQ-2 impregnated with phosphotungstic acid were prepared and tested in the reaction in the presence or absence of CTAB as phase transfer catalyst. The results are shown in Table 4.8.

Table 4.8 Effect of phosphotungstic acid supported on MCM-22 and ITQ-2 on esterification of glycerol with lauric acid in the presence or absence of CTAB

Catalysts	CTAB amount (wt.%)	Lauric acid conversion (mol%)	Monoglycerides yield (mol%)	Glycerides selectivity (%)	
				mono	di
				MCM-22	-
	2	32.1	27.0	83.9	16.0
ITQ-2	-	38.5	32.0	83.0	17.0
	2	36.8	31.5	85.6	17.3
20HPW/MCM-22	-	44.2	35.6	80.6	19.4
	2	35.9	29.5	82.1	17.9
20HPW/ITQ-2	-	47.1	38.5	81.8	18.2
	2	40.8	33.2	81.4	18.6

Reaction conditions: Catalyst amount, 4 wt.%; glycerol/lauric acid molar ratio, 1; reaction temperature, 110 °C; reaction time, 5 h.

The results revealed that phosphotungstic acid supported on MCM-22 and ITQ-2 showed higher activity than MCM-22 and ITQ-2, giving higher lauric acid conversion and yield of monoglycerides. It should be related to the increase of acidity derived from the impregnated phosphotungstic acid (Table 4.3). However, the presence of CTAB retarded the reaction in a similar manner to the results mentioned previously (Table 4.6).

4.2.6 Catalytic activity of MCM-22 and ITQ-2 impregnated with different amounts of phosphotungstic acid

In order to optimize the acidity of HPW/MCM-22 and HPW/ITQ-2 for the esterification, the phosphotungstic acid amount was varied in the range of 0 to 60 wt.% based on weight of support. The catalytic activity of HPW/MCM-22 and HPW/ITQ-2 with different amounts of phosphotungstic acid are presented in Table 4.9.

Table 4.9 Effect of phosphotungstic acid loading on lauric acid conversion and products distribution in esterification of glycerol over HPW/MCM-22 and HPW/ITQ-2

Catalysts	Lauric acid conversion (mol%)	Monoglycerides yield (mol%)	Glycerides selectivity (%)	
			mono	di
MCM-22	32.5	27.8	85.5	14.5
10HPW/MCM-22	35.3	28.9	81.7	18.3
20HPW/MCM-22	44.2	35.6	80.6	19.4
40HPW/MCM-22	48.4	40.7	83.9	16.1
60HPW/MCM-22	45.9	38.3	83.5	16.5
ITQ-2	38.5	32.0	83.0	17.0
10HPW/ITQ-2	44.2	35.4	80.2	19.8
20HPW/ITQ-2	47.1	38.5	81.8	18.2
40HPW/ITQ-2	57.4	45.5	79.3	20.7
60HPW/ITQ-2	53.4	42.1	78.9	21.1

Reaction conditions: Catalyst amount, 4 wt.%; glycerol/lauric acid molar ratio, 1; reaction temperature, 110 °C; reaction time, 5 h.

The results revealed that both HPW/MCM-22 and HPW/ITQ-2 exhibited a significant increase in the lauric acid conversion and the monoglycerides yield when increased the amount of phosphotungstic acid in the catalysts. It should be due to an enhancement of the catalyst acidity. However, when the loading reached 60 wt.%, the acid conversion and the monoglycerides yield were dropped. It was informed by the

nitrogen adsorption-desorption results that the specific surface area of HPW/MCM-22 and HPW/ITQ-2 decreased with increasing in the loading of phosphotungstic acid (Table 4.2). The surface area of 40HPW/ITQ-2 was 259 m²/g, while the loading amount was increased to 60 wt.%, resulting in a loss of surface area to 215 m²/g. Therefore, the higher activity of 40HPW/ITQ-2 should be due to the higher surface area that promoted better dispersion of phosphotungstic acid when compared to 60 HPW/ITQ-2.

By comparing between HPW/MCM-22 and HPW/ITQ-2 with the same phosphotungstic acid loading, HPW/ITQ-2 showed higher lauric acid conversion and the monoglycerides yield. It should be due to the higher surface area and the better dispersion of phosphotungstic acid. Based on these results, the highest lauric acid conversion (57.4%) and monoglycerides yield (45.5%) were obtained over 40HPW/ITQ-2. Hereafter, 40HPW/ITQ-2 was used as the catalyst to investigate the suitable conditions for the esterification of glycerol with lauric acid.

4.3 Parameters affecting esterification of glycerol with lauric acid

4.3.1 Effect of molar ratio of glycerol to lauric acid

The effect of molar ratio of glycerol to lauric acid on the esterification over 40HPW/ITQ-2 was studied. The results are shown in Table 4.10.

Table 4.10 Effect of molar ratio of glycerol to lauric acid on lauric acid conversion and products distribution in esterification of glycerol over 40HPW/ITQ-2

Glycerol : lauric molar ratio	Lauric acid conversion (mol%)	Monoglycerides yield (mol%)	Glycerides selectivity (%)	
			mono	di
1	57.4	45.5	79.3	20.7
3	23.6	23.6	100.0	0

Reaction conditions: Catalyst amount, 4 wt.%; reaction temperature, 110 °C; reaction time, 5 h.

It was found that the lauric acid conversion and the monoglycerides yield were decreased when the molar ratio of glycerol to lauric acid increased. However, the formation of diglycerides was suppressed. Since the catalyst surface and the glycerol molecule are hydrophilic, the increase in the amount of glycerol added should enhance the amount of glycerol adsorbed on the surface of the catalyst. Therefore, the diffusion of fatty acid molecules to the catalytically active sites was reduced seriously. Based on these results, the molar ratio of glycerol to lauric acid of 1 was the suitable ratio for the esterification of glycerol with lauric acid.

4.3.2 Effect of reaction temperature

To determine the effect of reaction temperature on the esterification of glycerol with lauric acid, the experiments were conducted at temperatures ranging from 100 °C to 130 °C. Table 4.11 summarizes the results attained.

Table 4.11 Effect of reaction temperature on lauric acid conversion and products distribution in esterification of glycerol over 40HPW/ITQ-2

Reaction temperature (°C)	Lauric acid conversion (mol%)	Monoglycerides yield (mol%)	Glycerides selectivity (%)	
			mono	di
100	20.7	19.4	94.1	5.9
110	57.4	45.5	79.3	20.7
120	59.3	44.2	74.6	25.5
130	62.1	43.8	70.5	29.5

Reaction conditions: Catalyst amount, 4 wt.%; glycerol/lauric acid molar ratio, 1; reaction time, 5 h.

The conversion of lauric acid and the formation of glyceride products were promoted when the reaction temperature was raised from 100 °C to 110 °C. As the reaction temperature was increased, all the reactant molecules would gain more kinetic energy that eventually accelerated the mass transfer rate between the reactant-catalyst phases, resulting in the formation of monoglycerides in a shorter time. The highest monoglycerides yield (45.5%) was obtained at the reaction temperature of 110 °C. However, the selectivity to monoglycerides was decreased with increasing the temperature, reducing the yield of monoglycerides. Since monoglycerides were transformed into diglycerides by the reaction of monoglycerides with lauric acid, the temperature elevated enhanced also the energy required for this consecutive reaction. According to these results, the reaction temperature of 110 °C was the suitable one.

4.3.3 Effect of catalyst amount

The effect of catalyst amount on the lauric acid conversion and the products distribution were investigated by varying different amounts of 40HPW/ITQ-2 in the esterification of glycerol and lauric acid. The catalyst amount was adjusted in the range of 0 to 6 wt.% based on weight of lauric acid.

Table 4.12 Effect of catalyst amount on lauric acid conversion and products distribution in esterification of glycerol over 40HPW/ITQ-2

Catalyst mass (wt.%)	Lauric acid conversion (mol%)	Monoglycerides yield (mol%)	Glyceride selectivity (%)	
			mono	di
0	22.2	18.9	85.3	14.7
2	34.5	29.5	85.4	14.6
4	57.4	45.5	79.3	20.7
6	51.5	39.9	77.5	22.5

Reaction conditions: Glycerol/lauric acid molar ratio, 1; reaction temperature, 110 °C; reaction time, 5 h.

As shown in Table 4.12, an increase in the yield of monoglycerides with increasing the catalyst amount was expected due to the increase of the catalytically active sites. The highest conversion (57.4%) and yield (45.5%) were obtained at the catalyst amount of 4 wt.%. However, further increase in the catalyst amount to 6 wt.% rendered the yield of monoglycerides decreased. This could be explained by an agglomeration of the excess catalyst, which reduced the mass transfer of glycerol and lauric acid to the active sites. Based on these results, the typical catalyst amount used in the experiments was 4 wt.% based on weight of lauric acid.

4.3.4 Effect of reaction time

The effect of reaction time on the esterification of glycerol with lauric acid over 40HPW/ITQ-2 were investigated by varying the reaction course in the range of 0.5-8 h.

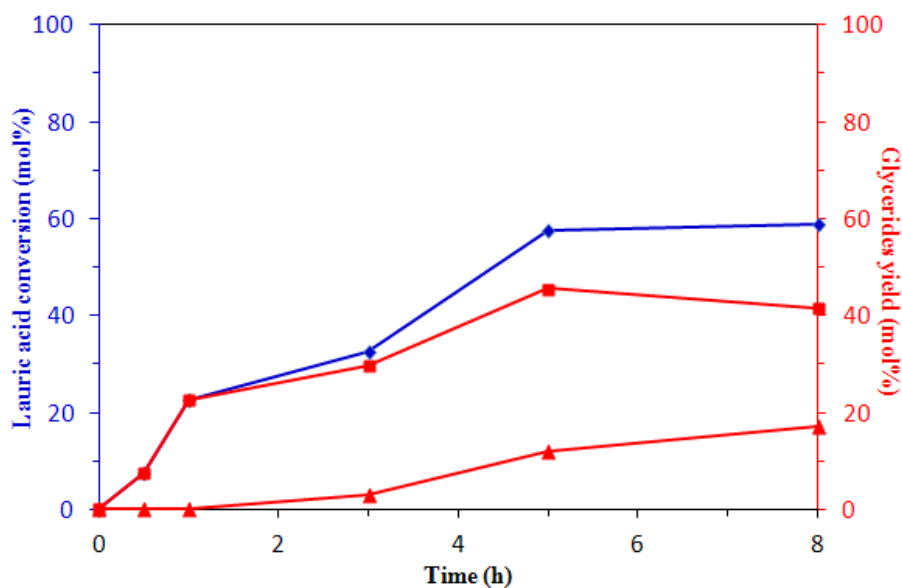


Figure 4.17 Effect of reaction time on glycerides yield and products distribution in esterification of glycerol over 40HPW/ITQ-2. Reaction conditions: Catalyst amount, 4 wt.%; glycerol/lauric acid molar ratio, 1; reaction temperature, 110 °C. (Symbols: (♦) lauric acid conversion, (■) monoglycerides yield, and (▲) diglycerides yield).

As shown in Figure 4.18, the monoglycerides yield was increased with increasing the reaction time from 0.5 to 5 h at which the amount of monoglycerides was obviously enhanced from 7.5% to 45.5%. When the reaction time continued to increase over 5 h, the monoglyceride yield was slightly decreased. It should be caused by the transformation of the monoglycerides to diglycerides by the consecutive reaction of monoglycerides with lauric acid. Therefore, the reaction time at 5 h was the suitable reaction course to attain the highest yield of monoglycerides.

CHAPTER V

CONCLUSIONS AND RECOMMENDATIONS

5.1 Conclusions

MCM-22(P) was synthesized by using hydrothermal method under rotating conditions. MCM-22 and ITQ-2 were successfully prepared by calcination and delamination of MCM-22(P), respectively. The intercalation of MCM-22 with CTAB and TPAOH or TBAOH can be prepared by refluxing MCM-22(P) with the solution of TPAOH/CTAB or TBAOH/CTAB, respectively, at 80 °C for 16 h. MCM-22 and ITQ-2 supported phosphotungstic acid catalysts were achieved by impregnation method.

The delamination of MCM-22 increased the total surface area of the resulting catalyst, increasing the amount of acid sites. Moreover, the impregnation of phosphotungstic acid onto MCM-22 and ITQ-2 increased the acidity of MCM-22 and ITQ-2. However, the total surface area of the catalysts was decreased with increasing the loading of phosphotungstic acid. From the liquid-phase adsorption study, the adsorption capacity of MCM-22 intercalated with CTAB and TPAOH (or TBAOH) was lower than that of MCM-22 due to the present of CTAB and TPAOH (or TBAOH) molecules. However, the organic molecules introduced in between the MCM-22 layers can enhance the hydrophobicity of the catalyst.

The catalytic activity test in the esterification of glycerol with lauric acid revealed that the separation of MWW layers from each other by the delamination process increased the lauric acid conversion and the monoglycerides yield. The presence of CTAB and TPAOH (or TBAOH) decreased the catalytic activity in the esterification. Furthermore, the impregnation of phosphotungstic acid onto MCM-22 and ITQ-2 enhanced the catalytic activity. By comparing between HPW/MCM-22 and HPW/ITQ-2 with the same phosphotungstic acid loading, HPW/ITQ-2 showed higher the lauric acid conversion and the monoglycerides yield. It was found that the highest lauric acid conversion (57.4%) and monoglycerides yield (45.5%) were obtained over 40HPW/ITQ-2 under the suitable conditions, the molar ratio of glycerol/lauric acid of 1, the catalyst mass of 4 wt.% base on weight of lauric acid, the reaction time of 5 h at 110 °C.

5.2 Recommendations

1) In the synthesis of ITQ-2, during the ultrasound treatment, care must be taken to ensure that temperature do not exceed 50 °C since at the high temperature, the undesired phase of MCM-41 is formed.

2) As the future work, the intercalation mechanism of quaternary ammonium salts into layer catalysts should be studied.

REFERENCES

- [1] Soares, V.L.P.; Lachter, E.R.; Rodrigues, J.A.; Batista, L.N. and Nascimento, R.S.V. New Applications for Soybean Biodiesel Glycerol. *Soybean-Applications and Technology*. (2011): 151-172.
- [2] Viinikainen, T.S.; Karinen, R.S. and Krause, A.O.I. Conversion of Glycerol into Traffic Fuels. *Catalysis for renewables: from feedstock to energy production*. (2007): 209–222.
- [3] Zheng, Y.; Chen, X. and Shen, Y. Commodity chemical derived from glycerol, an important biorefinery feedstock. *Chemical reserve*. 108(2008): 5253-5277.
- [4] Zhou, C.H.; Beltramini, J.N.; Fan, Y.X. and Lu, G.Q. Chemoselective catalytic conversion of glycerol as a biorenewable source to valuable commodity chemicals. *Chemical Society Reviews*. 37(2008): 527-549.
- [5] Lin, X.; Chuah, G.K. and Jaenicke, S. Base –funtionnalized MCM-41 as catalysts for the synthesis of monoglycerides Xuanhao. *Journal of Molecular Catalysis A: Chemical*. 150(1999): 287-294.
- [6] Machado, M.S.; Pérez-Pariente, J.; Sastre, E.; Cardoso, D. and Guereñu, A.M. Selective synthesis of glycerol monolaurate with zeolitic molecular sieves. *Applied Catalysis A: General*. 203(2000): 321–328.
- [7] Helwani, Z.; Othman, M.R.; Aziz, N., Kim, J. and Fernando, W.J.N. Solid heterogeneous catalysts for transesterification of triglycerides with methanol: A review. *Applied Catalysis A: General*. 363(2009): 1–10.
- [8] Corma, A.; Hamid, S.B.A.; Iborra, S. and Velty, A. Lewis and Bronsted basic active site on solid catalysts and their role in the synthesis of monoglycerides. *Journal of Catalysis*. 234(2005): 340-347.

- [9] Abdullah, A.Z.; Wibowo, T.Y. and Zakaria, R. Effect of tetramethyl ammonium hydroxide on the activity of LiOH-intercalated montmorillonite catalyst in the transesterification of methyl laurate with glycerol. *Chemical Engineering Journal*. 167(2011): 328-334.
- [10] Corma, A.; Iborra, S.; Miquel, S. and Primo, J. Catalyst for the production of fine chemical. *Journal of Catalysis*. 173(1998): 315-321.
- [11] Smith, K.; El-Hiti, G.A.; Gamal, A.; Jayne, A.J. and Butters, K. Acetylation of aromatic ethers using acetic anhydride over solid acid catalysts in a solvent-free system. Scope of the reaction for substituted ethers. *Organic and Biomolecular Chemistry*. 1(2003): 1560.
- [12] Clark, J.H. Solid Acids for Green Chemistry. *Accounts of Chemical Research*. 35(2002): 791–797.
- [13] Okamura, M.; Takagaki, A.; Toda, M.; Kondo, J.N.; Domen, K.; Tatsumi, T.; Hara, M.; and Hayashi, S. Acid-Catalyzed Reactions on Flexible Polycyclic Aromatic Carbon in Amorphous Carbon. *Chemistry of Materials*. 18(2006): 3039–3045.
- [14] Breck, D.W. Zeolite Molecular Sieves: Structure, Chemistry, and use, New York: John Wiley & Sons, 1997, 3.
- [15] Derouane, E.G. New aspects of molecular shape-selectivity: Catalytic by zeolite ZSM-5. *Studies Surface Science Catalysis*. 5(1980): 5.
- [16] Szostak, R. *Molecular Sieve Principles of Synthesis and Identification*. New Van Nostrand Reinhold, New York, 1988, 1.
- [17] Frontera, P.; Testa, F.; Aiello, R.; Candamano, S. and Nagy, J.B. Transformation of MCM-22(P) into ITQ-2: The role of framework aluminium. *Microporous and Mesoporous Materials*. 106(2007):107–114.

- [18] Aguilar, J.; Pergher, S.B.C.; Detoni, C.; Corma, A.; Melo, F.V. and Sastre, E. Alkylation of biphenyl with propylene using MCM-22 and ITQ-2 zeolites. *Catalysis Today*. 133–135(2008): 667–672.
- [19] Corma, A.; Diaz, U.; Garcia, T.; Sastre, G. and Velty, A. Multifunctional Hybrid Organic-Inorganic Catalytic Materials with a Hierarchical System of Well-Defined Micro- and Mesopores. *Journal of the American Chemical Society*. 132(2010): 15011-15021.
- [20] Zhang, Y.; Stanciulescu, M. and Ikura, M. Rapid transesterification of soybean oil with phase transfer catalysts. *Applied Catalysis A: General*. 366(2009): 176–183.
- [21] Wibowo, T.Y.; Abdullah, A.Z. and Zakaria, R. Organo-montmorillonites as catalysts for selective synthesis of glycerol monolaurate. *Applied Clay Science*. 50(2010): 280-281.
- [22] Pouilloux, Y.; Abro, S.; Vanhove, C. and Barrault, J. Reaction of glycerol with fatty acids in the presence of ion-exchange resins Preparation of monoglycerides. *Journal of Molecular Catalysis A: Chemical*. 149(1999): 243-254.
- [23] Otera, J. and Nishikido, J. Esterification: Methods, Reactions, and Applications. Germany: *WILEY – VCH*, 2010, 1.
- [24] The McGraw-Hill Companies. Reactions of Carboxylic Acids [Online]. Available from:<http://www.mhhe.com/physsci/chemistry/carey/student/olc/graphics/carey04oc/ref/ch19reactioncarboxylicacids.html#esters> [2010, October 3]
- [25] Nesaretnam, K.; Muhammad, B.; Chong, C.L. and Tan, Y.A. Selected readings on palm oil and its uses. *Palm Oil Research Institute of Malaysia*, 1989, 5.
- [26] Unsaturated fatty.acids [Online]. Available from: http://www.en.wikipedia.org/wiki/Fatty_acid [2011, August 2]

- [27] Activation energy [Online]. Available from: http://en.wikipedia.org/wiki/Activation_energy [2011, February 14]
- [28] Hagen, *Journal Industrial Catalysis*, New York, Weinheim Wiley, 1999.
- [29] Figueiredo, J.L.; Pereira, M.M. and Faria, J. *Catalysis from theory to application: an integrated course*. Portugal : *Imprensa Da Universidade De Coimbra*, 2008.
- [30] University of South Carolina. Building of a Heterogeneous Catalysis Reactor [Online]. Available from: http://www.che.sc.edu/centers/RCS/smith/jake_smith_reactor_page.html [2010, October 15]
- [31] Barrer, R. M. *Zeolite and Clay Minerals as sorbets and Molecular Sieves*. London: Academic Press, 1978.
- [32] Smart, L. and Moore, E. *Solid State Chemistry*. London: Chapman & Hall University, 1992, 184.
- [33] Szostak, R. *Molecular Sieves: Principle of synthesis and Identification*. New York: Van Nostrand Reinhold, 1989, 51.
- [34] Rollman, L. D. *Zeolites: Science and Technology*. Netherlands: Martinus Nijhoff, 1984, 109.
- [35] Breck, D. W. *Crystalline Zeolite Y*. US Patent No. 3,130,007, 1964.
- [36] Whattam, T. V. *Manufacture of Synthetic Zeolite*, US patent No. 4,016,246, 1977.
- [37] Crabtree, R. H. *The Organometallic Chemistry of transition metals*, New York: John Wiley & Sons, 1988, 200.
- [38] Gopalakrishnan, G.; Juttu, G. and Lobo, F.R. Characterization and catalytic properties of MCM-56 and MCM-22 zeolites. *Microporous and Mesoporous Materials*. 40(2000): 9.

- [39] Lin, Y.-H.; Yang, M.-H.; Yeh, T.-F. and Ger, M.-D. Catalytic degradation of HDPE over mesoporous and microporous catalytic in a fluidized-bed reactor. *Polymer Degradation and Stability*. 86(2004): 121.
- [40] Aguado, J.; Serrano, D.P.; Escola, J.M.; Garagorri, E. and Fernandez, J.A. Catalytic conversion of polyolefins into fuels over zeolite beta. *Polymer Degradation and Stability*. 69(2000): 11.
- [41] Rodriguez, I.; Climent, M.J.; Iborra, S.; Fornés, V. and Corma, A. Use of delaminated zeolites (ITQ-2) and mesoporous molecular sieves in the production of fine chemicals: preparation of dimethylacetals and tetrahydropyranlation of alcohols and phenols. *Journal of Catalysis*. 192(2000): 441–447.
- [42] Dehmlow, E.V. and Dehmlow, S.S. Phase Transfer Catalysis, 3 rd ed. *Weinheim: VCH*, 1993.
- [43] Starks, C.M.; Liotta, C. L. and Halpern, M. Phase-Transfer Catalysis, New York: *Chapman & Hall*, 1994.
- [44] Dharne, S. and Bokadee, V.V. Esterification of levulinic acid to n-butyl levulinate over heteropoly acid supported on acid-treated clay. *Journal of Natural Gas Chemistry*. 20(2011): 18-24.
- [45] Bhorodwaj, S.K. and Dutta, D.K. Heteropolyacid supported modified Montmorillonite clay: An effective catalyst for the esterification of acetic acid with sec-butanol. *Applied Catalysis A: General*. 378(2010): 221-226.
- [46] Blasco, T.; Corma, A.; Martinez, A. and Martinez-Escolano P. Supported Heteropolyacid (HPW) Catalysts for the Continuous Alkylation of Isobutane with 2-Butene: The Benefit of Using MCM-41 with Larger Pore Diameters. *Journal of catalysis*. 177(1998): 306-313.

- [47] Ferreira, P.; Fonseca, I.M.; Ramos, A.M.; Vital, J. and Castanheiro, J.E. Esterification of glycerol with acetic acid over dodecamolybdophosphoric acid encaged in USY zeolite. *Catalysis Communications*. 10(2009): 481-484.
- [48] Liu, Y.; Xu, L.; Xu, B.; Li, Z.; Jia, L. and Guo, W. Toluene alkylation with 1-octane over supported heteropoly acids on MCM-41 catalysts. *Journal of Molecular Catalysis A: Chemical*. 297(2009): 86-92.
- [49] Phosphotungstic acid [Online]. Available from: http://en.wikipedia.org/wiki/Phosphotungstic_acid [2011, November 28]
- [50] Xue, B.; Li, Y. and Deng, L. Selective synthesis of p-xylene by alkylation of toluene with dimethyl carbonate over MgO-modified MCM-22, *Catalysis Communications*. 10(2009): 1609–1614.
- [51] Calgaroto, C.; Scherer, R.P.; Calgaroto, S.; Oliveira, J.V.; Oliveira, D. and Pergher, S.B.C. Immobilization of porcine pancreatic lipase in zeolite MCM 22 with different Si/Al ratios. *Applied Catalysis A*. 394(2011): 101–104.
- [52] Ghesti, G.F.; Macedo, J.M.; Parente, V.C.I.; Dias, J.A.; Dias, S.C.L. Synthesis, characterization and reactivity of Lewis acid/ surfactant cerium trisdodecylsulfate catalyst for transesterification and esterification reactions. *Applied Catalysis A: General*. 355(2009): 139–147.
- [53] Fornes, V.; Guil, J.M., Corma, A.; Pergher, S.; Maesen, Th.L.M.; Buglass, J.G. Preparation, characterization and catalytic activity of ITQ-2, a delaminated zeolite. *Microporous and Mesoporous Materials*. 38(2000): 301.

APPENDIX

A reaction mixture from the esterification was quantitatively analyzed with an Agilent Technologies 7890A gas chromatograph (GC) equipped with a 15-m DB-5HT capillary column and a flame ionization detector (FID). Figure A-1 shows the chromatogram of reaction mixture obtained from the esterification of glycerol with lauric acid over 40HPW/ITQ-2 catalyst.

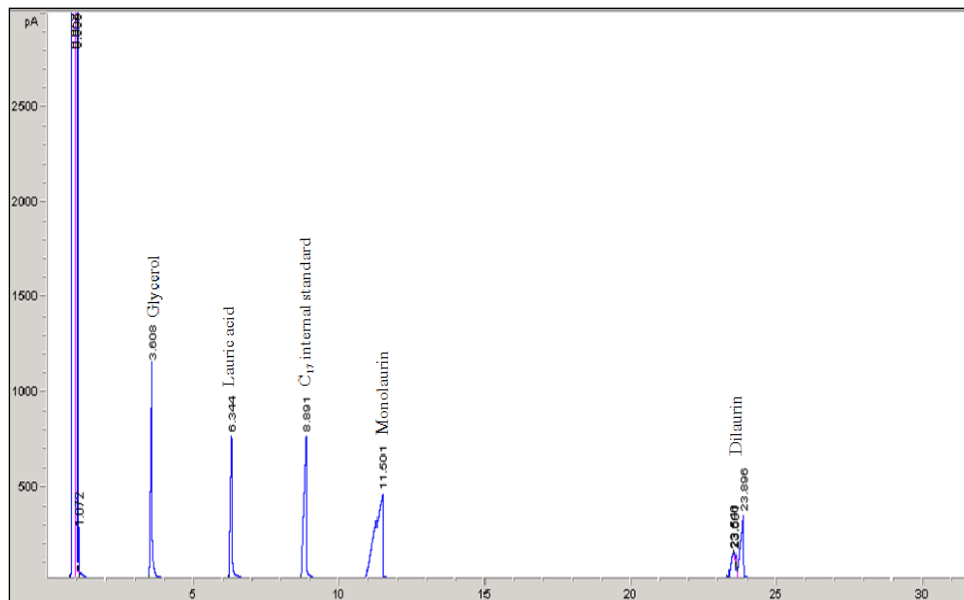


Figure A-1 Representative chromatogram of reaction mixture obtained from the esterification of glycerol with lauric acid over 40HPW/ITQ-2 catalyst.

The glyceride content was calculated based on the internal standardization method by using calibration curve of glyceride standard solution. Methyl heptadecanoate (C₁₇) was used as an internal standard. *N*-methyl-*N*-(trimethylsilyl)trifluoroacetamide (MSTFA) was used to convert the lauric acid and glycerol remaining and the products containing hydroxyl groups to more volatile derivatives. The calibration function was given by the following expression, obtained from the experimental data using the linear regression method.

Linear regression equation: $Y = aX + b$

$$X = \frac{\text{peak area of standard solution}}{\text{peak area of internal standard solution}}$$

$$Y = \frac{\text{mass of standard solution}}{\text{mass of internal standard solution}}$$

1) Calibration curve of glyceride standard solution

$$M_{\text{mono}}/M_{\text{c17}} = a_{\text{mono}}(A_{\text{mono}}/A_{\text{c17}}) + b_{\text{mono}}$$

$$M_{\text{di}}/M_{\text{c17}} = a_{\text{di}}(A_{\text{di}}/A_{\text{c17}}) + b_{\text{di}}$$

$$M_{\text{tri}}/M_{\text{c17}} = a_{\text{tri}}(A_{\text{tri}}/A_{\text{c17}}) + b_{\text{tri}}$$

$M_{\text{mono}}, M_{\text{di}},$ = mass of monolaurin, dilaurin and trilaurin, respectively (g)

M_{tri}

M_{c17} = mass of methyl heptadecanoate (g)

$A_{\text{mono}}, A_{\text{di}}, A_{\text{tri}}$ = peak area of monolaurin, dilaurin and trilaurin, respectively

A_{c17} = peak area of methyl heptadecanoate

$a_{\text{mono}}, b_{\text{mono}}$ = constant value of calibration curve of monolaurin standard solution

$a_{\text{di}}, b_{\text{di}}$ = constant value of calibration curve of dilaurin standard solution

$a_{\text{tri}}, b_{\text{tri}}$ = constant value of calibration curve of trilaurin standard solution

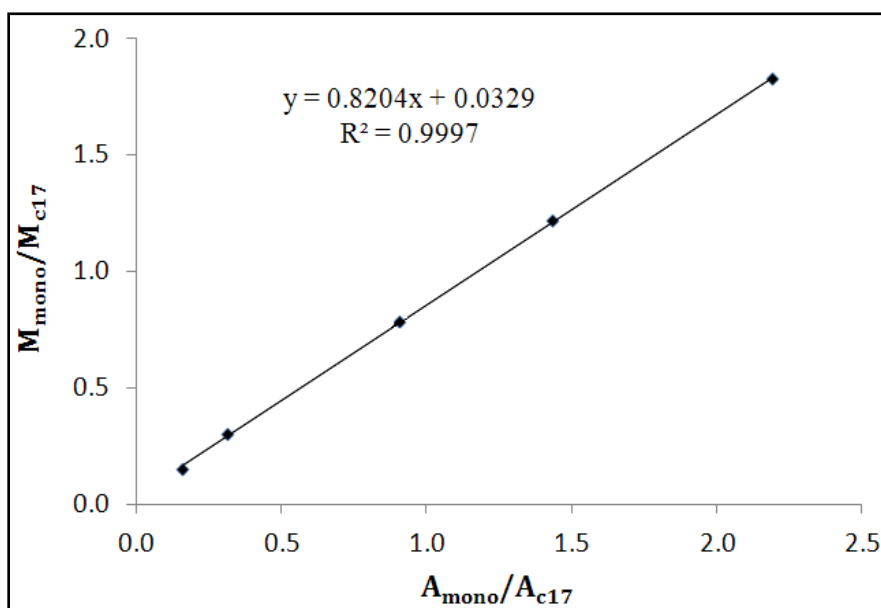


Figure A-2 Calibration curve of monolaurin standard solution.

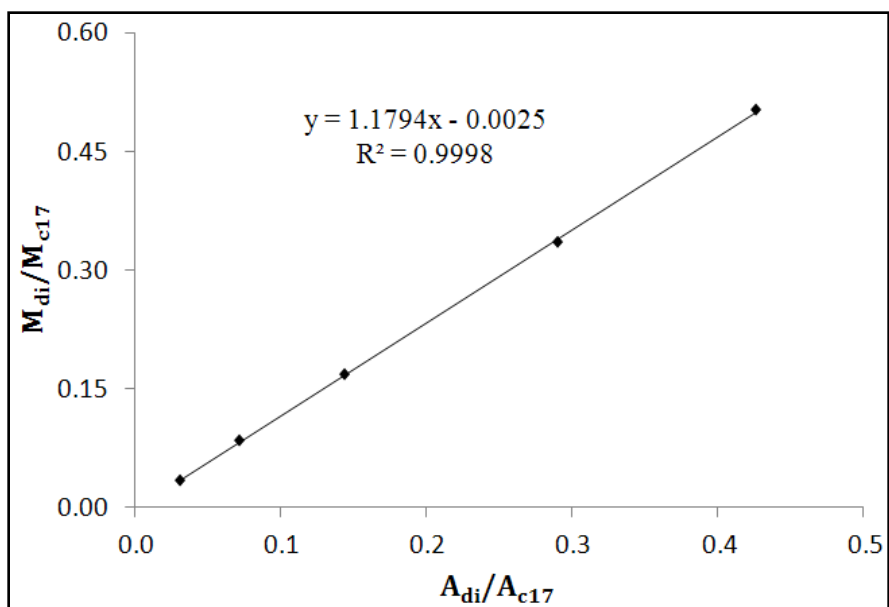


Figure A-3 Calibration curve of dilaurin standard solution.

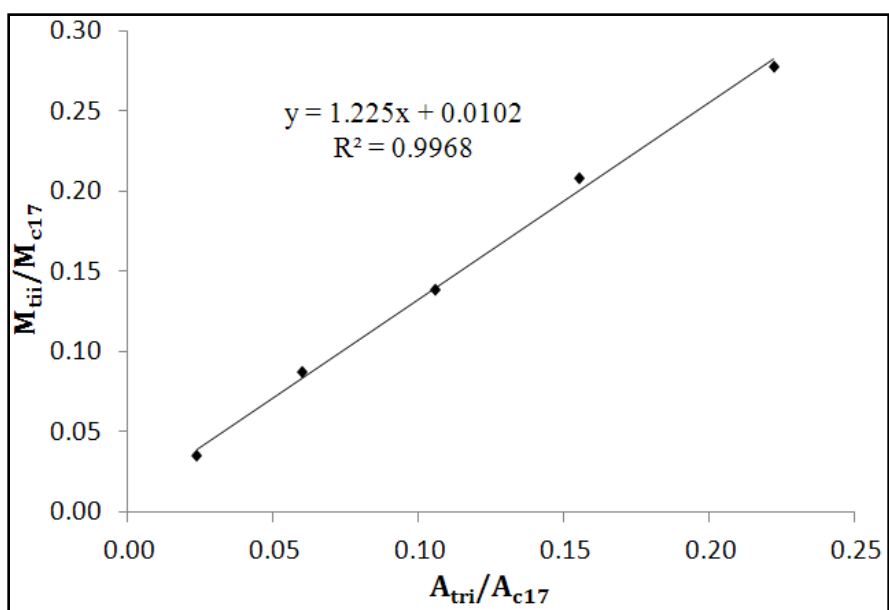


Figure A-4 Calibration curve of trilaurin standard solution.

2) Calibration curve of lauric acid standard solution

$$M_{\text{lauric}}/M_{\text{c17}} = a_{\text{lauric}}(A_{\text{lauric}}/A_{\text{c17}}) + b_{\text{lauric}}$$

M_{lauric} = mass of lauric acid (g)

M_{c17} = mass of methyl heptadecanoate (g)

A_{lauric} = peak area of lauric acid

A_{c17} = peak area of methyl heptadecanoate

$a_{\text{lauric}}, b_{\text{lauric}}$ = constant value of calibration curve of lauric acid standard solution

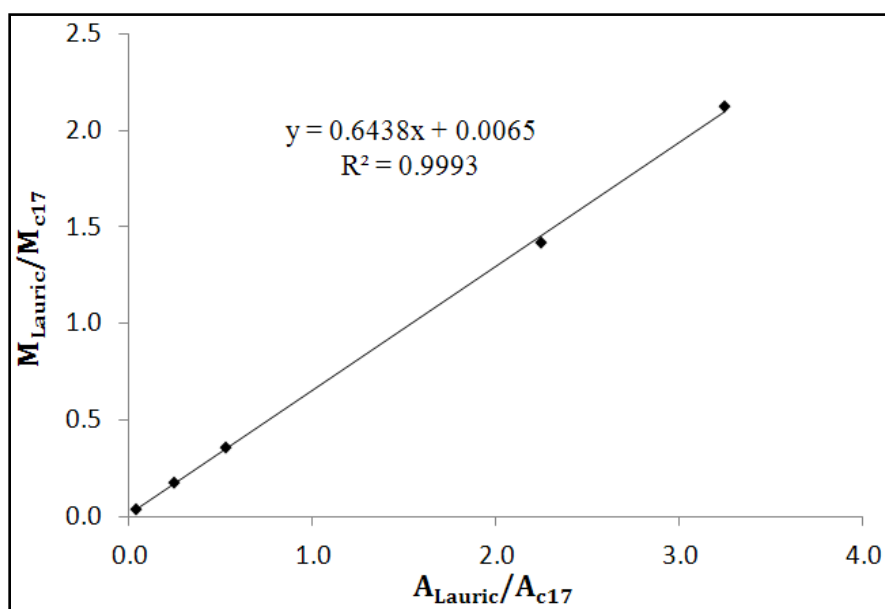


Figure A-5 Calibration curve of lauric acid standard solution.

3) Calibration curve of glycerol standard solution

$$M_{\text{glycerol}}/M_{\text{c17}} = a_{\text{glycerol}}(A_{\text{glycerol}}/A_{\text{c17}}) + b_{\text{glycerol}}$$

M_{glycerol} = mass of glycerol (g)

M_{c17} = mass of methyl heptadecanoate (g)

A_{glycerol} = peak area of glycerol

A_{c17} = peak area of methyl heptadecanoate

$A_{\text{glycerol}}, b_{\text{glycerol}}$ = constant value of calibration curve of glycerol standard solution

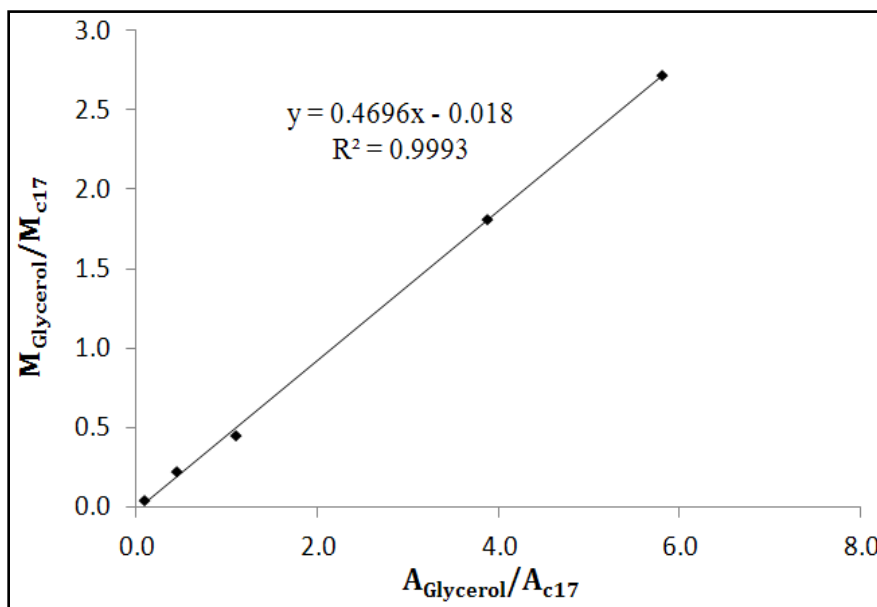


Figure A-6 Calibration curve of glycerol standard solution.

The amount of glyceride products in total reaction mixture (20 g) was calculated by comparing with the amount of glyceride products from calibration curve as show below:

M_{GC}	0.1xxx	g	M_{mono} or M_{di} or M_{tri}	A	mg
$M_{sampling + pyridine}$	B	g	M_{mono} or M_{di} or M_{tri}	C	mg
$M_{sampling}$	D	g	M_{mono} or M_{di} or M_{tri}	C	mg
$M_{total\ reaction}$	20	g	M_{mono} or M_{di} or M_{tri}	E	mg

M_{GC} = mass of reaction product for GC analysis (g)

$M_{mono}, M_{di}, M_{tri}$ = mass of monolaurin, dilaurin and trilaurin, respectively (g)

$M_{sampling + pyridine}$ = mass of sampling and pyridine (g)

$M_{sampling}$ = mass of sampling (g)

4) Calculation of yield percentage for glyceride products

$$\% \text{ yield of monolaurin} = \frac{\left(\frac{\text{mass of monolaurin (g)}}{\text{molecular weight of monolaurin (g/mol)}} \right)}{\left(\frac{\text{mass of lauric acid initial (g)}}{\text{molecular weight of lauric acid (g/mol)}} \right)} \times 100$$

$$\% \text{ yield of dilaurin} = \frac{\left(\frac{\text{mass of dilaurin (g)}}{\text{molecular weight of dilaurin (g/mol)}} \right)}{\left(\frac{\text{mass of lauric acid initial (g)}}{\text{molecular weight of lauric acid (g/mol)}} \right)} \times 100$$

$$\% \text{ yield of trilaurin} = \frac{\left(\frac{\text{mass of trilaurin (g)}}{\text{molecular weight of trilaurin (g/mol)}} \right)}{\left(\frac{\text{mass of lauric acid initial (g)}}{\text{molecular weight of lauric acid (g/mol)}} \right)} \times 100$$

5) Calculation of selectivity percentage for glyceride products

$$\% \text{ selectivity to monolaurin} = \frac{Y_{\text{mono}}}{Y_{\text{mono}} + Y_{\text{di}} + Y_{\text{tri}}} \times 100$$

$$\% \text{ selectivity to dilaurin} = \frac{Y_{\text{di}}}{Y_{\text{mono}} + Y_{\text{di}} + Y_{\text{tri}}} \times 100$$

$$\% \text{ selectivity to trilaurin} = \frac{Y_{\text{tri}}}{Y_{\text{mono}} + Y_{\text{di}} + Y_{\text{tri}}} \times 100$$

Y_{mono} = percent yield of monolaurin

Y_{di} = percent yield of dilaurin

Y_{tri} = percent yield of trilaurin

6) Calculation of percentage of lauric acid conversion

$$\% \text{ conversion of lauric acid} = \frac{[M_{\text{lauric, I}} - M_{\text{lauric, F}}]}{M_{\text{lauric, I}}} \times 100$$

$M_{\text{lauric, I}}$ = mass of lauric acid initial (g)

$M_{\text{lauric, F}}$ = mass of lauric acid remaining (g)

Example 1 Calculation of glycerides yield and selectivity to monolaurin and dilaurin products from the esterification of glycerol with lauric acid over 40HPW/ITQ-2. Reaction conditions: Catalytic amount, 4 wt.%; glycerol/lauric acid molar ratio, 1; reaction temperature, 110°C; reaction time, 5 h.

Glyceride products	A _{glyceride}	A _{C17}	A _{glyceride} /A _{C17}	M _{glyceride} /M _{C17}	M _{glyceride} (mg)	M _{glyceride} total (g)	Yield (mol%)	Selectivity (%)
Monolaurin	7501	4966	1.51	1.27	3.9905	8.5497	45.53	79.27
Dilaurin	2341	4966	0.47	0.55	1.7363	3.7201	11.90	20.72

M _{GC}	0.0985	g	M _{mono}	3.9905	mg
M _{sampling + pyridine}	5.3787	g	M _{mono}	217.91	mg
M _{sampling}	0.5107	g	M _{mono}	217.91	mg
M _{total reaction}	20.0378	g	M _{mono}	8549.84	mg = 8.5499 g

$$\begin{aligned}
 \% \text{ yield of monolaurin} &= \frac{\left(\frac{\text{mass of monolaurin (g)}}{\text{molecular weight of monolaurin (g/mol)}} \right)}{\left(\frac{\text{mass of lauric acid initial (g)}}{\text{molecular weight of lauric acid (g/mol)}} \right)} \times 100 \\
 &= [(8.5499/274.4)/(13.7078/200.32)] \times 100 \\
 &= 45.53 \%
 \end{aligned}$$

$$\begin{aligned}
 \% \text{ selectivity to monolaurin} &= \frac{Y_{\text{mono}}}{Y_{\text{mono}} + Y_{\text{di}}} \times 100 \\
 &= \frac{45.53}{45.53 + 11.90} \times 100 \\
 &= 79.27 \%
 \end{aligned}$$

Example 2 Calculation of conversion of lauric acid from the esterification of glycerol with lauric acid over 40HPW/ITQ-2. Reaction conditions: Catalytic amount, 4 wt.%; glycerol/lauric acid molar ratio, 1; reaction temperature, 110°C; reaction time, 5 h.

A_{lauric}	A_{C17}	$A_{\text{lauric}}/A_{\text{C17}}$	$M_{\text{lauric}}/M_{\text{C17}}$	M_{lauric} (mg)	M_{lauric} total (g)	Lauric acid conversion (mol%)
7247	4966	1.4593	0.9460	2.9676	6.3582	53.62

$$\begin{aligned}
 \% \text{ conversion of lauric acid} &= \frac{[M_{\text{lauric, I}} - M_{\text{lauric, F}}] \times 100}{M_{\text{lauric, I}}} \\
 &= \frac{(13.7078 - 6.3582) \times 100}{6.3582} \\
 &= 53.62 \%
 \end{aligned}$$

VITAE

Mr. Chitatat Numnim was born on November 29, 1985 in Bangkok, Thailand. He received a Bachelor Degree of Science, major in Chemistry from Silpakorn University in 2007. Since 2009, he has been a graduate student in the program of Petrochemistry and Polymer Science, Faculty of Science, Chulalongkorn University and completed his Master of Science Degree in 2012.

His present address is 24, Soi Sangchuto 17, Sangchuto Road, Pak Phraek district, Kanchanaburi, Thailand 71000.